UCLA Samueli
School of Engineering

Office of Academic and Student Affairs
UCLA Samueli School of Engineering
420 Westwood Plaza, 6288 Boelter Hall, Los Angeles, CA, 90095-1600
310.825.9478 | www.samueli.ucla.edu

UCLA Samueli
School of Engineering

SUMMER UNDERGRADUATE SCHOLARS PROGRAM

2018

Poster Symposium | August 17, 2018

11:00 AM Begin Poster Symposium in Lobby

11:45 AM Hors d' oeuvres Served

12:55 PM Begin SUSP Closing Ceremony in CNSI Auditorium

1:00 PM Welcome: Dean Murthy

1:05 PM Acknowledgements: William Herrera

1:15 PM Best Poster and Poster Presentation Awards

1:30 PM Presentation of Certificates of Completion

2:00 PM SUSP Ceremony Concludes

Table of Contents

Student Research Abstracts & Posters

DEAN'S MESSAGE

The Summer Undergraduate Scholars Program (SUSP) provides participants with an intensive 8-week summer research experience in a wide range of engineering fields. Undergraduate students participate in research with UCLA Samueli School of Engineering faculty and research teams to gain real-world lab experience. As part of this program, SUSP students:

- Meet and network with peers who have similar goals and interests
- Learn to communicate research outcomes by participating in weekly Journal Club meetings
- Create a professional scientific poster of their research
- Write and publish a research abstract
- Present a detailed Summary of Project
- Become more competitive when applying to engineering graduate schools

This year, 43 Samueli undergraduate students were selected to join the first-ever SUSP cohort. I would like to congratulate this SUSP class on completion of their amazing research projects. Creating new knowledge is a very important, and very difficult, task. These high-performing students have done an outstanding job balancing their normal academic course load with the rigorous demands of research. They should be very proud of the abstracts and posters they have published today. I encourage you to meet the students, ask questions about their projects, and learn about the amazing new knowledge that is being created here at the UCLA Samueli School of Engineering.

Sincerely,

Jayathi Murthy
Ronald and Valerie Sugar Dean

Ksenia Afonicheva

Chemical Engineering

Sophomore

LAB NAME

Simonetti Research Group

FACULTY ADVISOR

Dante Simonetti

DAILY LAB SUPERVISOR

Eric Lin

DEPARTMENT

Chemical and Biomolecular Engineering

Effects of Ion Exchanged Zeolite Catalysts & Isobutane Cofeed on the Mechanistic Pathways of Butanal

Zeolite catalysis can be used in the conversion of biomass to biofuels by forming fuel-range alkanes from small oxygenates, providing a renewable alternative to fossil fuels. Zeolites have reaction sites that catalyze variable reaction pathways that potentially lead to undesired byproducts. This research investigated the effect of ion-exchanged zeolites and cofeed on mechanistic pathways of zeolite catlyzed butanal with the final goal of promoting alkane formation. Butanal, a biomass derivable molecule, was upgraded using H-BEA, Cu-BEA, and Zn-BEA catalysts with and without isobutane cofeed. Studies were carried out at 250 Celsius, 1 atm with 2 μL/min butanal flow. To quantify reaction mechanism preferences, butanal was flowed through a catalyst bed and analyzed using a GC-MS to identify product distribution. Based on product selectivity, it was found that H-BEA and Cu-BEA promoted longer C8 and C7 molecules in absence of isobutane. Cu-BEA additionally showed C8 and C4 alkane formation. Zn-BEA favored moderate C8 and C4 formation. The same experiment was executed with the addition of isobutane to observe cofeed effects. Isobutane, acting as a hydrogen donor, allowed for dehydration pathways to affect product distribution. In the case of H-BEA, product selectivity favored smaller C3-C5 molecules and additionally promoted C5, C7, C8, and C9 alkanes. Zn-BEA experienced diminishing C4 and increased C8 selectivity as well as C3 alkane production. Finally, Cu-BEA promoted C8 and C4 with minor C3 selectivity. In summary, alkane promoting mechanisms were achieved by running butanal through Cu-BEA without cofeed and by running butanal through Zn-BEA and H-BEA with isobutane cofeed.

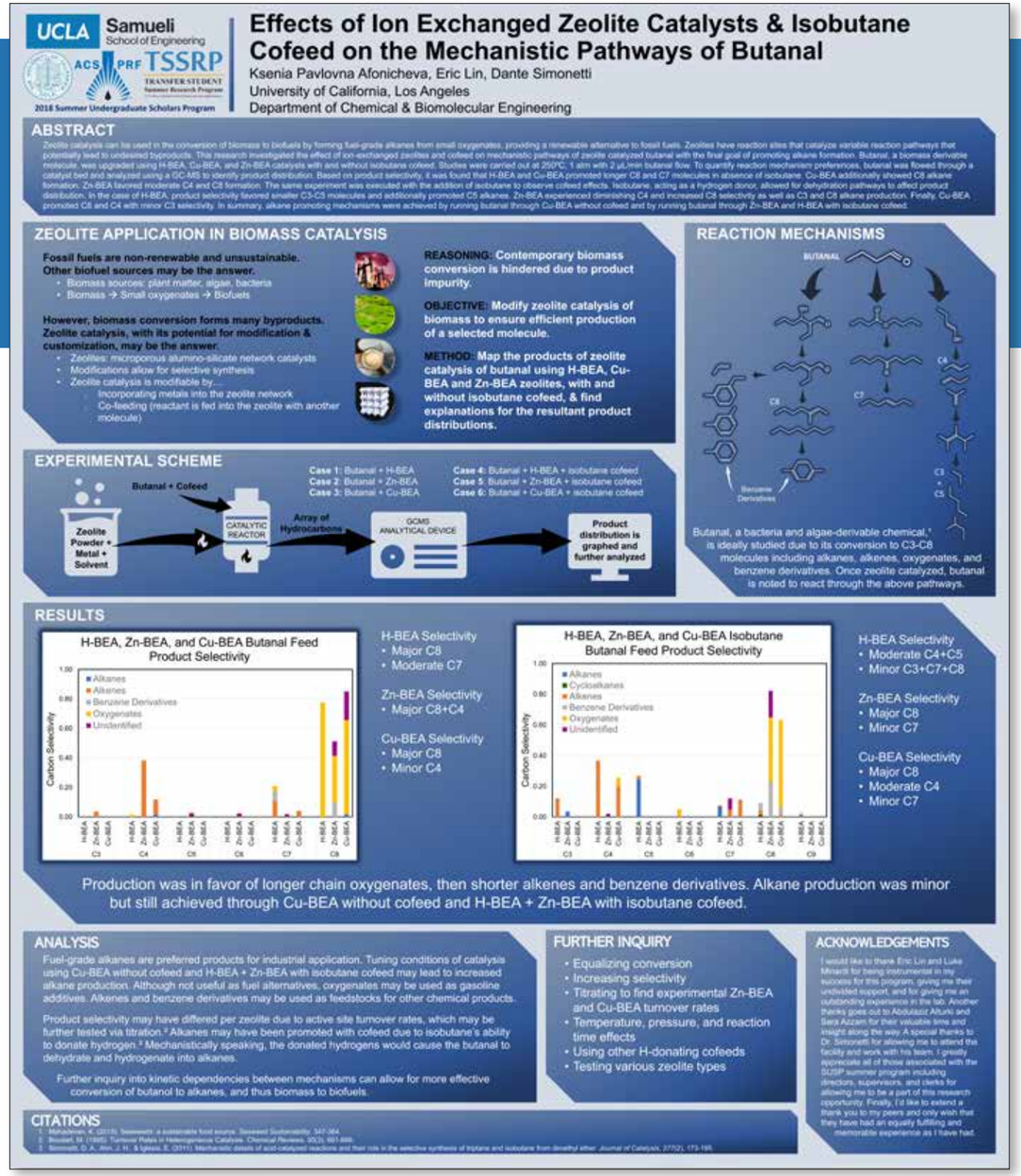

Nate Atkinson

Electrical Engineering

Sophomore

LAB NAME

Terahertz Devices and Intersubband Nanostructures Laboratory

FACULTY ADVISOR

Ben Williams

DAILY LAB SUPERVISOR

Chris Curwen

DEPARTMENT

Electrical and Computer Engineering

Automating data collection for a quantum cascade external cavity laser

There has been relatively little technological advancement within photonics concerning the terahertz frequency range, due in part to the historically poor performance and inconvenience of terahertz sources and components. Recent developments in the field have witnessed the creation of quantum cascade lasers with external optical cavities coupled to active reflectarray surfaces loaded with quantum cascade gain (the THz QC-VECSEL). These new designs have produced single-mode, near-diffraction limited beam patterns as well as optical powers above 5 mW in continuous wave, and peak pulse-powers greater than 1 W at 77 K.

Another strength of the THz QC-VECSEL is its ability to be tuned over a large frequency bandwidth. However, performing such measurements requires considerable manpower and time. Here, we present a method of automation for the experimental data collection, designed to decrease collection time and eliminate the need for human interaction. A LabVIEW program controls multiple devices simultaneously, supplying necessary input parameters and recording data to respective files on a personal computer. All the incorporated instruments are successfully able to communicate directly—or indirectly, through the employment of additional software as an intermediary communication protocol—with LabVIEW. Excluding the initialization of input parameters, the program runs autonomously. Results indicate an 81% reduction in execution time compared to manual operation.

Automating data collection for a quantum cascade external cavity laser

Nathan Atkinson, Pranav Balgi, Christopher Curwen, and Benjamin Williams

Department of Electrical and Computer Engineering, University of California, Los Angeles

INTRODUCTION

QC-VECSEL Active Region Geometry

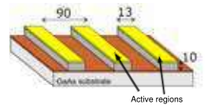

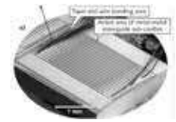

Xu, L., et al. *Applied Physics Letters,* **107**, (2015).

- Quantum cascade vertical external-cavity surface-emitting laser (QC-VECSEL) operating within THz frequencies
- Metasurface contains array of active regions, acts as amplifying mirror
- Output coupler reflects and transmits light
- Various properties of beam controlled and measured by different devices
- **GOAL**: automate operation of devices for collection of spectral and electromagnetic properties

VECSEL DESIGN

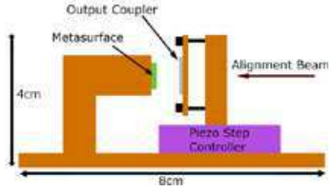

The position of the output coupler can be shifted using a piezoelectric controller, slightly altering the laser's wavelength. Consequently, the VECSEL is tunable over a short range of frequencies.

INITIALIZATION

User-defined inputs must be generated prior to program execution.

- Pulse generator: voltage range, pulse frequency, pulse width/delay, output impedance, gate frequency
- FT-IR: spectrum type, resolution, wavenumber range, aperture size
- Piezoelectric controller: step magnitude, step range, direction
- DMM: voltage/current calibration

BEAM PROPERTIES

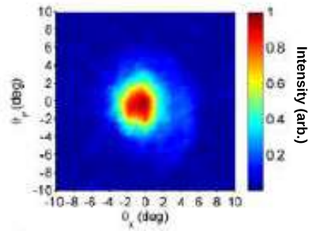

Xu, L., et al. *Applied Physics Letters,* **107**, (2015).

Pyroelectric sensor measures intensity over cross-sectional area of output beam, which provides a visualization of the beam pattern.

Other properties of focus include:

- peak power
- voltage and current at lasing threshold
- absorbance, transmittance, and single beam interference spectra

DATA COMMUNICATION PATHWAYS

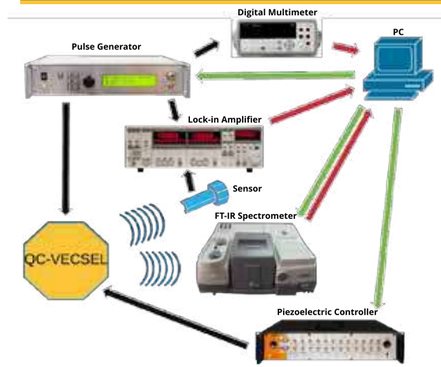

Pulse Generator

- Fires laser in pulsed "packets"
- Short pulses (~7 kHz)
- Gated signal (~30 Hz)

Lock-in Amplifier

- Amplifies signal at gate frequency
- Isolates signal from noise

FT-IR Spectrometer

- Produces frequency spectrum for the laser
- Uses OMNIC through LabVIEW

Piezoelectric Stepper

- Adjusts output coupler
- Tunes frequency

IMPROVEMENTS THROUGH AUTOMATION

The "Manual" bar represents the fastest recorded completion time for a human operator out of ten trials. The "Automated" bar presents the LabVIEW program's average execution time out of ten runs.

FT-IR Spectrum

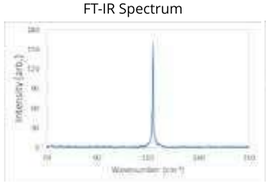

V-I and L-I Curves

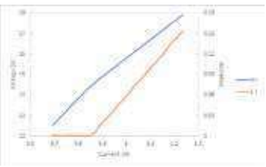

The FT-IR single beam signal response spectrogram of the laser, as well as voltage and power measurements from the DMM and pyroelectric sensor, respectively, are recorded, saved to file, and plotted automatically by LabVIEW. Automation allows for accurate data collection without human interaction, thus conserving manpower for use elsewhere.

REFERENCES

Faist, J., Capasso, F., Sivco, D. L., Sirtori, C., Hutchinson, A. L., & Cho, A. Y. (1994). Quantum cascade laser. *Science, 264*(5158), 553-556.

Mirzaei, B., Silva, J. R., Hayton, D., Groppi, C., Kao, T. Y., Hu, Q., . . . Gao, J. R. (2017). 8-beam local oscillator array at 4? THz generated by a phase grating and a quantum cascade laser. *Optics Express,25*(24), 29587. doi:10.1364/oe.25.029587

Verdeyen, J. T. (1995). *Laser electronics*. Englewood Cliffs: Prentice Hall.

Williams, B. S., Kumar, S., Callebaut, H., Hu, Q., & Reno, J. L. (2003). Terahertz quantum-cascade laser at λ≈100 μm using metal waveguide for mode confinement. *Applied Physics Letters,83*(11), 2124-2126. doi:10.1063/1.1611642

Xu, L., Curwen, C. A., Hon, P. W., Chen, Q., Itoh, T., & Williams, B. S. (2015). Metasurface external cavity laser. *Applied Physics Letters, 107*(22), 221105. doi:10.1063/1.4936887

We would like to thank the National Science Foundation Research Experience for Undergraduates Program and the Functional Nanomaterials Summer Scholar Program for providing funding for our undergraduate research, as well as the UCLA Electrical Engineering Fast Track to Success Program for its continued support of undergraduate research and studies.

LAB NAME

Communications Systems Lab

FACULTY ADVISOR

Richard Wesel

DAILY LAB SUPERVISOR

NA

DEPARTMENT

Electrical and Computer Engineering

Alex Baldauf

Electrical Engineering

Senior

Efficient Computation of Convolutional Decoder Reliability without a CRC

When a convolutional encoder sends a codeword over a noisy channel, the noise distorts the codeword bits. This distortion can cause the Viterbi decoder at the receiver to select the wrong codeword. Sometimes a cyclic redundancy check (CRC) is used to detect these decoding errors, but this requires extra bits for the CRC. The reliability-output Viterbi algorithm (ROVA) of Raghavan and Baum computes the probability that a Viterbi decoding result is in error, allowing unreliable decoding to be identified without the overhead of a CRC. Although ROVA gives an exact probability that the selected codeword is the correct codeword, its complexity brings about a desire for a lower complexity alternative. Polyanskiy et al. proposed accumulated information density (AID) as a stopping criterion for VL codes and used it for theoretical analysis. This work compares ROVA and AID in terms of performance and complexity. AID sums the estimated information content of each received bit in the codeword. While less complex, AID turns out to perform far worse than ROVA in detecting Viterbi decoding errors. We propose a third metric, codeword information density (CID) that calculates the information content of the overall received codeword. CID turns out to be mathematically equivalent to ROVA and reveals a lower complexity approach to computing ROVA.

Efficient Computation of Convolutional Decoder Reliability Without a Cyclic Redundancy Check

A. Baldauf, A. Belhouchat, N. Wong, R.D. Wesel

Department of Electrical and Computer Engineering, University of California, Los Angeles

Introduction

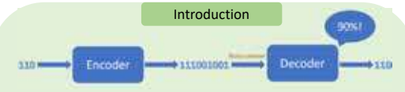

- Cyclic redundancy checks (CRCs) have overhead for short block-lengths
- Three methods to compute decoder reliability without overhead:
  - Reliability output Viterbi algorithm (ROVA) calculates probability of correct decoding
  - Accumulated information density (AID) sums information content of each bit in codeword
  - Codeword information density (CID) finds information density of entire codeword
- Goal: determine the best metric (in terms of accuracy and complexity) and develop a model to set a threshold to control the error rate

Metric	Complexity	Accuracy
ROVA	High	High
AID	Low	???
CID	Medium	???

Materials/Methods

- Run simulations to generate histograms of ROVA, AID, and CID values
  - Keep track of correctly and incorrectly decoded codewords
  - Measure time taken to complete simulations using ROVA, AID, and CID separately
- Data analysis:
  - Separation between correct and incorrect histograms tells us effectiveness of metric
  - Determine best metric from analysis
- Design a model to fit distribution of chosen metric
  - Use model to find:
    - Probability of undetected error P(E)
    - Probability of correctness P(C)
    - Probability of rejection P(NACK)

Results

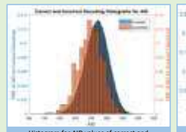

Histogram for AID values of correct and incorrect decodings. The lack of separation between blue and orange curves indicates that AID is a poor metric for detecting errors.

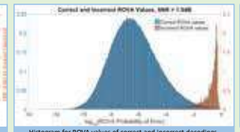

Histogram for ROVA values of correct and incorrect decodings. The clear separation between blue and orange curves indicates that ROVA is a good metric for detecting errors. The histograms follow the same distribution as CID.

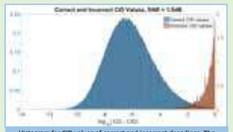

Histogram for CID values of correct and incorrect decodings. The clear separation between blue and orange curves indicates that CID is a good metric for detecting errors. The histograms follow the same distribution as ROVA.

Histogram of ROVA values with model overlaid. The model is a piecewise of various Gaussian distributions and functions of Gaussian distributions.

Graph of throughput vs. undetected error rate for AID and ROVA. A good metric should have high throughput for a low undetected error rate, which ROVA offers and AID does not.

Throughput: ratio of accepted messages to total received messages.

Undetected error rate: ratio of errors not detected by the metric.

	AID	CID	ROVA
Number of operations	3.0×10^6	2.7×10^6	1.8×10^7
Runtime (ms) (10000 decodings)	1.7×10^3	1.3×10^3	2.7×10^3

Complexity and time comparisons of ROVA, AID, and CID. Note that the number of operations doesn't include the operations for Viterbi decoding.

$$\mathrm{ROVA} = \frac{f_{Y|X}(y^n|\hat{x}^n)}{\sum_{x^n \in \mathcal{C}} P(x^n) f_{Y|X}(y^n|x^n)} = \frac{1}{1+E}$$

where E is a sum of weighted skew log-normals

Conclusion

- AID is fastest, ROVA is slowest, CID is in between
- AID is too inaccurate
- CID has an equivalent distribution to ROVA
- Because CID is equivalent to ROVA and faster than ROVA, CID is the best metric to assess decoder reliability

References

C.-Y. Lou, B. Daneshrad, and R. D. Wesel, "Convolutional-code specific CRC code design," IEEE Transactions on Communications, vol. 63, no. 10, pp. 3459–3470, Oct 2015.

A. Raghavan and C. Baum, "A reliability output Viterbi algorithm with applications to hybrid ARQ," IEEE Trans. Inf. Theory, vol. 44, no. 3, pp. 1214–1216, May 1998.

A. R. Williamson, M. J. Marshall, and R. D. Wesel, "Reliability-output decoding of tail-biting convolutional codes," IEEE Transactions on Communications, vol. 62, no. 6, pp. 1768–1778, Jun 2014.

Y. Polyanskiy, H. V. Poor, and S. Verdu, "Feedback in the non-asymptotic regime," IEEE Trans. Inf. Theory, vol. 57, no. 8, pp. 4903 – 4925, August 2011.

Future Work

- Find analytic expression describing distribution of CID
- Use equation to determine relationship between threshold and P(E), P(C), and P(NACK)

Acknowledgements

This work used computational and storage services associated with the Hoffman2 Shared Cluster provided by UCLA Institute for Digital Research and Education's Research Technology Group.

Pranav Balgi

Electrical Engineering

Sophomore

LAB NAME

Terahertz Devices and Intersubband Nanostructures Laboratory

FACULTY ADVISOR

Ben Williams

DAILY LAB SUPERVISOR

Chris Curwen

DEPARTMENT

Electrical and Computer Engineering

Automating data collection for a quantum cascade external cavity laser

There has been relatively little technological advancement within photonics concerning the terahertz frequency range, due in part to the historically poor performance and inconvenience of terahertz sources and components. Recent developments in the field have witnessed the creation of quantum cascade lasers with external optical cavities coupled to active reflectarray surfaces loaded with quantum cascade gain (the THz QC-VECSEL). These new designs have produced single-mode, near-diffraction limited beam patterns as well as optical powers above 5 mW in continuous wave, and peak pulse-powers greater than 1 W at 77 K.

Another strength of the THz QC-VECSEL is its ability to be tuned over a large frequency bandwidth. However, performing such measurements requires considerable manpower and time. Here, we present a method of automation for the experimental data collection, designed to decrease collection time and eliminate the need for human interaction. A LabVIEW program controls multiple devices simultaneously, supplying necessary input parameters and recording data to respective files on a personal computer. All the incorporated instruments are successfully able to communicate directly—or indirectly, through the employment of additional software as an intermediary communication protocol—with LabVIEW. Excluding the initialization of input parameters, the program runs autonomously. Results indicate an 81% reduction in execution time compared to manual operation.

Automating data collection for a quantum cascade external cavity laser

Nathan Atkinson, Pranav Balgi, Christopher Curwen, and Benjamin Williams

Department of Electrical and Computer Engineering, University of California, Los Angeles

INTRODUCTION

QC-VECSEL Active Region Geometry

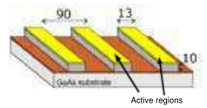

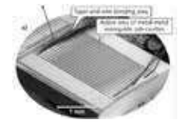

Xu, L., et al. *Applied Physics Letters,* **107**, (2015).

- Quantum cascade vertical external-cavity surface-emitting laser (QC-VECSEL) operating within THz frequencies
- Metasurface contains array of active regions, acts as amplifying mirror
- Output coupler provides feedback to form laser resonator
- Frequency tunable by altering position of output coupler
- **GOAL**: automate operation of spectral and electromagnetic data collection instruments

VECSEL DESIGN

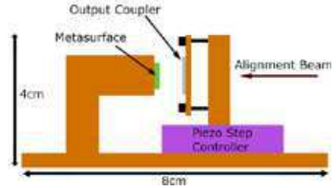

The position of the output coupler can be shifted using a piezoelectric controller, slightly altering the laser's wavelength. Consequently, the VECSEL is tunable over a short range of frequencies.

INITIALIZATION

User-defined inputs must be generated prior to program execution.

- Pulse generator: voltage range, pulse frequency, pulse width/delay, output impedance, gate frequency
- FT-IR: spectrum type, resolution, wavenumber range, aperture size
- Piezoelectric controller: step magnitude, step range, direction
- DMM: voltage/current calibration

BEAM PROPERTIES

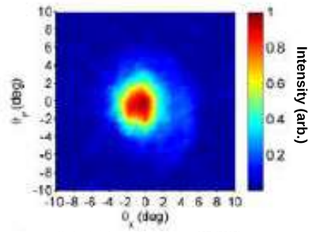

Xu, L., et al. *Applied Physics Letters,* **107**, (2015).

Pyroelectric sensor measures intensity over cross-sectional area of output beam, which provides a visualization of the beam pattern.

Other properties of focus include:

- peak power
- voltage and current at lasing threshold
- atmospheric absorption

DATA COMMUNICATION PATHWAYS

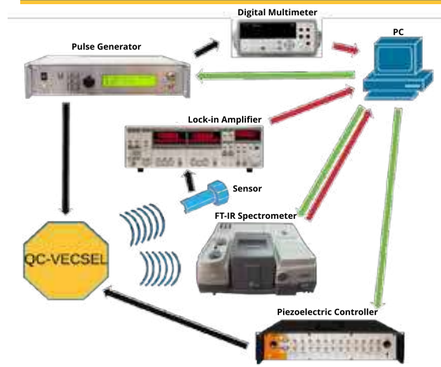

Pulse Generator

- Fires laser in pulsed "packets"
- Short pulses (~7 kHz)
- Gated signal (~30 Hz)

Lock-in Amplifier

- Amplifies signal at gate frequency
- Isolates signal from noise

FT-IR Spectrometer

- Produces frequency spectrum for the laser
- Uses OMNIC through LabVIEW

Piezoelectric Stepper

- Adjusts output coupler
- Tunes frequency

IMPROVEMENTS THROUGH AUTOMATION

51% faster

1.54 hours saved

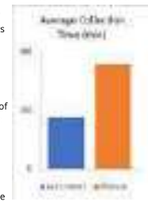

The "Manual" bar represents the fastest recorded completion time for a human operator out of ten trials. The "Automated" bar presents the LabVIEW program's average execution time out of ten runs.

FT-IR Spectrum

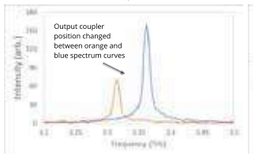

V-I and L-I Curves

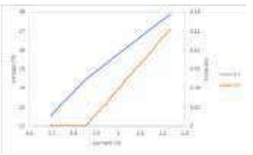

The FT-IR single beam signal response spectrogram of the laser, as well as voltage and power measurements from the DMM and pyroelectric sensor, respectively, are recorded, saved to file, and plotted automatically by LabVIEW. Automation allows for accurate data collection without human interaction, thus conserving manpower for use elsewhere.

ACKNOWLEDGEMENTS

We would like to thank the National Science Foundation Research Experience for Undergraduates Program and the Functional Nanomaterials Summer Scholar Program for providing funding for our undergraduate research, as well as the UCLA Electrical Engineering Fast Track to Success Program for its continued support of undergraduate research and studies.

LAB NAME
Sensors and Technology Laboratory

FACULTY ADVISOR
Robert Candler

DAILY LAB SUPERVISOR
Jimmy Wu

DEPARTMENT
Electrical and Computer Engineering

Michaella Baltazar

Electrical Engineering

Sophomore

Circuit Analysis of Micromachined Electromagnet Quadruple Devices

The increasing interest in higher-energy FEL for medical and particle imaging calls for new focusing technology. The fabrication process outlined in Harrison et. al. [1] allows for the micromachining of an electromagnet, with a field parallel to the substrate plane, which makes possible the MEMS magnetic quadrupole in Harrison et. al. [2]. These quadrupoles can be utilized for FEL emission in the 100-10 nm wavelength spectrum in shorter distances than allowed by current technology. After the machining of a handful of quadrupole devices for FEL focusing on a 4mm x 4mm die, multiple technical issues surfaced surrounding the machining process, mostly shortages and other node faults, which prevent experimentation. By means of a stereoscope and probe station, identification consisted of thorough resistance mapping across individual devices, which were analysed for shorts in the electromagnet windings. This resulted in resistance fluctuation during measurement, and resistance mappings pointed to shorts located at the vias. To allow for furthering of the initial project, current was applied across shorted pads to burn the shorts; this technique working points towards “whiskers” -- small strands of metal created by the fabrication process -- being the primary cause of shortage for some devices. Some electromagnets were found to be disconnected, leading to future investigations involving FIB incision and SEM imaging.

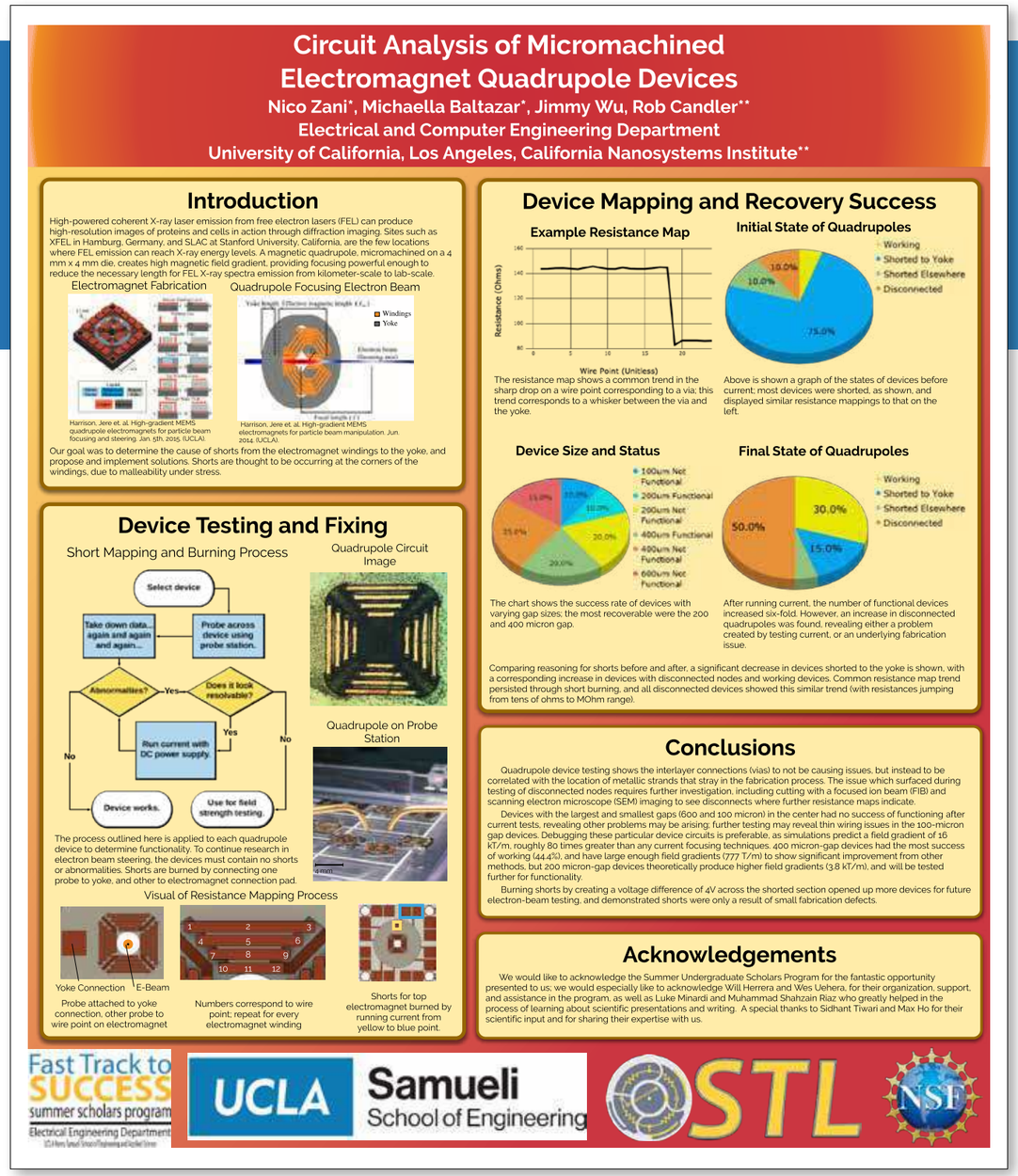

Cory Barnes

Chemical Engineering

Senior

LAB NAME

Christofides Lab

FACULTY ADVISOR

Panagiotis Christofides

DAILY LAB SUPERVISOR

Anh Tran and Carlos Garcia

DEPARTMENT

Chemical and Biomolecular Engineering

Phthalic Anhydride Synthesis Optimization via Computational Fluid Dynamics

The simulation of fixed bed catalytic reactors is an important resource in gaining a better understanding of reactor fluid dynamics. The focus of this research will be on the modeling of phthalic anhydride synthesis from the partial oxidation of o-xylene in a fixed bed catalytic reactor. This is an exothermic process that will generate considerable heat, and a simulation of this type will help to identify and mitigate the formation of hot spots in the reactor. Phthalic anhydride is widely used as a plasticizer for polyvinyl chloride and other plastics. It is also an important precursor for pharmaceutical drugs like cellulose acetate phthalate which helps fight viral diseases. Previous researchers have used computational fluid dynamics to create simulations for the fixed bed catalytic reactor synthesis of phthalic anhydride to study the relationship between product yield and the stability and activity of the catalyst. The most accurate of these simulations use three-dimensional modeling, making them computationally expensive. It is the goal of this project to develop a two-dimensional model of the fixed bed catalytic reactor that will be both accurate and computationally affordable. This two-dimensional model will represent a cross-section of the reactor along its axis and will account for the radial space between the center of the pipe and the pipe wall. Because it is assumed that the pipe is symmetrical with respect the angular cylindrical coordinate, the two-dimensional plot can be rotated about the x-axis to generate a three-dimensional representation of the fixed bed catalytic reactor. The decision to take advantage of the reactor symmetry in this way enables the generation of a computationally affordable two-dimensional simulation with the same output of meaningful data as a computationally expensive three-dimensional model. Improvements to the computational efficiency of fixed bed catalytic reactor simulations will enable improvements to engineering controls, which will in-turn improve the consistency and safety of process plant operations.

Phthalic Anhydride Synthesis Optimization via Computational Fluid Dynamics

Cory Barnes, Carlos Garcia, Anh Tran, Zhihao Zhang
Zhe Wu, and Panagiotis D. Christofides
UCLA Department of Chemical and Biomolecular Engineering

Introduction

The simulation of fixed bed catalytic reactors is an important resource in gaining a better understanding of reactor fluid dynamics. The focus of this research will be on the modeling of phthalic anhydride synthesis from the partial oxidation of o-xylene in a fixed bed catalytic reactor. This is an exothermic process that will generate considerable heat, and a simulation of this type will help to identify and mitigate the formation of hot spots in the reactor. Phthalic anhydride is widely used as a plasticizer for polyvinyl chloride and other plastics. It is also an important precursor for pharmaceutical drugs like cellulose acetate phthalate which helps fight viral diseases. Previous researchers have used computational fluid dynamics to create simulations for the fixed bed catalytic reactor synthesis of phthalic anhydride to study the relationship between product yield and the stability and activity of the catalyst. The most accurate of these simulations use three-dimensional modeling, making them computationally expensive. It is the goal of this project to develop a two-dimensional model of the fixed bed catalytic reactor that will be both accurate and computationally affordable. This two-dimensional model will represent a cross-section of the reactor along its axis and will account for the radial space between the center of the pipe and the pipe wall. Because it is assumed that the pipe is symmetrical with respect the angular cylindrical coordinate, the two-dimensional plot can be rotated about the x-axis to generate a three-dimensional representation of the fixed bed catalytic reactor. The decision to take advantage of the reactor symmetry in this way will allow for the generation of a computationally affordable two-dimensional simulation with the same output of meaningful data as a computationally expensive three-dimensional model. Improvements to the computational efficiency of fixed bed catalytic reactor simulations will enable improvements to engineering controls, which will in-turn improve the consistency and safety of process plant operations.

Materials and Methods

- Single fixed bed catalytic reactor
  - Diameter: 0.025 m ; Length: 4 m
  - V_2O_5/TiO_2 catalyst
  - Partial oxidation of o-xylene to phthalic anhydride
- Simulation to display a steady state reactor with parameters varying in the axial and radial direction
  - Temperature
  - Concentrations
  - Pressure
  - Velocity
- Ansys Fluent and Aspen Simulation software will be used to generate the data for the reactor.
- Two-dimensional modeling is used to improve computational affordability compared with three-dimensional modeling.

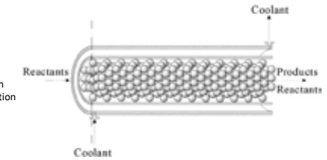

Figure 1 – General diagram of a fixed bed catalytic reactor with a co-current cooling jacket.

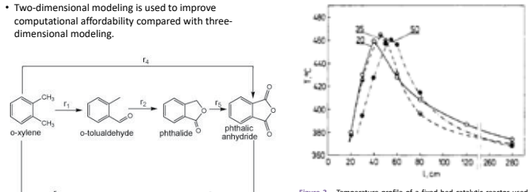

Figure 3 – Simplified reaction mechanism for production of phthalic anhydride from the partial oxidation of o-xylene

Figure 2 – Temperature profile of a fixed bed catalytic reactor used for phthalic anhydride synthesis. The temperature spike is a result of the exothermic reaction that occurs as the reaction initiates as the reactants contact the catalyst. (Anastasov, 1992)

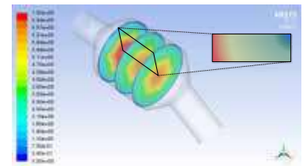

Figure 4 – Three-dimensional model of velocity gradients in a fixed bed catalytic reactor as generated by the Ansys Fluent software. Reactants enter the reactor in the upper left of the diagram and the products exit on the lower right. The rectangle on the right represents the two-dimensional segment of the reactor that is modeled in this research.

Pseudo Homogeneous Model

The pseudo homogeneous model represents the mass and energy transport of the fixed bed catalytic reactor. This model makes the assumption that the presence of the solid phase can be neglected and that the fluid can be modeled as having ideal plug flow.

$$D_{er}\left(\frac{\partial^2 c}{\partial r^2}+\frac{1}{r}\frac{\partial c}{\partial r}\right) - u_z\frac{\partial c}{\partial z} - r_{A\ B} = 0$$

$$k_{er}\left(\frac{\partial^2 T}{\partial r^2}+\frac{1}{r}\frac{\partial T}{\partial r}\right) - u_z\ \rho_f c_p\frac{\partial T}{\partial z} + (-\Delta H) r_{A\ B} = 0$$

ε_B : Void fraction of the catalytic bed
D_{er} : Effective diffusivity in the radial direction
C : Concentration of a single reactant
u_z : Superficial velocity
r_A : Reaction rate based on component A
ρ_B : Catalyst bulk density
c_p : Specific heat
ΔH : Heat of the reaction
ρ_f : Density of the Fluid
T : Temperature
k_{er} : Effective thermal conductivity in the radial direction

Heterogeneous Model

The heterogeneous model represents the mass and energy transport of the fixed bed catalytic reactor. This model utilizes the governing equations for both the fluid and solid phases.

Fluid:

$$D_{er}\left(\frac{\partial^2 c}{\partial r^2}+\frac{1}{r}\frac{\partial c}{\partial r}\right) - u_z\frac{\partial c}{\partial z} - k_f a_v\left(c - c_s'\right) = 0$$

$$\rho_f c_{pf}\left(\frac{\partial^2 T}{\partial r^2}+\frac{1}{r}\frac{\partial T}{\partial r}\right) - u_z\ \rho_f c_{pf}\frac{\partial T}{\partial z} + h_f a_v\left(T_s' - T\right) = 0$$

Solid:

$$k_f a_v\left(c - c_s'\right) - \eta r_A = 0$$

$$k_{es}\left(\frac{\partial^2 T}{\partial r^2}+\frac{1}{r}\frac{\partial T}{\partial r}\right) + h_f a_v\left(T_s' - T\right) + (-\Delta H)\ \rho_B r_A = 0$$

η : Effectiveness factor based on the catalyst
k_f : Film mass transfer coefficient
a_v : Particle surface area to unit bed volume ratio
k_{es} : Effective thermal conductivity in the radial direction for the solid phase
k_{ef} : Effective thermal conductivity in the radial direction for the fluid phase

Results and Discussion

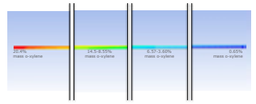

Figure 5 – Compressed and segmented concentration gradient of o-xylene as it is consumed while traveling through the reactor. Fluid enters the reactor on the left and exits to the right.

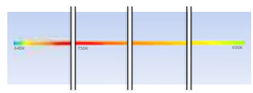

Figure 6 – Compressed and segmented temperature gradient in the reactor. The exothermic reaction produces significant heat causing the spike in temperature. Fluid enters the reactor on the left and exits to the right.

- The images to the left depict two-dimensional models of the fixed-bed catalytic reactor.
- In order to create an accurate representation of the reactor, it was necessary to create user defined functions for the following profiles:
  - Catalyst bed porosity
  - Inertial resistance
  - Viscous resistance
  - Volumetric rate of reaction
- These results are representative of the physical experimental results from past literature.

Conclusion

This research has shown that it is possible to generate a two-dimensional simulation that produces the same level of effective data as a three-dimensional model with a fraction of the computational cost. Based on the results of the temperature, pressure, velocity, and concentration profiles generated via the Fluent simulation, it can be seen that these are accurate when compared to the results of past simulations and physical experiments found in the literature. Future work will include further optimization of this process simulation.

Reference

Anastasov, A. I.; Nikolov, V. A. Pretreatment of Vanadia-Titania Catalyst for Partial Oxidation of o-Xylene under Industrial Conditions. *Ind. Eng. Chem. Res.*, 1992, *Vol. 31*, No. 1.

Acknowledgements

Department of Energy
National Science Foundation
2018 UCLA Summer Undergraduate Scholars Program

Adam Belhouchat

Electrical Engineering

Junior

LAB NAME

Communications Systems Laboratory

FACULTY ADVISOR

Richard Wesel

DAILY LAB SUPERVISOR

NA

DEPARTMENT

Electrical and Computer Engineering

Efficient Computation of Convolutional Decoder Reliability without a CRC

When a convolutional encoder sends a codeword over a noisy channel, the noise distorts the codeword bits. This distortion can cause the Viterbi decoder at the receiver to select the wrong codeword. Sometimes a cyclic redundancy check (CRC) is used to detect these decoding errors, but this requires extra bits for the CRC. The reliability-output Viterbi algorithm (ROVA) of Raghavan and Baum computes the probability that a Viterbi decoding result is in error, allowing unreliable decoding to be identified without the overhead of a CRC. Although ROVA gives an exact probability that the selected codeword is the correct codeword, its complexity brings about a desire for a lower complexity alternative. Polyanskiy et al. proposed accumulated information density (AID) as a stopping criterion for VL codes and used it for theoretical analysis. This work compares ROVA and AID in terms of performance and complexity. AID sums the estimated information content of each received bit in the codeword. While less complex, AID turns out to perform far worse than ROVA in detecting Viterbi decoding errors. We propose a third metric, codeword information density (CID) that calculates the information content of the overall received codeword. CID turns out to be mathematically equivalent to ROVA and reveals a lower complexity approach to computing ROVA.

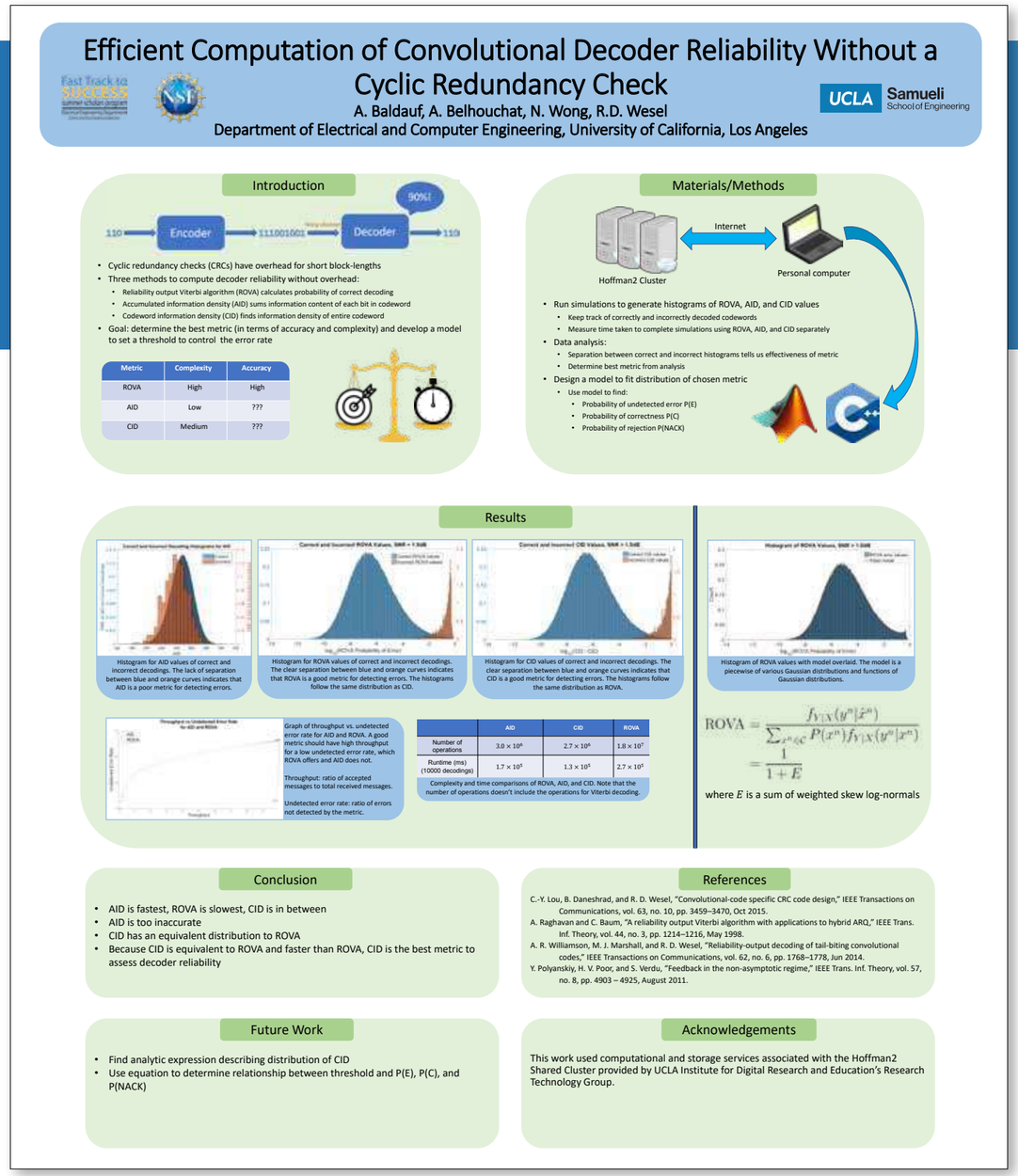

Vinya Bhuvan

Chemical Engineering

Junior

LAB NAME

Chen Lab

FACULTY ADVISOR

Yvonne Chen

DAILY LAB SUPERVISOR

Patrick Ho

DEPARTMENT

Chemical and Biomolecular Engineering

Developing a high-throughput screening platform to optimize intracellular target-dependent cytotoxic switches

Adoptive T-cell (ACT) therapy is a promising cancer therapy which uses engineered T cells to target tumor cells based on extracellular signatures. However, its dependence on extracellular markers which are rarely unique to tumor cells limits its specificity and the scope of its application. Here, we propose to genetically fuse a T-cell cytotoxic molecule, granzyme B, to intracellular tumor marker-specific nanobodies to generate molecules called Cytoplasmic Oncoprotein VErifier and Response Triggers (COVERT) to reduce off-tumor toxicity in ACT. These molecules are designed to exhibit one of two target-dependent cytotoxic switch behaviors: activity exclusively in the presence of a marker unique to tumor cells or activity exclusively in the absence of a marker unique to healthy cells. Furthermore, since protein folding of individual variants is difficult to predict, we are developing a retroviral cytotoxicity assay (RVCA) to identify high-performing COVERT switches from a pool of variants. As proof of concept, we generated a library of 10^4 COVERT variants simultaneously using transposition cloning. EGFP-responsive clones were then isolated from a RVCA screen. Screening via RVCA resulted in an enrichment of forward, in-frame nanobody insertions and we hypothesize that next-generation DNA sequencing will reveal enrichment of COVERT variants that exhibit cytotoxic activity dependent upon the presence of EGFP. In the future, this strategy may be generalized to a wide variety of intracellular tumor markers to improve the specificity and safety of ACT.

Developing a high-throughput screening platform to optimize intracellular target-dependent cytotoxic switches

[1]Vinya Bhuvan, [1]Patrick Ho, [1]Yvonne Chen

[1]Department of Chemical and Biomolecular Engineering, University of California – Los Angeles

Improving the specificity of adoptive T-cell therapy

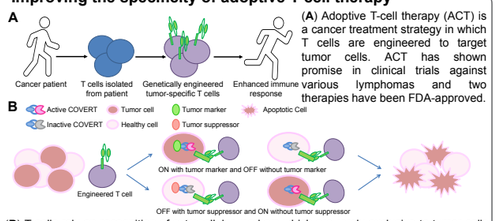

(**A**) Adoptive T-cell therapy (ACT) is a cancer treatment strategy in which T cells are engineered to target tumor cells. ACT has shown promise in clinical trials against various lymphomas and two therapies have been FDA-approved.

(**B**) T cells rely on recognition of extracellular markers which are rarely exclusive to tumor cells making ACT prone to misidentifying healthy tissue. To increase the specificity of ACT, we propose to develop cytotoxic switch proteins termed Cytoplasmic Oncoprotein VErifier and Response Triggers (COVERT), which can be delivered by engineered T cells to selectively kill tumor cells that either express an intracellular tumor marker or lack expression of an intracellular tumor suppressor.

Generating a diverse library of COVERT variants

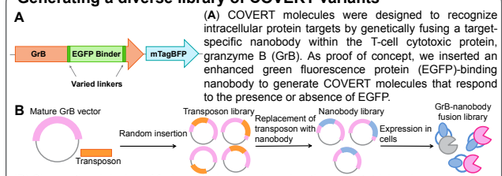

(**A**) COVERT molecules were designed to recognize intracellular protein targets by genetically fusing a target-specific nanobody within the T-cell cytotoxic protein, granzyme B (GrB). As proof of concept, we inserted an enhanced green fluorescence protein (EGFP)-binding nanobody to generate COVERT molecules that respond to the presence or absence of EGFP.

(**B**) Since rational design of fusion proteins remains a low-throughput, trial-and-error process, a library of 10^4 variants was simultaneously generated via transposition cloning to insert an EGFP-binding nanobody into random sites in the mature GrB sequence.

Transposition cloning yields an unbiased library of nanobody insertion variants

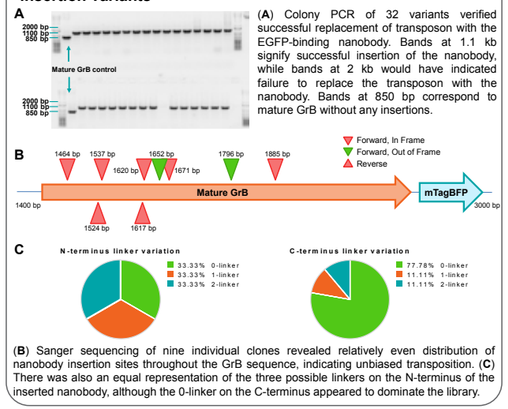

(**A**) Colony PCR of 32 variants verified successful replacement of transposon with the EGFP-binding nanobody. Bands at 1.1 kb signify successful insertion of the nanobody, while bands at 2 kb would have indicated failure to replace the transposon with the nanobody. Bands at 850 bp correspond to mature GrB without any insertions.

(**B**) Sanger sequencing of nine individual clones revealed relatively even distribution of nanobody insertion sites throughout the GrB sequence, indicating unbiased transposition. (**C**) There was also an equal representation of the three possible linkers on the N-terminus of the inserted nanobody, although the 0-linker on the C-terminus appeared to dominate the library.

High-throughput screening to isolate high performing variants

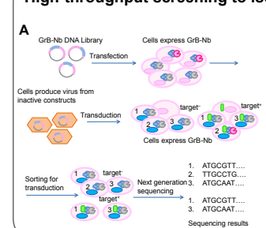

(**A**) A retroviral cytotoxicity assay (RVCA) was developed to screen the library for cytotoxic switch behavior. Retrovirus was produced in either target$^+$ (EGFP$^+$) or target$^-$ cells. Both target$^+$ and target$^-$ cells were transduced and sorted to enrich for in-frame insertions. Due to the cytotoxic behavior of active variants, we anticipate that comparison of the surviving variants from both transduced populations by next-generation DNA sequencing may reveal enrichment of EGFP-responsive switches. We hypothesize that multiple rounds of screening may reveal greater enrichment of functional variants.

RVCA results in an enrichment of productive constructs

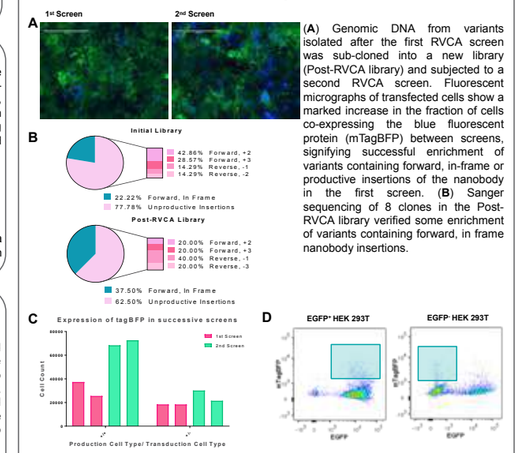

(**A**) Genomic DNA from variants isolated after the first RVCA screen was sub-cloned into a new library (Post-RVCA library) and subjected to a second RVCA screen. Fluorescent micrographs of transfected cells show a marked increase in the fraction of cells co-expressing the blue fluorescent protein (mTagBFP) between screens, signifying successful enrichment of variants containing forward, in-frame or productive insertions of the nanobody in the first screen. (**B**) Sanger sequencing of 8 clones in the Post-RVCA library verified some enrichment of variants containing forward, in frame nanobody insertions.

(**C**) We observed an greater increase in the number of mTagBFP$^+$ cells isolated from EGFP$^+$ cells than EGFP$^-$ cells between the first and second screens, suggesting possible enrichment of variants that are inactivated by EGFP. (**D**) Representative fluorescence dot plots of EGFP$^+$ and EGFP$^-$ cells before sorting. Turquoise boxes indicate gates for sorting.

Conclusions and future work

We developed a novel RVCA screening platform that may enrich COVERT sequences containing productive insertions of the EGFP-specific nanobody. We anticipate that next-generation DNA sequencing will reveal an enrichment of high functioning cytotoxic switches. Future work will include the application of transposition cloning and RVCA to a variety of clinically relevant tumor markers and suppressors to improve the specificity and safety of adoptive T-cell therapy

This work was supported by the National Science Foundation (CBET 1533767). V.B. is supported by an REU supplement to CBET 153767. P.H. is supported by the NIH Biotechnology Training in Biomedical Sciences and Engineering Program (T32 GM067555). V.B. is participating in the Summer Undergraduate Scholars Program at the Henry Samueli School of Engineering at UCLA.

Nathan Chen

Electrical Engineering

Sophomore

LAB NAME

Interconnected and Integrated Bioelectrics Laboratory

FACULTY ADVISOR

Sam Emaminejad

DAILY LAB SUPERVISOR

Haisong Lin

DEPARTMENT

Electrical and Computer Engineering

In-Situ Biofluid Management by Magnetic Field for Lab on the Body Application

Sweat biomarker sensing and general biofluid management has been a topic of research for years, yet limited applications have been investigated for actively controlling sweat droplets. Our group experiments with electric and magnetic actuation of sweat droplets to actively transport biofluids through wearable microfluidic channels, achieving a “lab on the body” platform for sweat glucose sensing. Conventional wearable sweat sensing platforms are inefficient and prone to contamination, as sweat is passively transported or the sensing area must be placed in direct contact with sweat on the skin. In comparison, our platform allows continual sensing over time through active sweat transport, while avoiding contamination by separating skin from the sensing area on the device. Our device prototype is capable of generating homogeneous sweat droplets (~600um diameter). This consistency of droplet sizes has the potential to allow controlled, specific concentrations of sweat to be actively transported by an array of electro-magnets on a printed circuit board we designed and analyzed by a sweat glucose sensor on the device. The results of the experiment demonstrate the efficacy of actively moving sweat from the body to the sensor, implicating future develop-ments in executing lab on a chip functions in a miniaturized, wearable, “lab on the body” platform.

Fernando Cruz

Computer Science

Sophomore

LAB NAME

Networked and Embedded Systems Lab

FACULTY ADVISOR

Mani Srivastava

DAILY LAB SUPERVISOR

Kevin Zhengxu Xia and Eun Sun Lee

DEPARTMENT

Electrical and Computer Engineering

Automated Grading of Embedded Systems Assignments, Version 2.0

Grading embedded system assignments requires time-consuming interaction between students and instructors because of the experimental setup that is only available in the laboratory. Previous work to address this problem includes EmbedInsight, a system which automates the grading cycle by allowing students to submit their codes to a server. Submissions are graded in a queue by the instructor's grading microcontroller board, which creates a long delay in feedback when many students upload code within a short period of time. We propose EmbedInsight Version 2.0, which provides distributed grading and user-friendly debugging features by giving a grading board to each student. The three components to this system are the website, a grading board, and a student board. This system establishes communication between the website and the grading board by using Google Chrome's WebUSB feature, while the grading board communicates with the student board through the use of General Purpose Input/Output pins. The grading board tests whether or not the student programmed their board to carry out specific instructions. The new website has several features such as buttons that send commands to the board and the ability to simulate an oscilloscope. The concept of this project expands the functionality of microcontrollers and could also be a very powerful tool for education. It would allow instructors to easily assign and grade embedded systems assignments at all levels of education, while also giving students a way to get more feedback to improve their learning experience.

Automated Grading of Embedded Systems Assignments, Version 2.0

Manuel Rivas, Fernando Cruz, Zhengxu Xia, Eun Sun Lee, Mani Srivastava

Department of Electrical and Computer Engineering,

University of California, Los Angeles

2018 Summer Undergraduate Scholars Program

Motivation

- Embedded systems are a combination of computer hardware and software that is designed for a specific function within a larger system
- Grading embedded system assignments requires one-to-one meeting in a designated time slot
- Extreme time investment required from instructors and students
- Debugging devices like oscilloscopes are only available in lab facilities

Oscilloscopes are used to debug and grade these assignments. We aim to provide a similar feature that is accessible from the web with our project.

Previous Work: EmbedInsight

- Automates grading cycle by allowing students to submit their codes to a server
- Grades submissions in a queue.
- Creates a long delay in feedback when many students upload code within a short period of time
- Uses only a limited number of testbeds

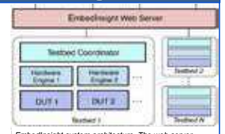

EmbedInsight system architecture. The web server communicates with multiple testbeds to grade multiple student's submissions

Introduction to EmbedInsight Version 2.0

- Provides a grading board to each student
  - Distributed grading
  - User-friendly debugging feature
- Our board communicates with the website using Google Chrome's WebUSB API
- Students' microcontroller board programmed as assigned
- Result read by the tester board through GPIO
- The tester microcontroller board facilitates communication between the browser and student board as well as the recording process

Student Board: NUCLEO-F746ZG

Tester Board: LPC1768

Example Assignment

- Example assignment: Timestamping Pulse Width Modulation (PWM) waves
- A PWM wave is an electric wave that alternates between "on" and "off"
- Dependent on two factors: period and duty cycle
- Period = time for one cycle
- Duty Cycle = (time on) / period

An example of a PWM wave that could be generated by a student's board.

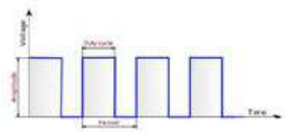

Overall Architecture

- The browser sends commands to the Tester Board, which sends signals to the Student Board
- The Student Board interprets the data as a period and duty cycle and generates a PWM wave
- The Tester Board measures the waveform coming from the Student Board and reports the data back to the browser
- The browser analyzes, grades, and then displays the data from the Tester Board

Results and Website

- Oscilloscope-like graphical user interface
- Graphs detected and expected waveform of the test case
- Displays grading feedback
- Other functions include turning lights on or off on the tester board
- Reliable and consistent communication between the 3 components

Conclusion and Future Work

Conclusion:

- Allow efficient distribution and grading of embedded systems assignments
- Improve students learning experience by providing user-friendly debugging features
- Give microcontrollers the capability of communicating with websites

Future Work:

- Record multiple signals simultaneously
- Flash grading algorithm directly to tester board via WebUSB
- Develop a user account system for students/instructors
- Test the current system with other types of assignments

Acknowledgements

University of California, Los Angeles (UCLA);

Networked and Embedded Systems Lab (NESL), UCLA;

Wireless Health Institute (WHI), UCLA

LAB NAME

Process and Control Lab

FACULTY ADVISOR

Vasilios Manousiouthakis

DAILY LAB SUPERVISOR

Masih Jorat

DEPARTMENT

Chemical and Biomolecular Engineering

Austin Cullen

Chemical Engineering

Senior

Sustainable Region Identification Algorithm for N-Dimensional Temporal Systems, Using the Novel Concept of Sustainability Over Sets

As defined by the American Institute of Chemical Engineering, Sustainability represents the path of continuous improvement over time. A word association game for the word “sustainably” would quickly generate as response the expression “forever”. Thus, it becomes apparent that to characterize a system as being sustainable, its behavior must be studied over an infinite period of time. Second, the inherent understanding associated with the word “sustainability” is that it provides an indication as to whether a system’s dynamic behavior meets some preconceived notions of what is acceptable. However, since such notions vary from person to person, the question “is a system sustainable or not?” may lead to different answers depending on who asks the question. Thus, to evolve this concept to the level of scientific scrutiny whereby the question receives always the same answer, independently of who asks the question, human input regarding what is deemed acceptable must be incorporated in the definition of sustainability. By including the mentioned criteria in the system sustainability definition, the article “Sustainability Over sets (SOS)” published by Jorat and Manousiouthakis (2017) defines a system to be sustainable over a chosen set if and only if its state remains within the set’s bounds for infinite time. For this definition to be practical a tool must exist capable of finding such invariant sustainable regions. In this work we present a computational algorithm that can identify sustainable sets in the state-space for N-dimensional systems. This evolution of the SOS concept can be efficiently applicable to a variety of systems regardless of their complexity in dimension and the selected criteria for their sustainability. To demonstrate the practical applicability of the developed algorithm, it identifies the sustainable nonconvex regions of multispecies systems.

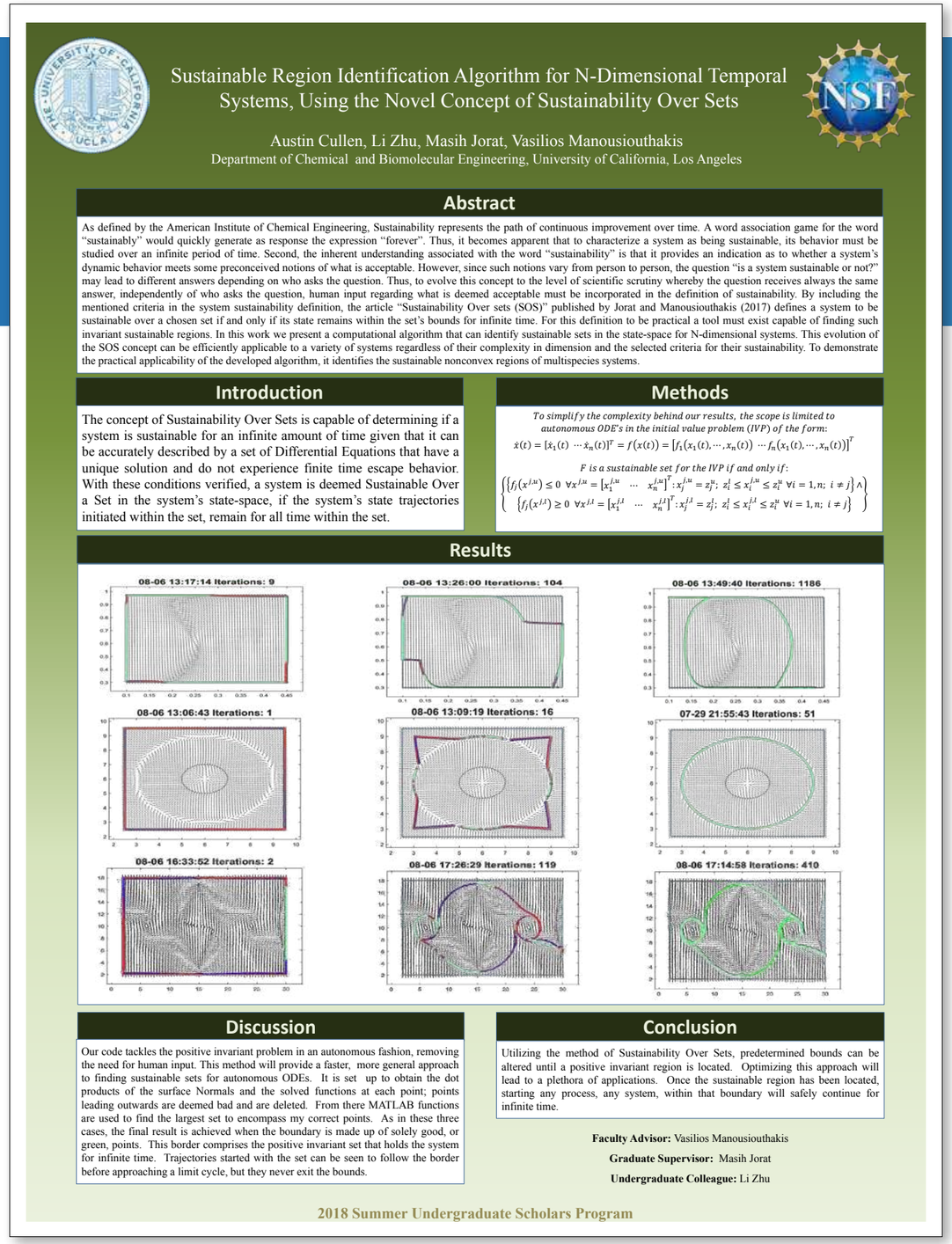

Kathy Daniels

Electrical Engineering

Sophomore

LAB NAME
ARNI

FACULTY ADVISOR
Christina Fragouli

DAILY LAB SUPERVISOR
Gaurav Agarwal

DEPARTMENT
Electrical and Computer Engineering

Exploring Secure Capacity for Communication in 1-2-1 Networks

Millimeter wave communication allows for very high data transfer rates; however, transmitting over large distances poses the issue of high information loss due to path loss. In order to minimize this path loss, we utilize beamforming, in which transmitting and receiving nodes align their antennae in order to establish a communication link. 1-2-1 networks serve as models for millimeter wave communication networks which use beamforming such that any intermediate node can only receive from and transmit to one node at a time. In our research, we analyze the secure capacity of these 1-2-1 networks in the presence of a passive adversary who has access to any K channels of her choice. Using the number of node and edge-disjoint paths of a network, we can calculate the lower and upper bounds on the secure capacity. For randomly generated graphs, we find and compare these capacity bounds with the rate achieved using a novel scheme. In our scheme, rather than starting with node-disjoint paths of a graph (which corresponds to the lower bound on capacity region), this scheme starts with edge-disjoint paths and maximizes path use while minimizing adversary access. Plotting the results of our scheme with upper and lower capacity bounds will allow us to analyze the specific network parameters that may yield a tighter lower bound.

UCLA Samueli School of Engineering | Summer Undergraduate Scholars Program

Fast Track to SUCCESS Summer Scholars Program — Electrical Engineering Department — UCLA Henry Samueli School of Engineering and Applied Science

Wireless Health UCLA

On Secure Capacity for Communication in 1-2-1 Networks

UCLA Department of Electrical and Computer Engineering

K. Daniels, N. Woo, G. Agarwal, C. Fragouli

NSF

Algorithmic Research in Network Information Flow (ARNI)

Millimeter Wave Communication

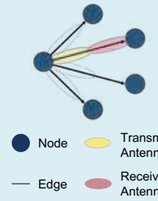

- Utilized in 5G wireless communication systems
- High frequency communication
- Large bandwidth, small components
- **Challenge**: Short range and physical barriers
- **Solution:** Utilize beamforming: two beams must align to establish a communication link

1-2-1 Network Model

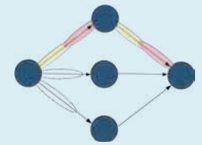

Example of a 1-2-1 Network

- Models millimeter wave communication
- Unit capacity edges
- Each node can point its transmitting/receiving beam to at most one node
- Source: can transmit to at most M nodes
- Destination: can receive from at most M nodes

Unsecure Capacity

- Unsecure capacity: Maximum flow in the absence of adversary

$$C_u = \min(M, H_e)$$

M = number of antennae on source node
H_e = # of edge disjoint paths

Secure Capacity Bounds

- Secure capacity = # of information packets that can be sent given adversary has access to any K edges
- Secure capacity of the network is between the following bounds:
  - H_v = # of vertex disjoint paths
  - M = number of antennae on source node
  - H_e = # of edge disjoint paths
- Upper Bound: $H = \min(M, H_e)\left(1 - \frac{K}{H_e}\right)$
- Lower Bound: $L = \min(M, H_v)\left(1 - \frac{K}{H_v}\right)$

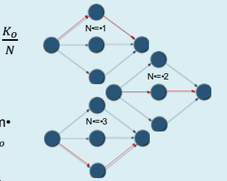

Arbitrary Network Graph

$H_e = 3 \rightarrow H = \min(1,3)\left(1 - \frac{1}{3}\right) = \frac{2}{3}$

$H_v = 2 \rightarrow L = \min(1,2)\left(1 - \frac{1}{2}\right) = \frac{1}{2}$

$$L \leq Secure\ Rate \leq H$$

Approximating Tighter Lower Bound on Secure Capacity

- The secure flow rate for any graph is given by: $R = \frac{(M*N)-K_o}{N} = M - \frac{K_o}{N}$

N = number of times network is used
K_o = number of symbols intercepted by adversary on her K channels

- We must choose paths of traversal from source to destination such that either K_o is minimized or N is maximized
- Continuously alternate paths such that adversary is severely limited

Given:
M<=1, K<=1
Secure Rate = $1 - \frac{1}{3} = \frac{2}{3}$

Scheme for Choosing Optimal Paths

Bin-Choosing Scheme

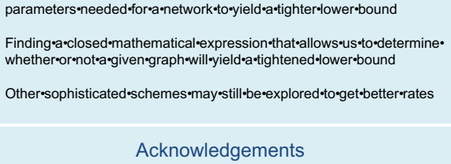

*Relates to complexity of graph

1. Group all edge disjoint paths into node disjoint bins
2. Choose paths from M different bins every iteration, always starting with the biggest bins
3. If there are any leftover paths left, use them if doing so will generate a greater overall rate

Conclusions and Future Work

- We observed that scheme 1 was able to yield a rate better than the lower bound in some cases
- Further generalizations can be made regarding the specific parameters needed for a network to yield a tighter lower bound
- Finding a closed mathematical expression that allows us to determine whether or not a given graph will yield a tightened lower bound
- Other sophisticated schemes may still be explored to get better rates

Acknowledgements

We would like to thank the Summer Undergraduate Scholars Program, the UCLA Electrical and Computer Engineering Department, Professor Christina Fragouli, and Gaurav Agarwal for their continuous guidance and for this opportunity to explore research in the field of network security.

LAB NAME
LEMUR

FACULTY ADVISOR
Akur Mehta

DAILY LAB SUPERVISOR
Wenzhong Yan

DEPARTMENT
Electrical and Computer Engineering

Emily Evans

Mechanial Engineering

Sophomore

STEM Education Revolutionized with Paper Robots

As the number of robots has been increasing in the world, so has their presence in our daily lives. Students are getting exposed to robotics from a younger age and some classes have even started using it as a tool for learning. However, these robots are quite expensive and challenging to make. Our lab has developed a design environment that generates a 2D pattern that an average user can print, cut, and fold to make a 3D structure for a robot. We aim to use this cheap and easy method of fabricating robots to teach middle school students a plethora of math and science topics. We have created robot designs of varying difficulty levels and built them ourselves. We have also developed lesson plans highlighting exciting activities that connect these robots to STEM concepts. We will test these lesson plans on middle school students and enhance them based on the results. This will give us a clear idea about their skill level, curiosity for learning, and what we should deliver accordingly. In using robots to teach math and science, students will be more engaged and interested in the topic as they will be learning by doing. Integrating simple and inexpensive robots into the classroom at an earlier age will give young students a fun introduction to the world of robotics.

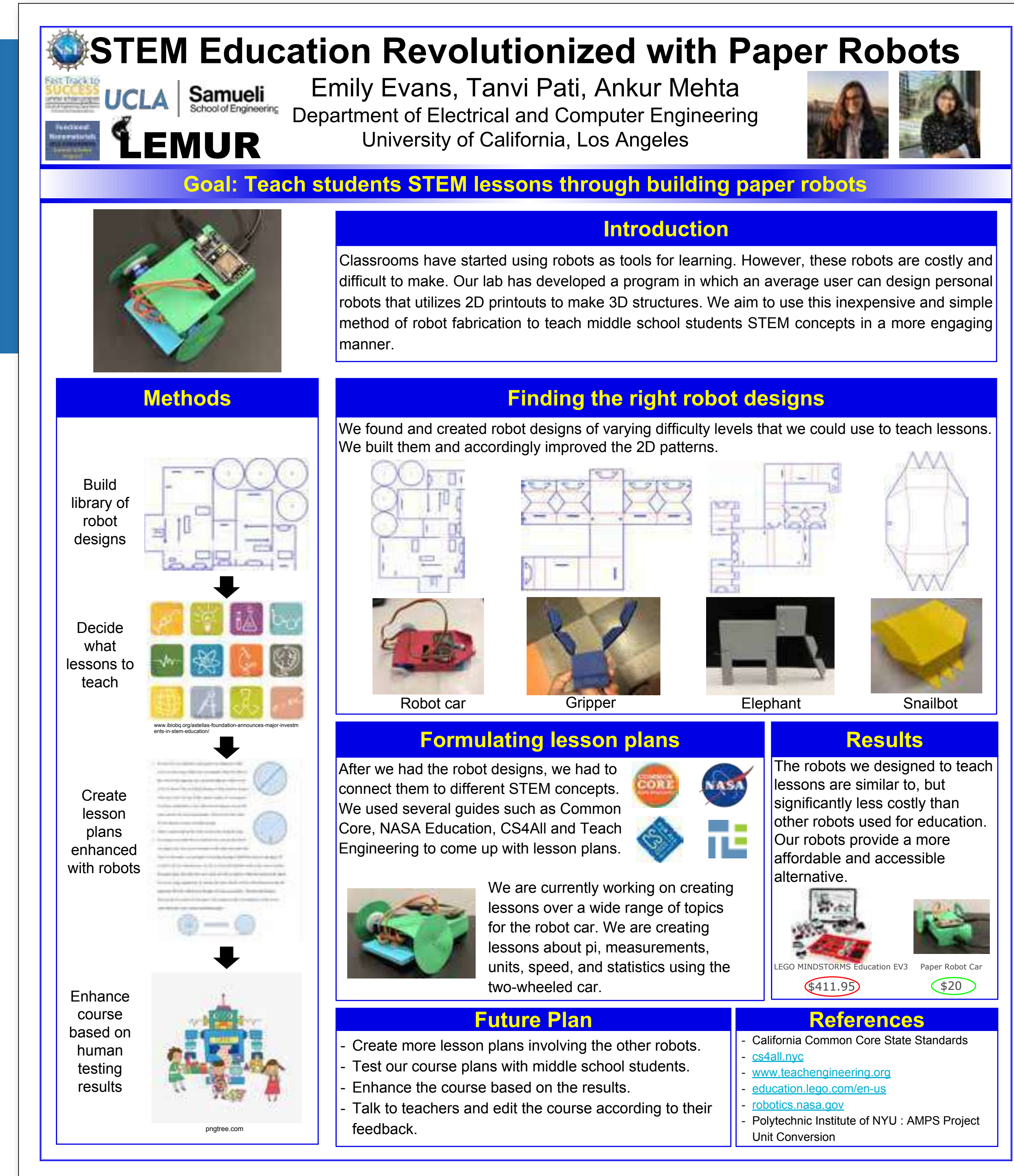

Honor Fisher

Civil Engineering

Sophomore

LAB NAME

Geotechnical Engineering Research Lab

FACULTY ADVISOR

Scott J. Brandenberg

DAILY LAB SUPERVISOR

Paolo Zimmaro

DEPARTMENT

Civil and Environmental Engineering

Data Analysis Tools for the Next-Generation Liquefaction (NGL) Case-History Database

Soil liquefaction is a major cause of damage to structures, infrastructure, and lifelines during strong earthquakes. This phenomenon occurs when saturated sand loses substantial strength due to seismically induced pore pressure increase. Liquefaction triggering models are heavily reliant on data as they are typically developed using empirical or semi-empirical procedures. Current models often provide different outcomes in predicting liquefaction due to inconsistent and incomplete data sets, different methods of data interpretation, and potential errors in data analysis. Additionally, traditional spreadsheets hinder the processing of such massive data sets and unnecessarily incorporate repeated information. The Next-Generation Liquefaction (NGL) database is an open-source resource designed to store and organize liquefaction case-histories. A case-history in NGL comprises three components: (1) earthquake event, (2) geotechnical site characterization, and (3) post-earthquake observation. The NGL database will constitute a platform for researchers and practitioners to share soil liquefaction information, eliminating the repetitive nature of traditional data collections and condensing important information into readable tables and figures. We produced post-processing and data analysis tools for the NGL database using python with jupyter notebook. Our tools can be used to create interactive maps of geotechnical investigation data and earthquake events. Such maps directly interact with the NGL database and include charts and information relevant to each test. We also developed tools to perform liquefaction triggering analysis based on field investigation results. We envision that the civil engineering community will utilize the NGL case history database and associated data analysis tools to produce improved prediction models and broaden the understanding of liquefaction-related phenomena.

Data Analysis Tools for the Next-Generation Liquefaction (NGL) Case History Database

Honor Fisher, Allison Lee, Paolo Zimmaro, Scott J. Brandenberg

Department of Civil and Environmental Engineering; *University of California, Los Angeles*

2018 Summer Undergraduate Scholars Program

Soil Liquefaction:

Liquefaction describes the phenomenon that occurs when saturated deposits of loose sand lose substantial strength due to pore pressure increase during an earthquake and can cause sinkholes, soil ejecta, lateral spreading, and damage to buildings, lifelines, and infrastructure.

Figure 1: Soil Liquefaction, Niigata Earthquake (NOAA/NGDC, 1964)

An earthquake induced the liquefaction of the soil beneath the foundation of these buildings. As a result, some structures were tilted dramatically, and others were completely overturned.

Figure 2: Soil Liquefaction Analysis (Sutherland, 2017)

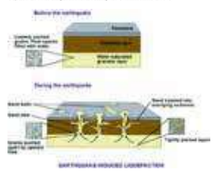

This image gives a cross-sectional view of the complex soil liquefaction, depicting how earthquakes cause saturated loose soil to eject and seep onto the surface.

Current Issues:

- Liquefaction triggering models are empirical or semi-empirical
- Alternate liquefaction models provide different outcomes
- Small, incomplete, and inconsistent data sets
- Potential errors in data analysis
- Different methods for data interpretation and extrapolation beyond data range
- Lack of communication between researchers

Figure 3: Current Discrepancies in Prediction Models (Idriss and Boulanger, 2010)

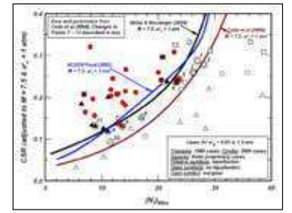

The variance in these liquefaction prediction models stresses the need for collaboration among modelers to produce improved prediction models based on an updated and larger case history database.

Next-Generation Liquefaction Relational Database

Relational Database:

A structured body of interrelated condensed tables connected by keys. The following gives an example of how tables relate to each other.

Table 1: Earthquake Event Table (Brandenberg et al., 2018)

This table consolidates the earthquake name and magnitude.

Table 2: Recording Station Table (Brandenberg et al., 2018)

This table consolidates the recording station name and time-averaged shear wave velocity in the upper 30 meters.

Compared to Traditional Spreadsheets, a Relational Database:

- Eliminates unnecessary repetition
- Avoids null fields
- Enforces data format consistent with parameter (INT, CHAR, BOOL)
- Enables data to be queried
- Allows development of post-processing tools

Table 3: Ground Motion Table (Brandenberg et al., 2018)

The IDs relate the respective information and minimize repetition in reporting information recorded by each station for each earthquake in this hypothetical scenario.

NGL Project:

The multi-year research project aims to develop a relational database to collect high-quality liquefaction case histories worldwide.

A **case history** comprises of three components:
1. Earthquake events
2. Site characterizations
3. Post-earthquake observations

Primary Key Foreign Key

Figure 4: Tables from NGL Database Schema (Brandenberg et al., 2018)

This subset of tables collect site characterization data from the Next-Generation Liquefaction database. These are the parameters of borehole, standard penetration, and cone penetration test data.

Data Organization and Analysis Tools

NGL Post-Processing Tools:

We developed the following tools to organize and present information from the database:
- Interactive map that queries information from relational database
- Plots of test data
- Markers to represent test and earthquake sites

Software Development:

We used the following systems for the tool development.
- Anaconda (Python distribution)
- Jupyter Notebook
- MAMP
- MySQL Workbench
- Folium

Figure 6: CPT Test Popup

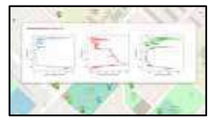

Blue markers indicate soil information from Cone Penetration Test through charts plotting cone tip resistance, sleeve friction resistance, and pore water pressure at various depths.

Figure 7: Earthquake Popup

Beachballs summarize the earthquake event mechanism. Information about the earthquake is displayed when the marker is clicked.

Figure 8: SPT Test Popup

Green markers indicate the location of a Standard Penetration Test, and their popups display the site name and chart of number of blow counts at various depth intervals.

Conclusions:

A more accurate model of predicting ground failure can be produced through this relational database, and the model become more precise as more researchers upload their work. Moving forward, we will develop tools to analyze the recorded data and produce triggering models for liquefaction. It is our hope that Civil and Geotechnical Engineers can use the NGL website to broaden the understanding of the liquefaction phenomenon.

Acknowledgements:
We would like to thank and acknowledge Scott J. Brandenberg and Paolo Zimmaro for teaching us about soil liquefaction, welcoming us into their lab, and taking steps to improve data sharing in geotechnical engineering. We would also like to acknowledge the UCLA Summer Undergraduate Scholars Program for giving us this opportunity to understand the various depths of the world of research.

References:
- NOAA/NGDC (1964). *NOAA National Geophysical Data Center.*
- Sutherland, S. (2017). "Japanese Structural Seismic Risk Prevention Techniques & Its Potential Performance in the Caribbean", *School of Architecture Urban Planning and Construction Engineering Academic Year 2016/2017.*
- Idriss, I.M. and Boulanger, R.W. (2010). *SPT-Based Liquefaction Triggering Procedures.* Center for Geotechnical Modeling
- Brandenberg, S. et al. (2018). "Next-Generation Liquefaction (NGL) Case History Database Structure", *Geotechnical Earthquake Engineering and Soil Dynamics V GSP 290.* pp. 426-433

Brendan Galvin

Chemical Engineering

Junior

LAB NAME

Process and Control Lab

FACULTY ADVISOR

Vasilios Manousiouthakis

DAILY LAB SUPERVISOR

Masih Jorat

DEPARTMENT

Chemical and Biomolecular Engineering

Sustainability Analysis of Infinite Dimensional Spatiotemporal Systems Through the Novel Concept of Sustainability over Sets

The notion of Sustainability is a loosely defined concept that can be interpreted to fit the desires of those accessing it. Historically, the word "sustainable" had conveyed the meaning of "bearable" or "defensible". The modern definition of sustainability consists of three fundamental dimensions, environmental, social, and economic, called the three pillars of sustainability. Different definitions of sustainability have been obtained focusing on harmonizing the interactions of these dimensions i.e. "sustainability is a wise balance among economic development, environmental stewardship, and social equity" (Sikdar). Moving towards the application of sustainability requires tools to be developed that are readily capable of determining the sustainability status of a system over time. In this regard, the article "Sustainability over Sets (SOS)" published by Jorat and Manousiouthakis (2017), mathematically formalized the incorporation of human input into the sustainability assessment process thus enabling definitive (yes or no) answers to the question "is a system sustainable?". SOS deems systems to be sustainable over a defined set in the system's state-space, if the system's trajectories initiated within that set, remain in it for all time. The previously presented studies of the (SOS) concept were limited to sustainability assessments of systems, whose behavior is modeled through a set of ordinary differential equations (ODEs). In this work a developed version of the SOS concept is presented which has the ability to assess the sustainability of infinite dimensional systems whose dynamic behavior has been captured by a system of Partial Differential Equations (PDEs). In this regard we present necessary and sufficient conditions for sustainability of systems, whose behavior is captured by parabolic and hyperbolic PDEs, commonly arising in chemical engineering, ecological, economic, and social applications. Furthermore, the practical applicability of the introduced conditions will be demonstrated through analysis of the population dynamics of a multi species system.

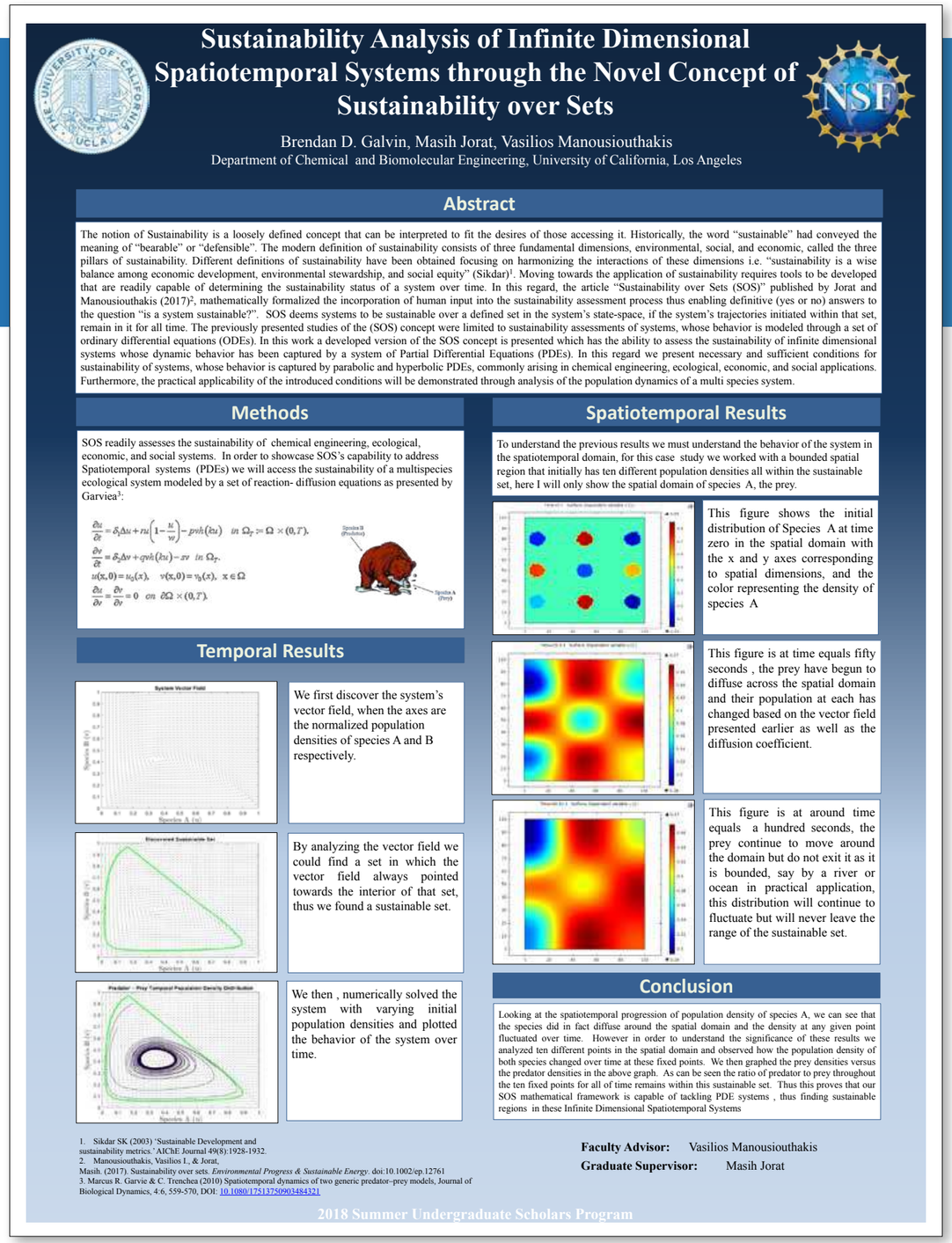

LAB NAME

Cognitive Reconfigurable Embedded Systems Lab

FACULTY ADVISOR

Danijela Cabric

DAILY LAB SUPERVISOR

Samer Hanna

DEPARTMENT

Electrical and Computer Engineering

Benjamin He

Electrical Engineering

Sophomore

RSSI-based Localization of IoT Devices Using Machine Learning Approaches

The Internet of Things (IoT), the idea of having all devices connected to the internet and to each other, is becoming increasingly prevalent in the modern world. IoT has countless applications including smart homes and intelligent traffic management. Beyond everyday applications, they can extend to military surveillance and natural habitat monitoring, among others. In many of those applications, it is important to find the location of a device in the IoT network. This can be accomplished with wireless network localization. In our project, we explore the feasibility of using machine learning methods--namely, support vector machines (SVM) and a neural network (NN)--to perform passive, cooperative network localization. Both localization algorithms use received signal strength indication (RSSI) values as their inputs, thus making the localization range-free. In the proposed SVM-based algorithm, the localization area is divided into halves recursively. A binary tree of SVMs is trained over these divisions, which is then used to determine the position of each test point based on their RSSI values. For the proposed NN-based algorithm, we train a multilayer perceptron with a training set consisting of each point's location and RSSI values. To localize each test point, its RSSI values are fed to the trained neural network which computes the estimated coordinates of the point. The accuracies of both algorithms are evaluated using the error calculated from the differences between the test data's predicted versus actual positions. The performances of these algorithms are also compared to the theoretical limits from model-based network localization methods.

RSSI-Based Localization of IoT Devices Using Machine Learning Approaches

Benjamin He, Yan Han, Samer Hanna, Danijela Cabric

Summer Undergraduate Scholars Program

Introduction

The Internet of Things (IoT) is the idea of connecting all devices to the internet and each other. Interest in this idea has been rapidly growing in recent years due to the countless applications it provides including:

- Smart homes & architecture
- Intelligent traffic management
- Military surveillance
- Natural habitat monitoring
- Precision agriculture
- Industrial process control

In many of these applications, it is important to locate the position of a particular device in the IoT network. This can be done using wireless network localization, which is the focus of this project.

- Range-free network localization often utilizes **received signal strength indicator (RSSI)**, which is a measure of the power of a device's received signal from another device.
  - Commonly used as the input for range-free localization in wireless networks.
- **Anchor nodes**, devices already aware of their position, are used as reference points for unknown devices to receive RSSI values from in order to localize that unknown device.
- However, there is often a lot of noise in RSSI measurements due to the environment.
  - **Support vector machines (SVM)** or **neural networks (NN)** are machine learning algorithms that may provide effective solutions for minimizing that noise for more accurate IoT localization.

Goal

To evaluate the feasibility of using machine learning methods--SVMs and NNs—for localization within an IoT wireless network for potential use in real-world applications.

Simulation Set-up

- Both machine learning localization algorithms are tested in MATLAB simulations (Figure 1):
  - Square **20 x 20 m²** area
  - **1 anchor node in each corner** of the area
- Data points are randomly generated within the localization area (blue circles in Figure 1).
  - These data points consist of their **locations** and their **RSSI values**.
  - **80%** of points used for **training** the algorithms
  - **20%** used for **testing** the trained algorithms.

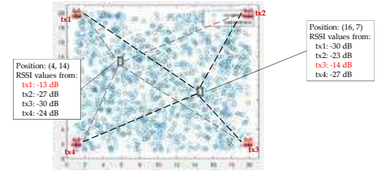

Figure 1

SVM-based Algorithm

- Using the training points, SVMs are recursively trained to **divide the localization area into halves** in x and y directions until the desired number of SVMs are obtained (Figure 2).

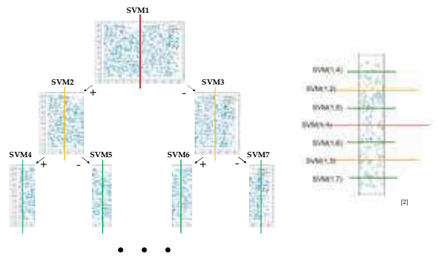

Figure 2

- Once all SVMs are trained, test points are localized by traversing a **binary search tree of the SVMs** (Figure 3) for both x and y directions until arrival at a leaf of the tree, which will indicate the respective estimated x and y coordinates of the test point.

NN-based Algorithm

- Neural networks operate by taking in **inputs**, **multiplying** those inputs with their respective **path weights** (indicated by the lines in the Figure 4), **summing** those products, then putting that sum into a function called a **transfer function** to produce the value of a node in the **next layer**.
- The training points are fed to a neural network called a **multilayer perceptron (MLP)** and a **backpropagation algorithm** is used to adjust the network path weights (θ).
  - Two multilayer perceptrons are tested—one with a **single hidden layer**, and one with **two hidden layers** (single hidden layer example shown below in Figure 4).
  - The transfer function for each hidden layer(t1) is **tanh** and the transfer function for the output layer (t2) is **purelin** because this MLP is performing a **regression** task.

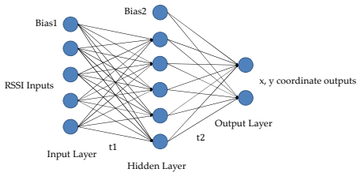

Figure 4

$$t1(input1, input2, input3, input4) = \tanh(\theta_{1,1} * input1 + \theta_{2,1} * input2 + \theta_{3,1} * input3 + \theta_{4,1} * input4 + \theta_{5,1} * Bias1)$$

$$t2(hid1, hid2, hid3, hid4, hid5) = \theta_{1,2} * hid1 + \theta_{2,2} * hid2 + \theta_{3,2} * hid3 + \theta_{4,2} * hid4 + \theta_{5,2} * hid5 + \theta_{6,2} * Bias2$$

- To localize test data, each test point's RSSI values are simply fed to the trained neural network, and the network calculates and outputs its estimated x and y coordinates.

Results & Discussion (In Progress)

Figure 5

- The **number** and **layout of anchor nodes** does not seem to significantly affect the performance of the SVM-based localization algorithm.

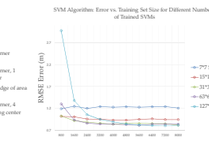

Figure 6

- Overall, **larger training sets** and **more trained SVMs** produce **the best performance**.
- However, a **small training set** with a **large number of SVMs** suffer **significant error** due to the inability for all the SVMs to be trained properly.

Preliminary Conclusions & Future Work

- The SVM-based algorithm reached an accuracy of approximately **0.8 m in a 20 x 20 m² area**, but significantly more work must be done before any solid conclusions can be drawn.
- Increasing the number of SVMs improves the localization accuracy of the algorithm, given a sufficiently large training set.

- More testing will be done on the proposed SVM-based localization algorithm.
- The proposed NN-based localization algorithm will also be developed and evaluated.
- These two algorithms will also be compared to other model-based wireless network localization methods.

Acknowledgements

I would like to thank the CORES Lab, the Summer Undergraduate Scholars Program, the UCLA EE Fast Track Program, and the UCLA Electrical & Computer Engineering Department for providing this valuable summer research opportunity for me.

References

[1] Y. Han, S. Chaudhari, D. Cabric, "RSSI-Based Localization in Wireless Sensor Network Using Support Vector Machines," in 2018 ECE Annual Research Review. 2018.

[2] A. A. Abdallah, S. Saab, Z. M. Kassas, "A machine learning approach for localization in cellular environments," in 2018 IEEE/ION Position, Location, and Navigation Symposium. IEEE 2018. IEEE Conference on, Apr. 2018.

Erik Hodges

Electrical Engineering

Senior

LAB NAME

Sensors and Technology Laboratory

FACULTY ADVISOR

Rob Candler

DAILY LAB SUPERVISOR

Jimmy Wu

DEPARTMENT

Electrical and Computer Engineering

Millimeter-Scale Electroplated Conformal Magnetic Shields

Recent advances in small-scale manufacturing have allowed for the fabrication of chip-scale atomic clocks. Portable atomic clocks have important applications. It is theoretically possible to perfectly track an object's position using an accelerometer if given the object's initial position and velocity. However, inadequately precise timekeeping makes this unrealizable in practice. Incorporating atomic clocks into mobile phones would allow for GPS-like tracking without sustaining battery draining communication with satellites. This technology will also enable precise positional tracking in caves and other places with no GPS access. However, atomic devices are highly sensitive to external magnetic fields, and current machining techniques used for magnetic shield fabrication are unable to cheaply produce small magnetic shields. It has also been mathematically and experimentally proven that multilayered magnetic shields are more effective than single layer shields of the same total thickness, but small multilayered shields are even more difficult to machine. Additionally, conventional machining is not capable of producing shields of complex geometries. We will fabricate shields by electroplating alternating layers of permalloy and copper onto a 3D printed mold. This method allows us to form thin, even layers of metal over any arbitrary geometry. Through COMSOL simulations, we determined that we can achieve an optimal longitudinal shielding factor of 3047 by electroplating a 2 layer shield of 500 µm total thickness. We will verify the shielding factor by applying a known magnetic field using an electromagnet and measuring the field inside the shield using a small magnetic sensor mounted on a flexible PCB.

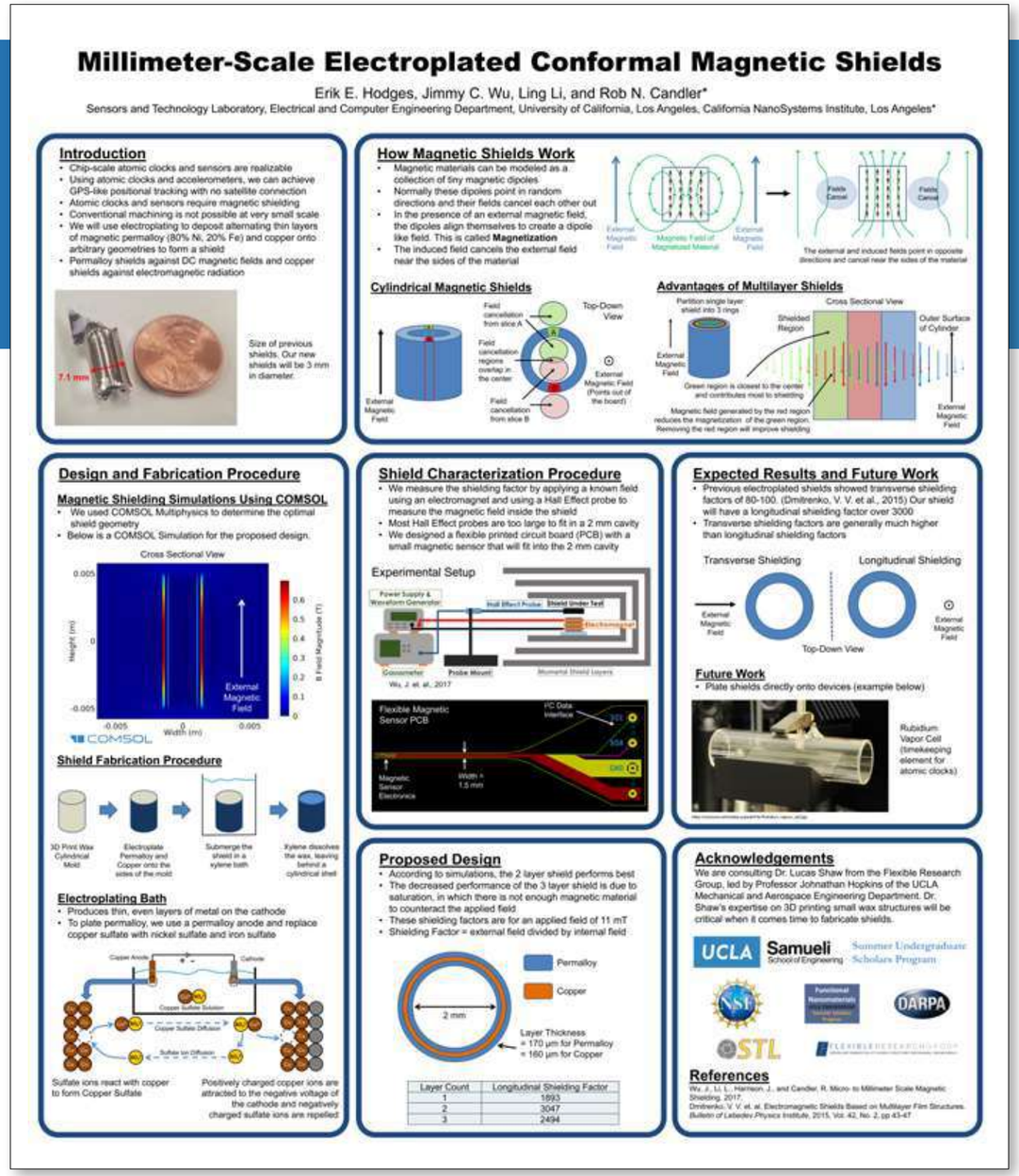

Donya Khashayar

Bio Medical Engineering

Junior

LAB NAME

Meyer Lab

FACULTY ADVISOR

Aaron Meyer

DAILY LAB SUPERVISOR

Song Yi Bae

DEPARTMENT

Bioengineering

Applying quantitative cell death measurements in evaluation of cancer cell drug response

Cancer treatments are not wide comprehensive and may not benefit one cancer patient as they do another. Despite significant development of therapeutics, some cancer cells persist even after treatment. In tumors, there are population of cells that are responsive to a drug and cells that are resistance to it. Therefore, the study of combination treatments can present more effective therapies for cancer. The quantification of drug response is essential in the development of therapeutics and the determination of cancer cell sensitivity and resistance. This is commonly evaluated by counting the number of live cells after compound treatment for certain amount of time. However, this method overlooks other phenotypic changes in cells such as cell growth and types of cell death. These details have important consequences on the immunological response in vivo and the arouse of resistance. Here, we suggest to quantitatively measure cell death simultaneously with cell growth in kinetics to enhance the understanding and prediction of the cancer cell response to anticancer therapeutics as well as possible drug combinations. In our assay system, Annexin V is used as an indicator of earlyapoptosis and YOYO3 as non-apoptotic cell death, such as necroptosis, in compound treated cells. The cell responses to drugs are evaluated by changes in cell confluence, Annexin V and/or YOYO3-positive signals over time. The observed signals varied across drugs and changed upon addition of another drug. Comparing these detected changes in cell growth and death signal with effectiveness of combined treatments, including synergy, additive and antagonism, may explain the drug responses in association to drug mechanism and possible drug resistance mechanisms. Thus, taking cell death into account for assessing cell response to therapeutics will benefit in designing optimal drug combination strategies.

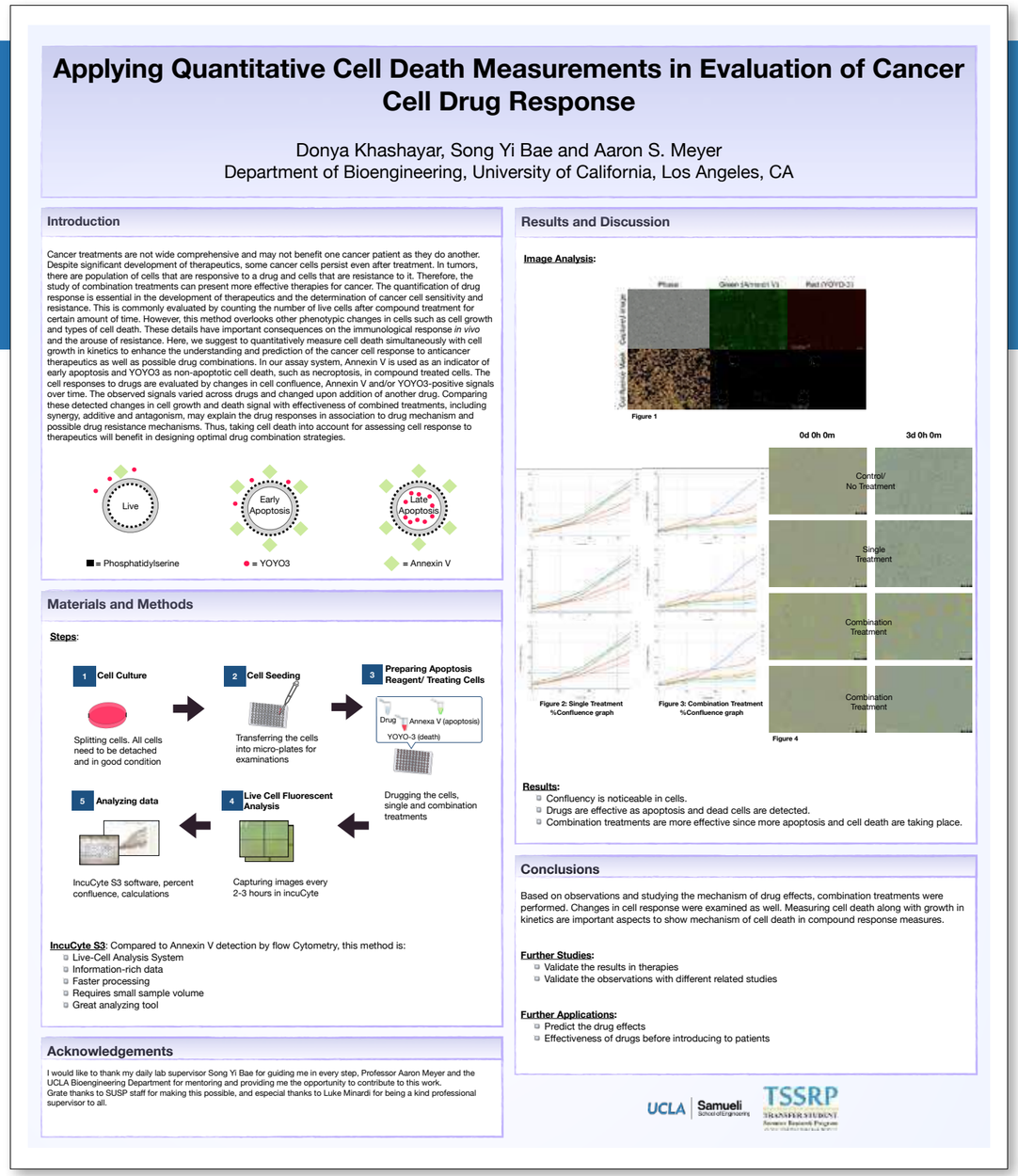

Applying Quantitative Cell Death Measurements in Evaluation of Cancer Cell Drug Response

Donya Khashayar, Song Yi Bae and Aaron S. Meyer

Department of Bioengineering, University of California, Los Angeles, CA

Introduction

Cancer treatments are not wide comprehensive and may not benefit one cancer patient as they do another. Despite significant development of therapeutics, some cancer cells persist even after treatment. In tumors, there are population of cells that are responsive to a drug and cells that are resistance to it. Therefore, the study of combination treatments can present more effective therapies for cancer. The quantification of drug response is essential in the development of therapeutics and the determination of cancer cell sensitivity and resistance. This is commonly evaluated by counting the number of live cells after compound treatment for certain amount of time. However, this method overlooks other phenotypic changes in cells such as cell growth and types of cell death. These details have important consequences on the immunological response *in vivo* and the arouse of resistance. Here, we suggest to quantitatively measure cell death simultaneously with cell growth in kinetics to enhance the understanding and prediction of the cancer cell response to anticancer therapeutics as well as possible drug combinations. In our assay system, Annexin V is used as an indicator of early apoptosis and YOYO3 as non-apoptotic cell death, such as necroptosis, in compound treated cells. The cell responses to drugs are evaluated by changes in cell confluence, Annexin V and/or YOYO3-positive signals over time. The observed signals varied across drugs and changed upon addition of another drug. Comparing these detected changes in cell growth and death signal with effectiveness of combined treatments, including synergy, additive and antagonism, may explain the drug responses in association to drug mechanism and possible drug resistance mechanisms. Thus, taking cell death into account for assessing cell response to therapeutics will benefit in designing optimal drug combination strategies.

Materials and Methods

Steps:

IncuCyte S3: Compared to Annexin V detection by flow Cytometry, this method is:

- Live-Cell Analysis System
- Information-rich data
- Faster processing
- Requires small sample volume
- Great analyzing tool

Acknowledgements

I would like to thank my daily lab supervisor Song Yi Bae for guiding me in every step, Professor Aaron Meyer and the UCLA Bioengineering Department for mentoring and providing me the opportunity to contribute to this work.
Grate thanks to SUSP staff for making this possible, and especial thanks to Luke Minardi for being a kind professional supervisor to all.

Results and Discussion

Image Analysis:

Figure 1

Figure 2: Single Treatment %Confluence graph

Figure 3: Combination Treatment %Confluence graph

Figure 4

Results:

- Confluency is noticeable in cells.
- Drugs are effective as apoptosis and dead cells are detected.
- Combination treatments are more effective since more apoptosis and cell death are taking place.

Conclusions

Based on observations and studying the mechanism of drug effects, combination treatments were performed. Changes in cell response were examined as well. Measuring cell death along with growth in kinetics are important aspects to show mechanism of cell death in compound response measures.

Further Studies:

- Validate the results in therapies
- Validate the observations with different related studies

Further Applications:

- Predict the drug effects
- Effectiveness of drugs before introducing to patients

UCLA Samueli | TSSRP

Sarina Kiani

Aerospace Engineering

Junior

LAB NAME

Micro and Nano Manufacturing

FACULTY ADVISOR

CJ Kim

DAILY LAB SUPERVISOR

Ning Yu

DEPARTMENT

Mechanical and Aerospace Engineering

Visually Determining the Wetting States of Underwater Superhydrophobic Surface

The wetting states, i.e., wetted or dewetted, are generally understood to determine the success or failure of the superhydrophobic surfaces submerged in water for intended applications, such as drag reduction or antifouling. Often, however, the key for the success lies with “partial” wetting, i.e., between the fully wetted and fully dewetted state. Unfortunately, the methods currently available to distinguish the partial wetting, such as confocal microscopy, are not portable and generally not useful to study applications. The Micro and Nano Manufacturing Lab has proposed a simple method that may allow users to determine the partially wetted states simply by looking at the superhydrophobic surface under water. To help study this new approach, I have developed an experimental setup that allows viewing of an underwater sample with different azimuth and altitude angles. The setup has a vertical plate, where three underwater endoscope cameras are mounted in an arc-shaped arrangement to view the sample from three different altitudes. The setup also includes a horizontally rotating stage, where a superhydrophobic sample is mounted to allow viewing of its surface from different azimuth directions. To assure the accuracies, camera positionings are calibrated with the actual CCD views. The multiple cameras are crucial so that the data from multiple angles are collected simultaneous because the detailed wetting state changes quickly over time. Lastly, the experimental setup has been developed in a way to allow confocal microscopy as well so that the accuracy and reliability of our new approach can be confirmed. With the setup developed, we are performing experiments with superhydrophobic samples in a water tank with the goal of applying the technique for the drag reduction tests with a motorboat in sea water.

Determining the Wetting States of Underwater Superhydrophobic Surface

Sarina Kiani, Ning Yu, Professor Chang-Jing “CJ” Kim

Mechanical and Aerospace Engineering Department, University of California Los Angeles

Introduction:

The Effect of Wetting States of on Drag Reduction:

- “Partial” wetting, i.e., between the fully wetted and fully dewetted state, determines the success or failure of the superhydrophobic surfaces submerged in water for intended applications, such as drag reduction and antifouling. The current available methods to distinguish the partial wetting states, such as confocal microscopy, are not portable for large scale experiments.

Approach:

- The Micro and Nano Manufacturing Lab has proposed a simple method that allows users to determine the partially wetted states by an underwater camera setup.
- The experimental setup has been developed in a way to allow confocal microscopy as well so that the accuracy and reliability of our new approach can be confirmed.

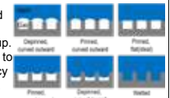

Figure a. Wetting States of Superhydrophobic Surface Under Water

Application:

- With the setup developed, experiments with superhydrophobic samples in a water tank are performed with the goal of applying the technique for the drag reduction tests with a motorboat in sea water.

Materials and Methods:

Camera Setup:

- The setup has a vertical plate, where three underwater endoscope cameras are mounted in an arc-shaped arrangement to view the sample from three different altitudes.
- The setup also includes a horizontally rotating stage, where a superhydrophobic sample is mounted to allow viewing of its surface from different azimuth directions.
- To assure the accuracies, camera positionings are calibrated with the actual CCD views.
- The multiple cameras are crucial so that the data from multiple angles are collected simultaneous

Camera Calibration → **Camera Setup, Water Tank, & Rotating Stage Construction** → **Simultaneous Data Collection With Confocal Microscopy**

Experimental Setup:

Figure b. Rotating Stage

Figure c. Camera Setup

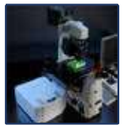

Figure d. Confocal Microscopy

Data collection with the prepared supersaturated and undersaturated water

Results and Discussion:

- **Camera Calibration Results:**
  - Camera One = 1.43 Degrees off center , Camera Two = 2.15 Degrees , Camera Three =0.95 Degrees

- **Superhydrophobic Wetting States For Undersaturated Water Results:**

Figure e.10 degree camera

Figure f. 20 degree camera

Figure g. 30 degree camera

- **Superhydrophobic Wetting States For Oversaturated Water Results:**

Figure h.10 degree camera

Figure i. 20 degree camera

Figure j. 30 degree camera

Conclusions:

The Application of the Collected Data:

The data collected by the camera setup allows the user to apply this technique on motorboat in sea water. The issue is not having enough collected data from various wetting states of superhydrophobic surface. To develop a more general technique, data must be collected from various wetting states.

Future Work:

Keeping the plastron from dissolution long enough for data collection is an issue. The next step is to develop a method to slow down the dissolution of air in water.

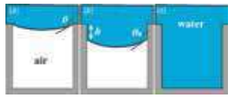

Figure k. Plastron Dissolution Diagram

Acknowledgments:

I would like to thank Professor CJ Kim and my DLS, Ning Yu, for allowing me to work in the lab and for helping me along the way. Great thanks to SUSP faculty, Luke Minardi, for being an understanding supervisor.

DARPA · NSF · TSSRP · UCLA Samueli School of Engineering

Keegan Kim

Chemical Engineering

Junior

LAB NAME

Process Control and Applied Mathematics Laboratory

FACULTY ADVISOR

Panagiotis Christofides

DAILY LAB SUPERVISOR

Roy Ding

DEPARTMENT

Chemical and Biomolecular Engineering

Optimizing Purge Times for PEALD of SiO2 Thin Films with Oxygen Plasma

As the microelectronic industry continues to move forward, new conformal deposition methods such as plasma-enhanced atomic layer deposition (PEALD) have been quickly adopted. However, sufficient control and monitoring of the process has lagged behind. Physical data gathering has proved impractical since the process requires extreme conditions within the reaction chamber. Multiscale computational fluid dynamic (CFD) models played a key role in the control of older deposition processes and it has been proven to be viable for PEALD as well in small scale tests. The deposition process requires a multiscale simulation that is modeled in two distinct domains: a macroscopic CFD model to capture the gas phase diffusion, and a microscopic kinetic Monte Carlo (kMC) film growth simulation that accounts for the atomic scale interactions of gases with the substrate material. With these two domains set up, they can interact through a set of dynamic boundary conditions where the two programs pass information between the macroscopic and microscopic phases. The precision of the mesh used in the macroscopic model and the complexity of the interactions occurring in it usually make the macroscopic domain the most computationally intensive part of the simulation to run. However, the use of a Bayesian artificial neural network (ANN) could make the process significantly more computationally efficient. This means that predictive control of PEALD systems could be attainable through this method, which would prove extremely useful for the microelectronics industry.

Optimizing Purge Times for PEALD of SiO_2 Thin Films with Oxygen Plasma

Keegan Kim[1], Yangyao Ding[1],
Yichi Zhang[1], Panagiotis D. Christofides[1,2]

[1] Department of Chemical and Biomolecular Engineering, University of California, Los Angeles
[2] Department of Electrical and Computer Engineering, University of California, Los Angeles

Motivation

Computer simulations proved to be the most viable method of controlling and monitoring reactions for the last generation of thin film growing techniques. However all current models for the more modern process of **plasma-enhanced atomic layer deposition (PEALD)** are either lacking realistic geometries or make very broad assumptions that limit the accuracy of the simulations. Simulations of the PEALD process could also help reveal some of the unknown causes of irregular film growth.

Fig. 1. Non uniform film growth is a major issue in the PEALD process. One of the main causes of film defects is incomplete purging in between precursor cycles, which leads to excess growth in locations where both precursors are present.

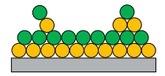

Our goal is to take the framework from the previous generation of simulations and update it with the new PEALD process. This would allow us to model the process more accurately than any current simulations and determine the most efficient conditions to run the reaction at.

Background Information

Our **plasma-enhanced atomic layer deposition** reaction consists of a cyclic process with four steps:

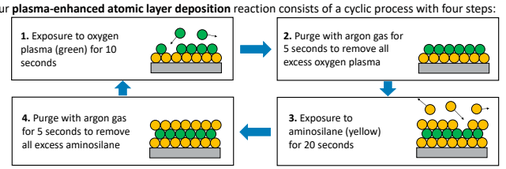

The process of alternating aminosilane and oxygen plasma (modeled by a 50:50 mixture of O_2 and O) causes them to react and form a thin film of silicon dioxide (SiO_2) layer by layer on the base material. This allows for extremely precise film thickness which is essential in today's microelectronic industry.

Materials and Methods

To model the PEALD process in ANSYS Fluent we must first construct the reactor geometry and write code to define the inlet flow rates, concentrations, and other conditions within the reactor.

The geometry of a PEALD reactor is designed in AutoCAD according to industry standards. Different reactor geometries can be tested to check for an optimal design.

ANSYS Meshing Editor is used to create a detailed grid for in interior of the reactor. A more detailed mesh gives more accurate results, but takes longer to run.

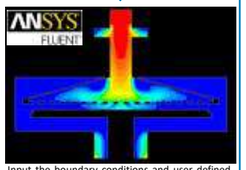

Input the boundary conditions and user defined functions into ANSYS Fluent simulations and set initial conditions.

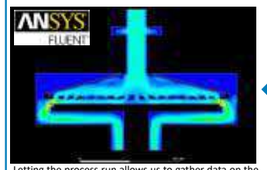

Letting the process run allows us to gather data on the dynamic flow of gases through the reactor and helps to visualize the process.

Results and Discussion

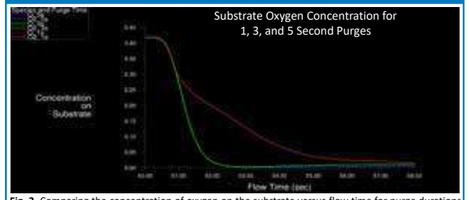

Fig. 2. Comparing the concentration of oxygen on the substrate versus flow time for purge durations of 1, 3, and 5 seconds. Only the 5 second purge lowers substrate oxygen concentrations to acceptable levels. The 3 second purge does not fully remove oxygen from the reactor. The 1 second purge removes minimal amounts of oxygen.

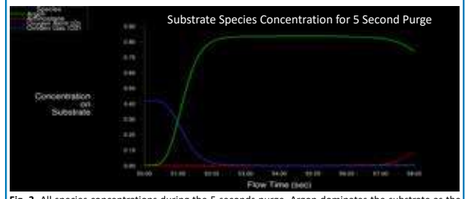

Fig. 3. All species concentrations during the 5 seconds purge. Argon dominates the substrate as the oxygen is removed to a safe level for processing to continue. Once aminosilane is present, less than 1% oxygen plasma remains on the substrate's surface.

Contours illustrating the successful 5 second purge are shown below

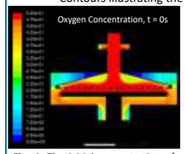

Fig. 4. The initial concentration of oxygen is shown after a 10 second exposure of oxygen plasma. The substrate is almost entirely covered by oxygen.

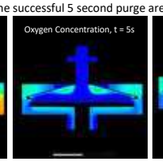

Fig. 5. After 5 seconds of exposure to argon, only small amounts of oxygen remain on the surface.

Fig. 6. The substrate is then exposed to 3 seconds of exposure to the second precursor. Almost no oxygen contacts the substrate.

Conclusions and Further Research

- An argon purge time of 5 seconds is required for this system to ensure that no oxygen is in contact with the substrate once aminosilane is present.
- Similar simulations can be run to determine the optimal reactor geometry, precursor concentrations, and other factors.
- Once integrated with our microscopic simulation we will be able to accurately model and optimize the entire PEALD process for SiO_2 film formation.

References

King, Sean. "Plasma Enhanced Atomic Layer Deposition of SiN:H and SiO_2." *Journal of Vacuum Science and Technology*, 24 May 2011, doi:10.1149/1.3485272.

Crose, Marquis, et al. "Multiscale Three-Dimensional CFD Modeling for PECVD of Amorphous Silicon Thin Films." *Computers & Chemical Engineering*, vol. 113, 14 Mar. 2018, pp. 184–195., doi:10.1016/j.compchemeng.2018.03.011.

Acknowledgements

Professor Panagiotis D. Christofides, Roy Ding, and the Process Control and Applied Mathematics Laboratory
UCLA Chemical and Biomolecular Engineering Department
UCLA Summer Undergraduate Scholars Program at the UCLA Henry Samueli School of Engineering and Applied Science
National Science Foundation REU Supplement

Michelle Lam

Electrical Engineering

Sophomore

LAB NAME

Digital Microwave Lab

FACULTY ADVISOR

Yuanxun Ethan Wang

DAILY LAB SUPERVISOR

Rustu Umut Tok

DEPARTMENT

Electrical and Computer Engineering

Magnetic Levitation System for Magnetic Pendulum Antenna to Reduce Mechanical Losses

Improved antenna efficiency is pertinent because it enables increased data transmission and enhanced signal strength, essentially translating into decreased production cost for bytes delivered. Mechanical antennas (Mechtennas) have been proposed to overcome the ohmic losses that accompany and limit the efficiency of conventional electrical antennas. Mechtennas radiate signals through a time-varying field that physically moves the electric charges in oscillations different from conventional electric antennas that accelerate charges via a current through a conductor. Physical movements overcome ohmic losses, so mechanical antennas have higher radiation efficiencies, meaning that the ratio of power radiated by the antenna to the power delivered to the antenna is higher. However, frictional loss from any moving part persists, preventing the maximum efficiency from being achieved. To address this aspect of energy loss, this work explores a magnetic levitation system to minimize the mechanical losses in order to increase antenna efficiency. By 3D printing the system and experimenting with aspects of the design, we can compare the energy loss between a magnetic levitation and bearing system in order to determine which is the most efficient. The data can be visualized through comparisons of the quality factor of each systems. Magnetic levitation systems significantly improve antenna efficiency by not only overcoming ohmic loss but also greatly decreasing friction loss as well.

Magnetic Levitation System for Magnetic Pendulum Antenna to Reduce Mechanical Losses

Michelle Lam, Rustu Umut Tok, Yuanxun Ethan Wang

Department of Electrical and Computer Engineering – University of California, Los Angeles

Ideas and Principles

Motivation

- Enhanced antenna efficiency essentially leads to increased signal strength and greater amount of data transmission.
- Frictional loss from any moving part persists, preventing the maximum efficiency from being achieved.
- A magnetic levitation system is explored to minimize mechanical losses in order to increase antenna efficiency.

Mechanical Antennas

- Mechanical antennas (Mechtennas) achieve higher efficiency radiation of signals.
- Mechtennas radiate signals through a time-varying magnetic field that physically oscillates electric charges, different from conventional electric antennas that accelerate charges via a current through a conductor.

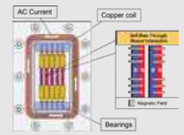

Fig. 1. *Magnetic Pendulum Array for Mechtennas.*

Proposed System Design

Magnetic Levitation System

- The system removes the application of bearings and uses unstable equilibrium of magnetic forces to “levitate”.

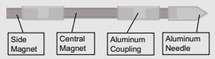

Fig. 2. *Magnetic Levitation System using Permanent Magnets.*

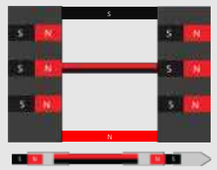

Fig. 3. *Aerial View of Magnetic Pole Format.*

- **Figure 2** shows the system with the permanent magnets removed.
- The axially magnetized magnets in the walls apply repulsive forces onto the “levitating” rod, as shown in **Figure 3**.

A bearing system was created with similar parameters to compare the quality factors between the two systems.

Bearing System

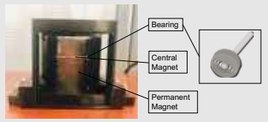

Fig. 4. *Bearing System using Permanent Magnets.*

- **Figure 4** demonstrates a design used in previous mechtennas via nested bearings.
- Frictional loss occurs as the magnet oscillates and remains in contact with the bearing.

Quality Factor Comparison via Resonance

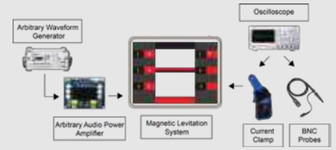

Fig. 5. *Data Collection from the Magnetic Levitation System.*

- In **Figure 5**, the input signal is generated by the waveform generator and amplified by the audio power amplifier before fed into the system. An oscilloscope is then used to measure the voltage and current running through the coil. Input impedance of the coil can be calculated to observe resonance and determine quality factor.
- Resonance frequency is the frequency at which the magnet oscillates with the greatest amplitude and radiates the maximal amount of electromagnetic waves.

Measured Input Impedance of the Coil

Fig. 5. *Measured Input Impedance of Bearing System*

Fig. 6. *Measured Input Impedance of Magnetic Levitation System*

- Resonance frequency is observed at the tallest peak in both **Figure 5** and **Figure 6**.
- The thinner bandwidth of the resonance frequency in **Figure 6** illustrates a higher quality factor since the variables have an inversely proportional relationship.

Quality Factor Comparison

$$Q = \frac{1}{R}\sqrt{\frac{L}{C}}$$

	Bearing System	Magnetic Levitation System
	R = L = C =	R = L = C =

Fig. 7. *Quality Factor Comparison between Bearing and Magnetic Levitation System.*

- **Figure 7** shows that the quality factor for the _____ system is higher, meaning that the oscillations last for a longer duration of time.

Conclusions

- The _____ system has a higher quality factor than that of the _____ system, demonstrating greater antenna efficiency.

Future Work

- Levitating an array of magnets, similar to the design of the mechtennas
- Stabilizing the magnet to prevent a sudden movement from displacing it

Acknowledgments

This work was supported by the National Science Foundation through the UCLA Summer Undergraduate Scholars Program managed by Will Herrera.

Amelia Lao

Bioengineering

Junior

LAB NAME

Seidlits Research Group

FACULTY ADVISOR

Stephanie Seidlits

DAILY LAB SUPERVISOR

Josh Karam and Jesse Liang

DEPARTMENT

Bioengineering

Development of a FRET System for Analysis of CD44 Clustering

Acute spinal cord injury is a debilitating condition with a lack of treatment options due to the complex pathophysiology of injury mechanisms. The severe inflammatory response causes deterioration of the extracellular matrix (ECM) and formation of a glial scar, resulting in programmed cell death and inhibition of neural regeneration. It has been shown that degradation of hyaluronan (HA), a major ECM component may induce inflammation upon binding to cell-surface receptors such as CD44. We have chosen to examine CD44 interactions with HA and hypothesize that HA molecular weight induces varying levels of CD44 clustering. A fluorescent resonance energy transfer (FRET) system was developed to measure clustering in HEK-293T cells cultured in various HA molecular weight solutions. When donor and acceptor fluorophores have spectral overlap and are located within a known distance, the donor emits a wavelength that excites the acceptor. By observing the energy transfer efficiency between the two molecules, we were able to quantify relative levels of CD44 clustering. In this work, we produced fluorescently-tagged CD44 viruses used to infect cells for FRET, characterized the viral transduction efficiency via flow cytometry, and performed the acceptor photobleaching FRET technique to compare two HA molecular weight conditions: 1M and 40K Da. Preliminary 1M HA experiments yielded a transfer efficiency of 38.39% for the positive control and 19.82% for the CD44 FRET pair, and 14.83% for the 40K FRET pair. The presence of FRET transfer and decrease in transfer efficiency in the 40K condition supports the validity of our FRET system.

Development of a FRET System for Analysis of CD44 Clustering

Amelia Lao, Josh Karam,
Jesse Liang, Stephanie Seidlits

Department of Bioengineering, University of California, Los Angeles

Background and Motivation

- Acute spinal cord injury (SCI) is a condition with devastating physiological effects including muscle weakness and paralysis, difficulty breathing, loss of bowel function, and blood pressure abnormalities.
- The lack of treatment options for SCI is largely due to the degradation of the extracellular matrix (ECM) and resulting inflammation and formation of a glial scar.

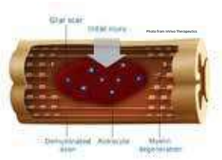

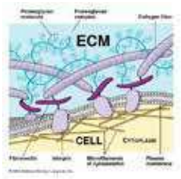

- The breakdown of hyaluronan (HA) in the ECM into low molecular weight forms is known to influence inflammatory responses via altered HA-CD44 receptor interactions.
- CD44 receptor clustering dependency on HA molecular weight can be investigated using a controlled fluorescence resonance energy transfer (FRET) system.

Materials and Methods

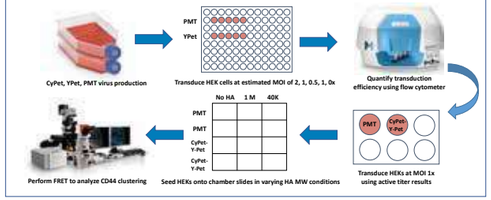

HEK Cell Transduction and Active Titer

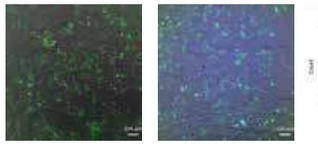

Calculating viral concentration using active titer:

$$\frac{\text{\# infectious particles}}{\text{ml}} = \frac{\text{\% cells infected} \times \text{\# cells seeded}}{100 \times \text{vol. virus added}} \times \text{dilution factor}$$

Optimizing HA MW in Hydrogel Delivery Systems

Goal: Engineer a biomimetic microenvironment to serve as a vehicle for stem cell delivery and scaffold to promote functional neuron recovery.

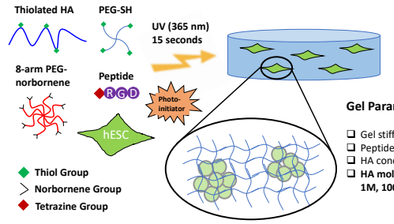

Gel Parameters

- Gel stiffness
- Peptide concentration
- HA concentration
- **HA molecular weight: 1M, 100K, 40K, 10K Da**

Acceptor Photobleaching FRET

- Bleach acceptor using laser and quantify increase in donor emission intensity using ImageJ analysis software
- FRET pair – CD44-CyPet (donor) and CD44-YPet (acceptor)
- Energy transfer efficiency depends on spectral overlap and distance between the two molecules
- Will be used to quantify relative levels of CD44 clustering

Experimental FRET Results

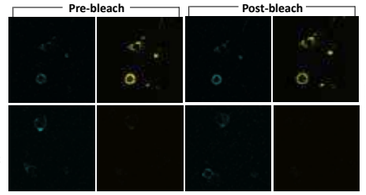

$$\text{FRET efficiency} = 1 - \frac{F_{pre}}{F_{post}}$$

F_{pre} = Integrated fluorescence intensity pre – bleach
F_{post} = Integrated fluorescence intensity post – bleach

PMT-CyPet-YPet	CD44-CyPet + YPet
49.98%	19.81%

The presence of FRET transfer validates our system and indicates CD44 receptor clustering in high (1M Da) HA.

Summary and Future Directions

- Acceptor Photobleaching FRET was used to quantify energy transfer from two fluorescently tagged CD44 molecules (CD44-CyPet and YPet).
- Future experiments include troubleshooting the system to achieve stronger signal, automating the analysis process, and testing the positive control and experimental condition in 100K, 40K, 10K, and no HA.

Special thanks to the UCLA Summer Undergraduates Scholars Program (SUSP), Seidlits Research Group, and the Microscopic Techniques Laboratory of the UCLA Brain Research Institute for support and resources, and the National Science Foundation (NSF) for funding on this project.

Allison Lee

Civil Engineering

Sophomore

LAB NAME

Geotechnical Engineering Research Lab

FACULTY ADVISOR

Scott J. Brandenberg

DAILY LAB SUPERVISOR

Paolo Zimmaro

DEPARTMENT

Civil and Environmental Engineering

Data Analysis Tools for the Next-Generation Liquefaction (NGL) Case-History Database

Soil liquefaction is a major cause of damage to structures, infrastructure, and lifelines during strong earthquakes. This phenomenon occurs when saturated sand loses substantial strength due to seismically induced pore pressure increase. Liquefaction triggering models are heavily reliant on data as they are typically developed using empirical or semi-empirical procedures. Current models often provide different outcomes in predicting liquefaction due to inconsistent and incomplete data sets, different methods of data interpretation, and potential errors in data analysis. Additionally, traditional spreadsheets hinder the processing of such massive data sets and unnecessarily incorporate repeated information. The Next-Generation Liquefaction (NGL) database is an open-source resource designed to store and organize liquefaction case-histories. A case-history in NGL comprises three components: (1) earthquake event, (2) geotechnical site characterization, and (3) post-earthquake observation. The NGL database will constitute a platform for researchers and practitioners to share soil liquefaction information, eliminating the repetitive nature of traditional data collections and condensing important information into readable tables and figures. We produced post-processing and data analysis tools for the NGL database using python with jupyter notebook. Our tools can be used to create interactive maps of geotechnical investigation data and earthquake events. Such maps directly interact with the NGL database and include charts and information relevant to each test. We also developed tools to perform liquefaction triggering analysis based on field investigation results. We envision that the civil engineering community will utilize the NGL case history database and associated data analysis tools to produce improved prediction models and broaden the understanding of liquefaction-related phenomena.

Data Analysis Tools for the Next-Generation Liquefaction (NGL) Case History Database

Honor Fisher, Allison Lee, Paolo Zimmaro, Scott J. Brandenberg

Department of Civil and Environmental Engineering; *University of California, Los Angeles*

2018 Summer Undergraduate Scholars Program

Soil Liquefaction:

Liquefaction describes the phenomenon that occurs when saturated deposits of loose sand lose substantial strength due to pore pressure increase during an earthquake and can cause sinkholes, soil ejecta, lateral spreading, and damage to buildings, lifelines, and infrastructure.

Figure 1: Soil Liquefaction, Niigata Earthquake (NOAA/NGDC, 1964)

An earthquake induced the liquefaction of the soil beneath the foundation of these buildings. As a result, some structures were tilted dramatically, and others were completely overturned.

Figure 2: Soil Liquefaction Analysis (Sutherland, 2017)

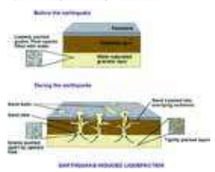

This image gives a cross-sectional view of the complex soil liquefaction, depicting how earthquakes cause saturated loose soil to eject and seep onto the surface.

Current Issues:

- Liquefaction triggering models are empirical or semi-empirical
- Alternate liquefaction models provide different outcomes
- Small, incomplete, and inconsistent data sets
- Potential errors in data analysis
- Different methods for data interpretation and extrapolation beyond data range
- Lack of communication between researchers

Figure 3: Current Discrepancies in Prediction Models (Idriss and Boulanger, 2010)

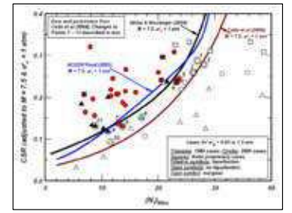

The variance in these liquefaction prediction models stresses the need for collaboration among modelers to produce improved prediction models based on an updated and larger case history database.

Next-Generation Liquefaction Relational Database

Relational Database:

A structured body of interrelated condensed tables connected by keys. The following gives an example of how tables relate to each other.

Table 1: Earthquake Event Table (Brandenberg et al., 2018)

This table consolidates the earthquake name and magnitude.

Table 2: Recording Station Table (Brandenberg et al., 2018)

This table consolidates the recording station name and time-averaged shear wave velocity in the upper 30 meters.

Compared to Traditional Spreadsheets, a Relational Database:

- Eliminates unnecessary repetition
- Avoids null fields
- Enforces data format consistent with parameter (INT, CHAR, BOOL)
- Enables data to be queried
- Allows development of post-processing tools

Table 3: Ground Motion Table (Brandenberg et al., 2018)

The IDs relate the respective information and minimize repetition in reporting information recorded by each station for each earthquake in this hypothetical scenario.

NGL Project:

The multi-year research project aims to develop a relational database to collect high-quality liquefaction case histories worldwide.

A **case history** comprises of three components:
1. Earthquake events
2. Site characterizations
3. Post-earthquake observations

Primary Key Foreign Key

Figure 4: Tables from NGL Database Schema (Brandenberg et al., 2018)

This subset of tables collect site characterization data from the Next-Generation Liquefaction database. These are the parameters of borehole, standard penetration, and cone penetration test data.

Data Organization and Analysis Tools

NGL Post-Processing Tools:

We developed the following tools to organize and present information from the database:
- Interactive map that queries information from relational database
- Plots of test data
- Markers to represent test and earthquake sites

Software Development:

We used the following systems for the tool development.
- Anaconda (Python distribution)
- Jupyter Notebook
- MAMP
- MySQL Workbench
- Folium

Figure 6: CPT Test Popup

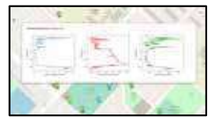

Blue markers indicate soil information from Cone Penetration Test through charts plotting cone tip resistance, sleeve friction resistance, and pore water pressure at various depths.

Figure 7: Earthquake Popup

Beachballs summarize the earthquake event mechanism. Information about the earthquake is displayed when the marker is clicked.

Figure 8: SPT Test Popup

Green markers indicate the location of a Standard Penetration Test, and their popups display the site name and chart of number of blow counts at various depth intervals.

Conclusions:

A more accurate model of predicting ground failure can be produced through this relational database, and the model become more precise as more researchers upload their work. Moving forward, we will develop tools to analyze the recorded data and produce triggering models for liquefaction. It is our hope that Civil and Geotechnical Engineers can use the NGL website to broaden the understanding of the liquefaction phenomenon.

Acknowledgements:
We would like to thank and acknowledge Scott J. Brandenberg and Paolo Zimmaro for teaching us about soil liquefaction, welcoming us into their lab, and taking steps to improve data sharing in geotechnical engineering. We would also like to acknowledge the UCLA Summer Undergraduate Scholars Program for giving us this opportunity to understand the various depths of the world of research.

References:
- NOAA/NGDC (1964). *NOAA National Geophysical Data Center.*
- Sutherland, S. (2017). "Japanese Structural Seismic Risk Prevention Techniques & Its Potential Performance in the Caribbean", *School of Architecture Urban Planning and Construction Engineering Academic Year 2016/2017.*
- Idriss, I.M. and Boulanger, R.W. (2010). *SPT-Based Liquefaction Triggering Procedures.* Center for Geotechnical Modeling
- Brandenberg, S. et al. (2018). "Next-Generation Liquefaction (NGL) Case History Database Structure", *Geotechnical Earthquake Engineering and Soil Dynamics V GSP 290.* pp. 426-433

Melissa Lee

Math/Applied Science

Sophomore

LAB NAME

CRESST

FACULTY ADVISOR

Greg Pottie

DAILY LAB SUPERVISOR

Jeffrey Jiang and Manie Tadayon

DEPARTMENT

Electrical and Computer Engineering

Using Hidden Marker Models and Embedded Devices to Facilitate the Learning of Physicals

Many other papers have shown the efficacy of using machine learning models to provide personalized feedback and instruction for purely cognitive tasks. Our research project addresses how to teach and assess upper body skills and provide personalized feedback and instruction. We take data from cameras to establish ground truth for our experiment. Then, we use gyroscopes and accelerometers to collect data on upper limb movement such as how fast the arm is moving and in what direction. This data is subsequently used to train a Hidden Markov Model to quantitatively evaluate upper body movements. Hidden Markov Models are a simple, probabilistic models that we chose to use due to their relatively easy to interpret structure and the small amount of data required to train them. Utilizing our evaluations, we can direct the student to exercises intended to correct any deficiencies in their understanding, optimizing the student's learning of that task. Our current experimental setup involves asking the participant to memorize a pattern of LEGOs and reproduce the pattern as accurately as possible. After the participant has finished, a picture of the original setup compared to their recreation will be shown to them and this will be repeated multiple times to assess if they are getting better or worse after each trial. Our results have wide applications in teaching physical skills pertaining to vocational training or supplementing the rehab process.

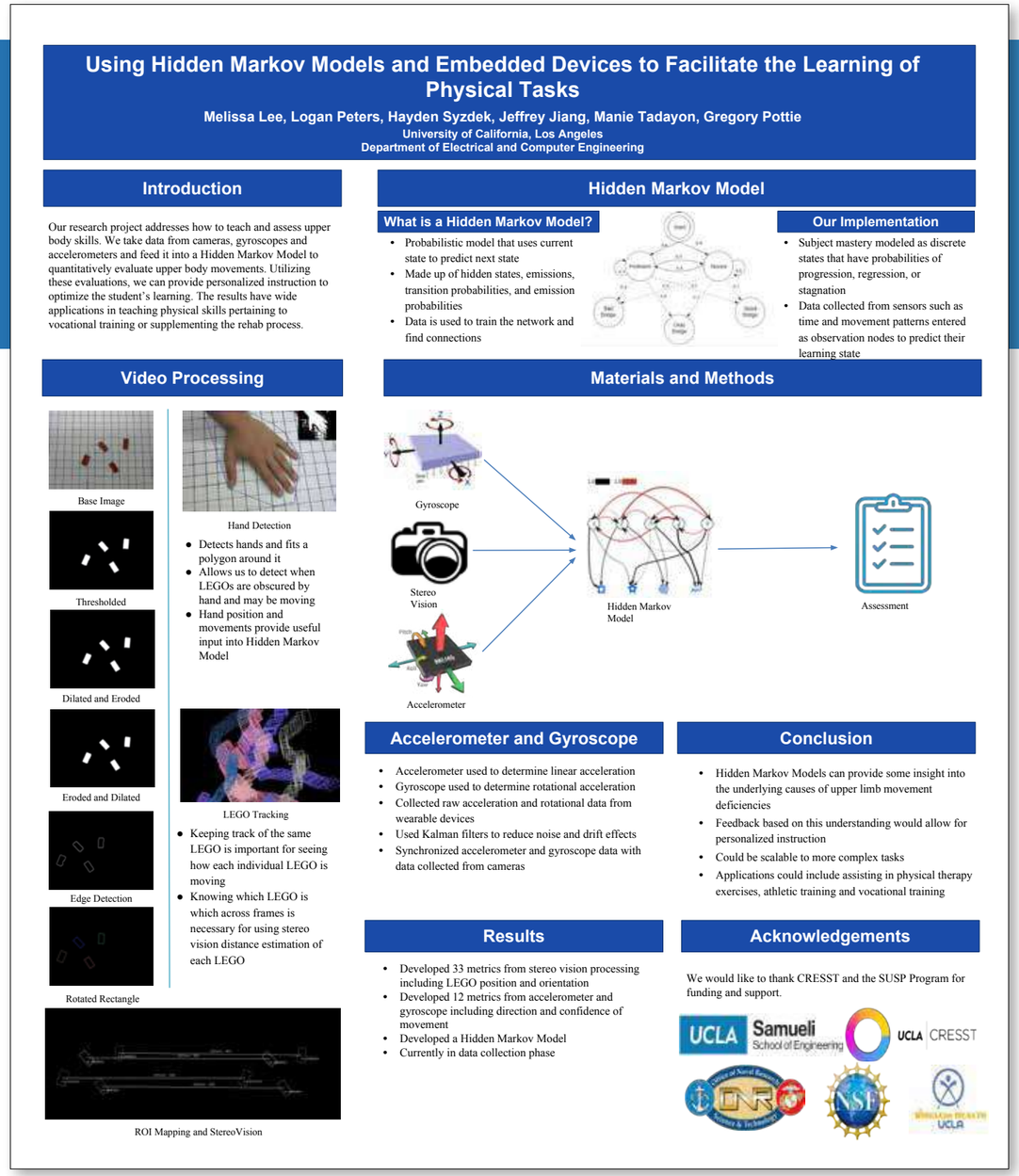

Using Hidden Markov Models and Embedded Devices to Facilitate the Learning of Physical Tasks

Melissa Lee, Logan Peters, Hayden Syzdek, Jeffrey Jiang, Manie Tadayon, Gregory Pottie

University of California, Los Angeles

Department of Electrical and Computer Engineering

Introduction

Our research project addresses how to teach and assess upper body skills. We take data from cameras, gyroscopes and accelerometers and feed it into a Hidden Markov Model to quantitatively evaluate upper body movements. Utilizing these evaluations, we can provide personalized instruction to optimize the student's learning. The results have wide applications in teaching physical skills pertaining to vocational training or supplementing the rehab process.

Hidden Markov Model

What is a Hidden Markov Model?

- Probabilistic model that uses current state to predict next state
- Made up of hidden states, emissions, transition probabilities, and emission probabilities
- Data is used to train the network and find connections

Our Implementation

- Subject mastery modeled as discrete states that have probabilities of progression, regression, or stagnation
- Data collected from sensors such as time and movement patterns entered as observation nodes to predict their learning state

Video Processing

Base Image

Thresholded

Dilated and Eroded

Eroded and Dilated

Edge Detection

Rotated Rectangle

Hand Detection

- Detects hands and fits a polygon around it
- Allows us to detect when LEGOs are obscured by hand and may be moving
- Hand position and movements provide useful input into Hidden Markov Model

LEGO Tracking

- Keeping track of the same LEGO is important for seeing how each individual LEGO is moving
- Knowing which LEGO is which across frames is necessary for using stereo vision distance estimation of each LEGO

ROI Mapping and StereoVision

Materials and Methods

Accelerometer and Gyroscope

- Accelerometer used to determine linear acceleration
- Gyroscope used to determine rotational acceleration
- Collected raw acceleration and rotational data from wearable devices
- Used Kalman filters to reduce noise and drift effects
- Synchronized accelerometer and gyroscope data with data collected from cameras

Conclusion

- Hidden Markov Models can provide some insight into the underlying causes of upper limb movement deficiencies
- Feedback based on this understanding would allow for personalized instruction
- Could be scalable to more complex tasks
- Applications could include assisting in physical therapy exercises, athletic training and vocational training

Results

- Developed 33 metrics from stereo vision processing including LEGO position and orientation
- Developed 12 metrics from accelerometer and gyroscope including direction and confidence of movement
- Developed a Hidden Markov Model
- Currently in data collection phase

Acknowledgements

We would like to thank CRESST and the SUSP Program for funding and support.

LAB NAME
Communications Systems Laboratory

FACULTY ADVISOR
Richard Wesel

DAILY LAB SUPERVISOR
Hengjie Yang

DEPARTMENT
Electrical and Computer Engineering

Ethan Liang

Electrical Engineering

Senior

Achieving a Target Frame Failure Rate with the Least Complexity in the Context of Convolutional Coding with an Optimized Cyclic Redundancy Check and the List Viterbi Algorithm

Necessary to the development of the internet of things is a short block-length code that guarantees each of the following: (1) low latency, (2) high reliability, and (3) low decoding complexity. List decoded convolutional codes offer a relatively low frame failure rate and decoding latency. A recent development allowing design of a cyclic redundancy check (CRC) that minimizes the probability of an undetected decoding error has renewed interest in list-decoded convolutional codes as a low-latency solution.

This work explores how complexity and performance in terms of undetected errors (UEs) and negative acknowledgements (NACKS) varies as the degree of the CRC and the number of states of the convolutional encoder (or the encoder constraint length) are varied.

UEs and NACKS are collectively referred to as frame failures. The relationship between the frame failure rate, probability of UE, and probability of NACK are analyzed as a function of cyclic redundancy check degree, constraint length of convolutional code, signal to noise ratio, and maximum list depth for the serial list Viterbi decoding algorithm. An expression to quantify the complexity of the serial list Viterbi decoder as a function of maximum list depth is introduced. Given a target frame failure rate and probability of undetected error, the list Viterbi decoded convolutional code is optimized to achieve the target parameters with the minimum complexity possible.

Achieving a Target FFR with the Least Complexity in the Context of Convolutional Coding with an Optimized Cyclic Redundancy Check and the List Viterbi Algorithm

Ethan Liang, Hengjie Yang, Richard D. Wesel
Department of Electrical and Computer Engineering
University of California, Los Angeles

2018 Summer Undergraduate Scholars Program

Introduction and Motivation:

The development of the internet of things requires a short block-length code that guarantees each of the following: (1) low latency, (2) high reliability, and (3) low decoding complexity. List decoded convolutional codes offer a relatively low frame failure rate and decoding latency. A recent development allowing design of a cyclic redundancy check (CRC) that minimizes the probability of an undetected decoding error has renewed interest in list-decoded convolutional codes as a low-latency solution.

This work explores how complexity and performance in terms of undetected errors (UEs) and negative acknowledgements (NACKS) varies as the degree of the CRC and the number of states of the convolutional encoder (or the encoder constraint length) are varied.

UEs and NACKS are collectively referred to as frame failures. The relationship between the frame failure rate, probability of UE, and probability of NACK are analyzed as a function of cyclic redundancy check degree, constraint length of convolutional code, signal to noise ratio, and maximum list depth for the serial list Viterbi decoding algorithm. An expression to quantify the complexity of the serial list Viterbi decoder as a function of maximum list depth is introduced. Given a target frame failure rate and probability of undetected error, the list Viterbi decoded convolutional code is optimized to achieve the latter target parameters with the minimum decoding complexity possible.

Materials and Methods:

C++ MATLAB Coffee

Overview of List Viterbi Decoding:

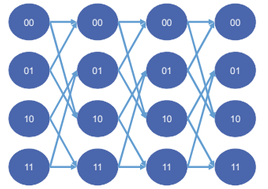

Example: Trellis List Decoder

The CRC Decoder performs CRC checks against decoded codewords from the Trellis Decoder until one of two exit conditions is met:
1. The decoded code word passes the CRC check.
2. The maximum number of iterations (max list depth) is reached and decoder declares a NACK).

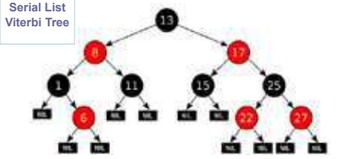

Example: Serial List Viterbi Tree
(Red-Black Tree with Max List =10)

Results:

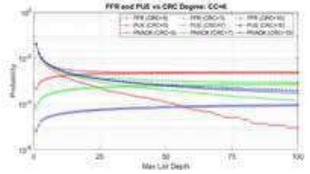

Analysis of varying CRC with constant CC/SNR: At very short list sizes (max list depth <5), the FFR and PNACK almost identical. The higher degree CRC is yields a large drop in the PUE without changing the shape of the curve. The FFR for an asymptotically large list size decreases as the degree of the CRC increases.

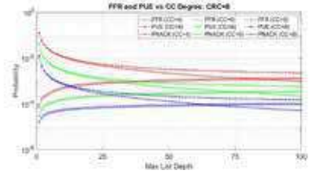

Analysis of varying CC with constant CRC/SNR: The FFR and PNACK exhibit large drops for very low list sizes (max list depth <5) as a result of larger CC degrees. Above this threshold, the FFR and PNACK have similar shapes. The PUE rises slower as a function of max list depth for a higher degree CCs.

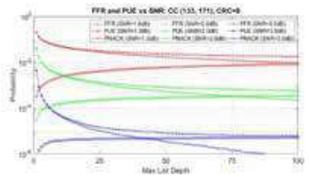

Analysis of varying SNR with constant CC/CRC: A higher SNR results in an improvement the FFR, PUE, and PNACK in both the short list size (max list depth <5), and asymptotically large list size regimes. The PNACK and PUE show larger drops and the PUE show smaller rises for short list sizes. The asymptotic FFR and PUE values are significantly lower for higher SNRs.

Complexity of the Serial List Viterbi Algorithm:

$$s\lfloor (k+r-2m)\times 2^{m+1}+(2^{m+1}+2^{m}+2^{m-1}+\cdots+4)\rfloor + s\lfloor (k+r-2m)\times 2^{m}+2^{m-1}+2^{m-2}+\cdots+1\rfloor + E[L]\times\left\lfloor\left(\frac{k+r}{2}\right)r+k+r\right\rfloor+(k+r+m)\times(2+\epsilon)\rfloor$$

$$where:\ \epsilon = P(insertion)*L$$

Key:
- k - length of information sequence.
- m - number of memory elements in the convolutional code.
- r - number of CRC bits.
- S - the precision of the comparison and add operations (in bits).
- L – max list depth.

Analysis of the serial list Viterbi Algorithm complexity: The complexity of the serial list Viterbi algorithm is a function of the expected list size. Choosing a maximum list size limits the complexity of the decoding process. The other figures give insight into CC/CRC/max list depth combinations that can achieve a target FFR, PUE, and PNACK with the low decoding complexity.

Conclusion:

- The serial list Viterbi decoding algorithm achieves a target frame failure rate and probability of undetected error for a given signal to noise ratio with less complexity than the soft Viterbi algorithm.
- The average complexity of the serial list Viterbi algorithm is a function of the expected list size, which can be designed by limiting the maximum list depth of the decoding algorithm.

Future Work:

- Model the variable list depth of the serial list Viterbi algorithm as an errors and erasures channel to calculate the mutual information and channel capacity.
- Extend this work to tail-biting convolutional codes. Develop complexity expression for a list decoded tail-biting convolutional code and calculate the associated frame failure rate and probability of undetected error.

References:

[1] Hengjie Yang and Richard Wesel, "Serial List Viterbi Decoding with CRC: Managing Errors, Erasures, and Complexity," 2018 IEEE Global Communications Conference, Dec. 9-13, 2018, Abu Dhabi, UAE.
[2] J. W. Kim, J. W. Tak, H. y. Kwak and J. S. No, "A New List Decoding Algorithm for Short-Length TBCCs With CRC," in IEEE Access, vol. 6, pp. 35105-35111, 2018.
[3] M. Roder and R. Hamzaoui, "Fast tree-trellis list Viterbi decoding," in *IEEE Transactions on Communications*, vol. 54, no. 3, pp. 453-461, March 2006.
[4] N. Seshadri and C. -. W. Sundberg, "List Viterbi decoding algorithms with applications," in *IEEE Transactions on Communications*, vol. 42, no. 234, pp. 313-323, Feb-Apr 1994.
[5] M. Mohammad, H. Ramchandran, J. Jong, C. Ravishankar and C. Barnett, "Comparing List Viterbi Algorithms with and without tail bits," *MILCOM 2008 - 2008 IEEE Military Communications Conference*, San Diego, CA, 2008, pp. 1-6.
[6] B. Chen and C. -. W. Sundberg, "List Viterbi algorithms for continuous transmission," in *IEEE Transactions on Communications*, vol. 49, no. 5, pp. 784-792, May 2001.

LAB NAME
eHealth Research Lab

FACULTY ADVISOR
Majid Sarrafzadeh

DAILY LAB SUPERVISOR
Kimmo Karkkainen

DEPARTMENT
Electrical and Computer Engineering

Arthur Lobins

Computer Science and Engineering

Junior

Mobile App for Tracking Mental Health

Mental illnesses affect millions of Americans each passing year and yet less than half of those affected receive proper treatment due to the associated stigma. Many people may not accept their condition or provide a socially desirable response in avoidance. The eHealth Research Lab proposes to use a smart phone sensor application to passively determine one's mental health state through an automated data collection system. The motivation for the application is to assist people in getting the help they need as soon as possible.

We are working with the U.S. Department of Veteran Affairs to determine whether a passive sensing approach can help resolve which veterans need immediate attention. Currently over 20 veterans commit suicide each day so there is a real issue with how care is provided. Veteran Affairs has limited resources to treat people, so an app like this could help them focus their attention on the individuals who are truly at risk.

The goal ofthis project is to track patients' depression and general mental health passively. That is, the method used to collect data on each patient will be unobtrusive to the individual's lifestyle without requiring active input. The challenge with depressed individuals is that they do not have the motivation to seek treatment when they need it, which is why a mobile app could help people in need connect with medical professionals. This app may also provide personalized guidance on how they may treat themselves.

2018 Summer Undergraduate Scholars Program

Mobile App for Tracking Mental Health

Arthur Lobins, Kimmo Kärkkäinen, Lionel Levine, Migyeong Gwak, Majid Sarrafzadeh

Department of Electrical Engineering University of California, Los Angeles

Abstract

Mental illnesses affect millions of Americans each passing year and yet less than half of those affected receive proper treatment due to the associated stigma. Many people may not accept their condition or provide a socially desirable response in avoidance. The eHealth Research Lab proposes to use a smart phone sensor application to passively determine one's mental health state through an automated data collection system. The motivation for the application is to assist people in getting the help they need as soon as possible.

Background

Current mechanisms for identifying patients at risk for severe mental health crises **have limited predictive success.**

Compounding this issue is that **many individuals** who would most need mental health interventions during crisis moments **fail to reach out** to receive help.

This project explores the **potential of smart devices**. Smart phones have many sensors in them that provide clues into a person's psyche. Moreover, studies done with smart devices provide an unobstructed and long-term data about patients' health. **Passive sensing data** that can interpret an individual's mental state could be an answer to the gap between the medical professional and a patient. **Detecting** the potential onset of a **mental health crisis** can potentially save lives.

Materials & Methods

Software

AWARE Framework is the library that allows our standalone iOS application to communicate with the iPhone sensors. The Framework consists of several sensors that are not limited to the ones shown to the right.

AWARE Dashboard also comes with the AWARE Framework software. It is a server used to store the data, otherwise known as a database. It is also a convenient way to run our studies and communicate with the users.

Sequel Pro is a data management program that allows us to view the data in an organized and accessible fashion.

The entirety of the application is made in the **Xcode** development environment and written in **Swift**. Swift is a high-performance system programming language that also allows access to old Objective-C code, which the AWARE Framework is written.

Sensors used for data collection

Ambient Noise · Linear Accelerometer · Location · Conversation · Battery · Screen · IOS ESM · Communication · Timezone

Current Work

The Application is **linked to a database** with both Sensor and ESM questionnaire data **successfully being uploaded**.

Working on **testing the app** on real devices and developing a friendly, **simple user interface. We don't** want the application to **frustrate patients**.

We are working on having this application **provide personalized guidance** on how patients under the study may **treat themselves** since many people tend to rely on self-treatment.

Our lab is also working on **algorithms to discover trends** within the data collected. **However, we need more information**. That is, **each person's story is quite different** so we must go deeper than what the numbers show us to **get the whole story** and from there determine the proper care and suitable treatment for each individual. Although it seems tricky to achieve the goals we have set, we hope our preliminary studies prove useful.

Flowchart for data extraction

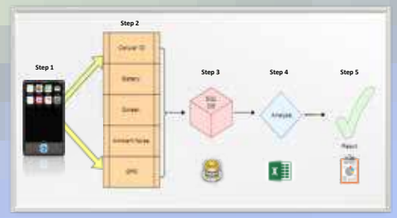

Step 1: Download the eWellness IOS App and accept terms and conditions for your study.

Step 2: A catalog will be made of various sensors based on the iPhone version.

Step 3: The program will automatically collect sensor data inside of a database (DB), and inputs of the questionnaires that the user desires.

Step 4: Data will be analyzed by algorithms developed by eHealth Research Lab.

Step 5: The results will then be verified by the patient's health care provider and given more personalized care when necessary.

Discussion

Wireless Health is the convergence of sensors, communication and health sciences. It is based on remote monitoring devices that allows healthcare providers to react to their patients much sooner.

Smart phones are ubiquitous in today's society, and have several embedded sensors that could provide useful information. Sensor data is used to **understand the daily activities and behaviors** of the users.

These **results would** open the way for novel interventions to **improve the treatment** of mental health patients.

Conclusion

This Application is part of the **Wireless Health Institute** studies which aims to **combine computer science, communications, and health sciences**.

This study is entirely from **passive sensing** from Smart Phones.

We are **currently working with** the U.S. Department of Veterans Affairs to help them **track which veterans need help**.

Future Work

Mobile App Development cycle

Testing the Application for **fine tuning**.

Getting **useful feedback** on as many features of the App as possible.

Work out any possible bugs and problems within the App **then distribute it** to those in need.

Train a machine learning model to automatically determine which patients are depressed from the sensor data.

In the future, we hope to no longer require the questionnaire and rely **only on the sensor data.**

Make use of the app by **assisting Veteran Affairs** with focusing their mental health treatment on veterans who truly need help.

References

Rui Wang, Gabriella Harariy, Peilin Hao, Xia Zhou, and Andrew T. Campbell. "SmartGPA: How Smartphones Can Assess and Predict Academic Performance of College Students." *UbiComp.* 7/15/2015. Osaka, Japan.

Rui Wang, Fanglin Chen, Zhenyu Chen, Tianxing Li, Gabriella Harari, Stefanie Tignor, Xia Zhou, Dror Ben-Zeev, and Andrew T. Campbell. "StudentLife: Assessing Mental Health, Academic Performance and Behavioral Trends of College Students using Smartphones". *UbiComp.* 9/17/2014, Seattle, WA. USA.

Acknowledgements

NSF · ERlab eHealth Research · Wireless Health Institute UCLA · UCLA Samueli School of Engineering

Adiba Majumder

Civil Engineering

Junior

LAB NAME
Jay Lab

FACULTY ADVISOR
Jenny Jay

DAILY LAB SUPERVISOR
Megyn Rugh

DEPARTMENT
Civil and Environmental Engineering

The Progression of Antibiotic Resistance and Persistence of Methicillin-Resistant *Staphylococcus aurous* After Fertilizer Application

The dissemination of antibiotic resistance from agriculture, specifically commercially brought fertilizer from Southern California, has created an urgency to further research the fate, transport and persistence of antibiotic resistant bacteria (ARB). ARB pose a serious health challenge that causes treatable illness to become untreatable, rendering life-saving drugs ineffective. Antimicrobials are commonly fed to animals to promote growth and prematurely prevent sickness. Methicillin resistant *Staphylococcus aurous* (MRSA), an ARB, is found in various fertilizers likely as a result of the antibiotic treatment used in agriculture, however, the severity and quantity of these bacteria are unknown. In this study, MRSA was isolated and analyzed specifically at two time points eight weeks apart. Potting soils such as manure, garden soils, food amendments and land amendments, were diluted with deionized water and sonicated. The homogenized solution was vacuum filtered and placed onto a CHROMAgar SA + Oxacillin plate. After incubation the plates reported approximately over 40 colony forming units per milliliter sample. The growth progression of the bacterial colonies was too numerous to count for time point eight and considering the detrimental health effects of MRSA infections, this raises concerning questions about ARB accumulation, as well as MRSA exposure in our communities. Future experiments will be indicative of the fate of ARB, while providing possible ways to combat this public health issue.

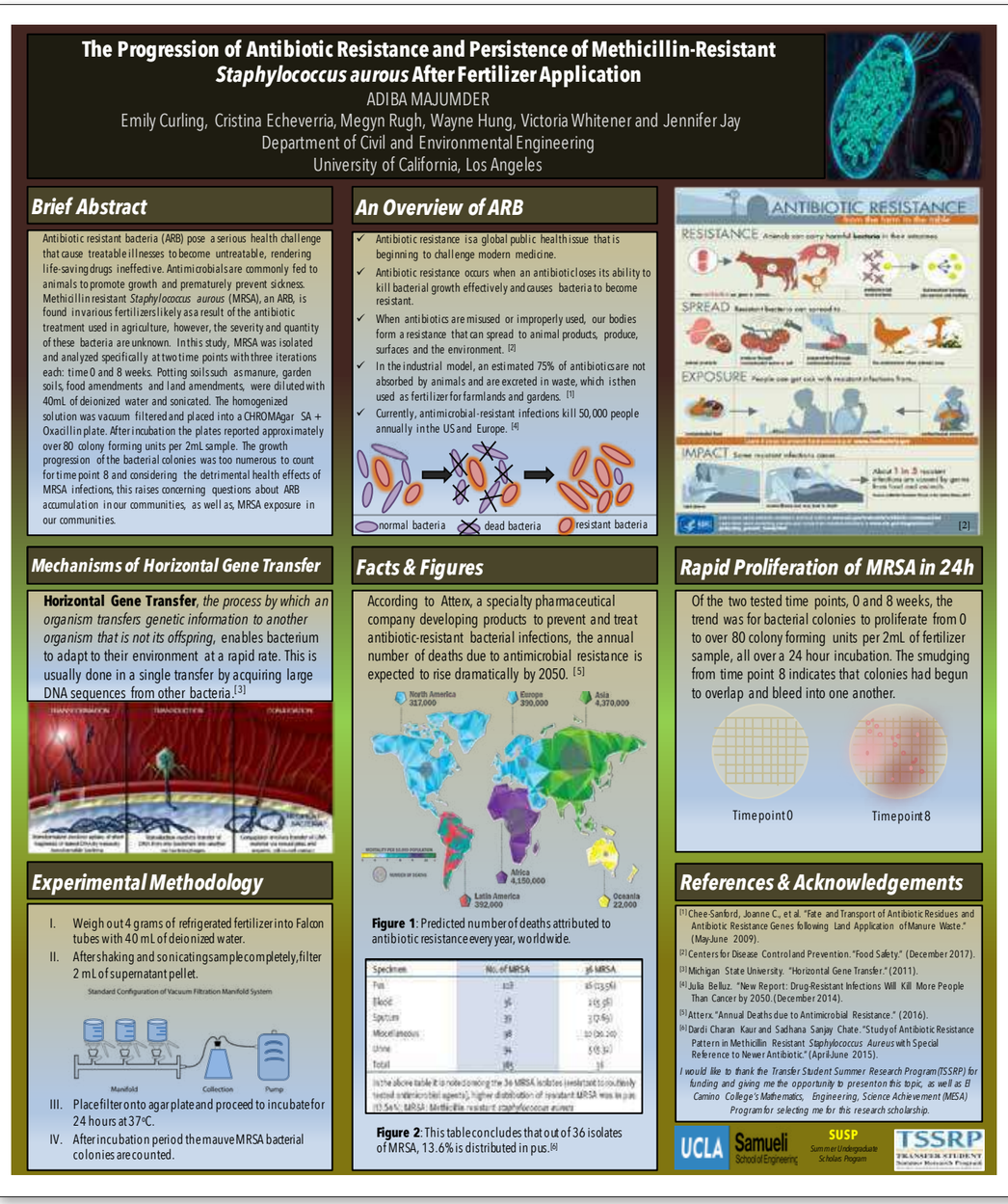

LAB NAME
Automated Reasoning Group

FACULTY ADVISOR
Adnan Darwiche

DAILY LAB SUPERVISOR
Arthur Choi

DEPARTMENT
Computer Science

Ingrid Mattinger

Linguistics and Computer Science, Mathematics of Computation

Senior

Integrating Grammars and Logic: From Context-Free to Context-Sensitive

A grammar is a set of rules which define the structure of a language. Context Free Grammars are a type of formal grammar which have been used to model both natural and programming languages. While Context Free Grammars are computationally more convenient, they cannot represent the full range of structures that appear in natural languages, which are Context Sensitive. However, Context Sensitive Grammars are computationally intractable. Here, we investigate the use of Sentential Decision Diagrams (SDDs), a representation of logical circuits that was recently proposed in the domain of Artificial Intelligence. In particular, we propose to use SDDs as a way of empowering grammars using logical constraints, to make them more context sensitive while maintaining tractability.

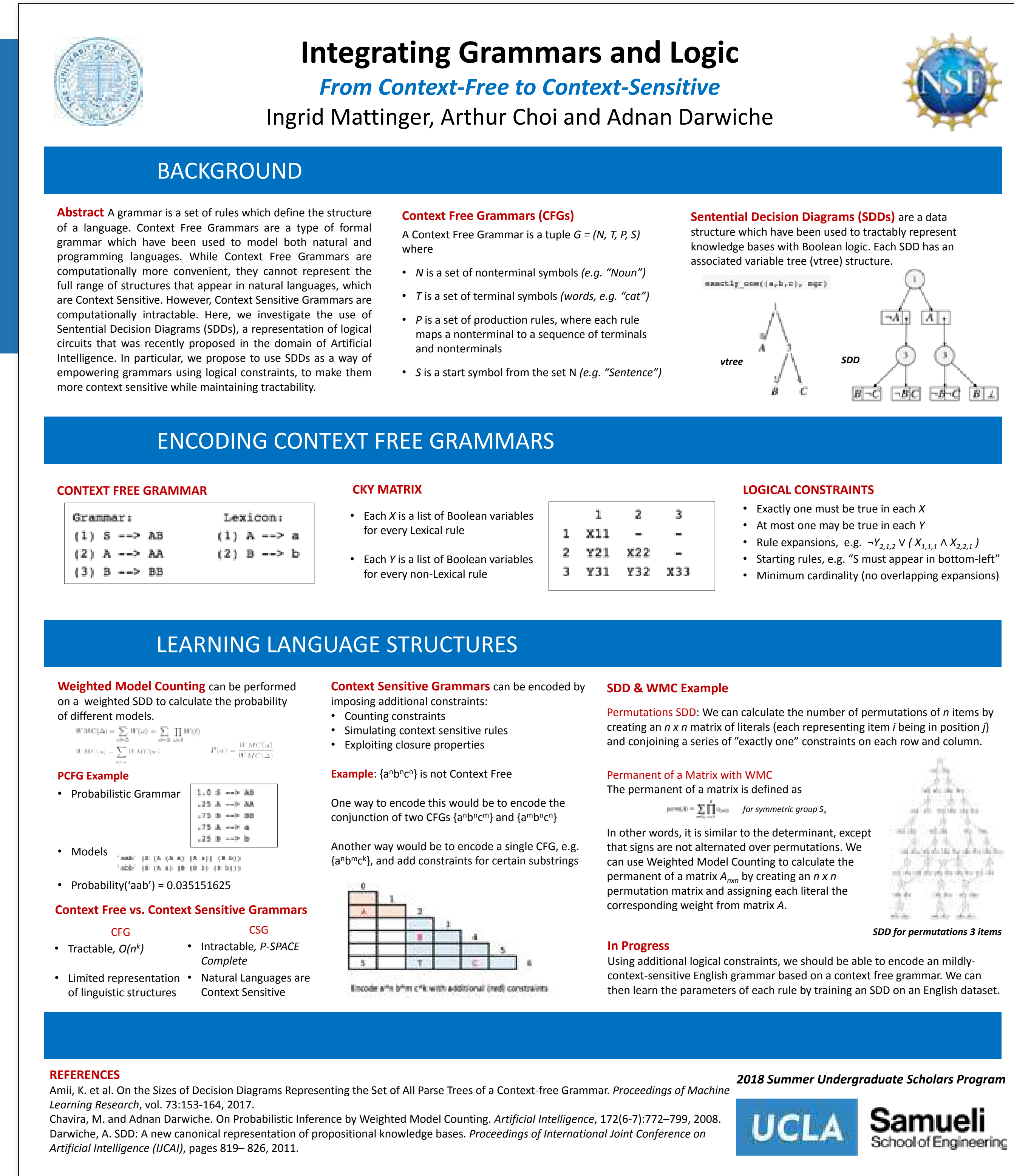

LAB NAME

Center for Heterogeneous Integration and Performance Scaling

FACULTY ADVISOR

Subramanian Iyer

DAILY LAB SUPERVISOR

Goutham Ezhilarasu

DEPARTMENT

Electrical and Computer Engineering

Michael Molter

Electrical Engineering

Sophomore

Design of a Multi-Electrode Array on FlexTrate™ for Electromyography

Electromyography is a method of measuring a person's muscular activity for the diagnosis of nerve and muscular disorders. We are working on a flexible electrode array EMG sensor for the benefit of showing spatial information about the nerve impulse and for the ability to determine conduction velocity, allowing doctors to better diagnose muscular and nerve disorders. The array is made on a flexible electronic material called Flextrate developed by the CHIPS lab at UCLA and is made up of 9 different copper, gold-plated electrodes in a grid. The different sized electrodes made on Flextrate needed to be characterized and compared to a standard surface electrode. The signal to noise ratio was calculated for different electrode diameters, and the power spectral density and maximum power in the power spectral density were found. These measurements served as performance validations of different sizes of electrodes. To switch between pairs of electrodes on the array, a multiplexer is hooked up to a microcontroller allowing for quick switching between the pairs of electrodes, allowing for the previously mentioned data to be gathered for analyzing.

Design of Multi-Electrode Array on FlexTrate™ for Electromyography

M. Molter, G. Ezhilarasu, S. S. Iyer

UCLA Electrical and Computer Engineering Department

Introduction and Background

Electromyography

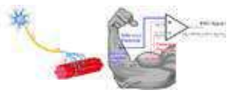

Electromyography is used to measure muscular activity by measuring muscle action potential. Electromyography can be used to help diagnose muscular and neurological disorders or injuries such as ALS. Emg machine consist of differential amplifiers that amplify the difference in the electrode signals.

FlexTrate™

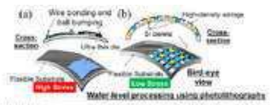

FlexTrate™ is a flexible electronics platform developed by the CHIPS lab at UCLA. It uses FOWLP with an elastic polymer substrate called PDMS. The use of small Si dies and flexible substrate allows for a flexible electronics platform with high interconnect density and small pitches. [1]

Materials and Data Collection

Setup

FlexTrate™ Electrodes

We tested different sizes of the copper FlexTrate electrode from 2 mm to 8 mm. For each electrode size we found the signal to noise ratio and the power spectral density in order to validate its performance.

EMG Circuit

myDAQ Data Collection

Data Processing and Collection

MATLAB

Design of Array Sensor

Electrode Array

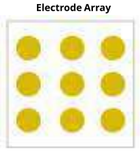

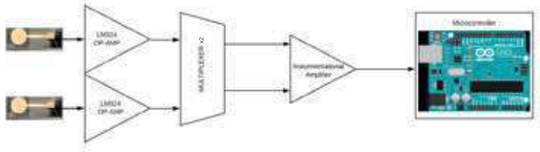

The electrode array is made up of 9 gold-plated copper electrodes. Each electrode is amplified individually, so it can be run through the multiplexer. The multiplexer allows us to select two electrodes to amplify and be sent to the microcontroller to be recorded.

Results

Processing of EMG Signal

- Processing using MATLAB
  - Low pass filter
    - 1000 Hz corner freq.
    - Tested 500 Hz corner freq.
  - High pass filter
    - 20 Hz corner freq.
    - Reduces motion artifact

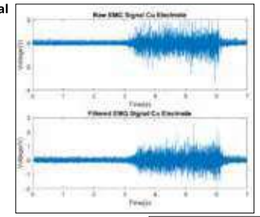

Comparison of Signal to Noise ratio

To help characterize the signal coming from the FlexTrate™ electrodes, we found the signal to noise ratio. The SNR is the ratio of the signal power to the noise in the signal. We see that the SNR decreases as the electrodes size decreases. We also see that the 8 mm, 7 mm, and 6 mm electrode have a similar or better SNR to the standard Ag/AgCl electrode.

Electrode	SNR (dB)
Ag/AgCl	18.86
8 mm	20.65
7 mm	18.52
6 mm	17.83
5 mm	13.94
4 mm	12.16
2 mm	8.76

Comparison of Power Spectral Density

To help characterize the signal coming from the FlexTrate™ electrodes, we found the Power Spectral Density. The frequency characteristics of an EMG electrode are important when used to diagnose neurological and muscular disorders. To ensure the frequency properties are similar, we compared the PSD of the Cu electrodes to the standard Ag/AgCl electrodes. We see that the PSD is similar in electrodes larger than 5 mm.

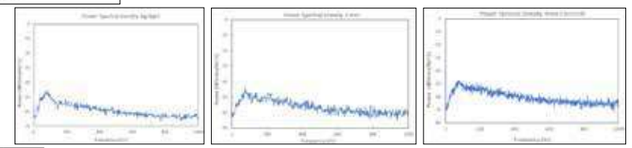

Electrode	Ag/AgCl	8 mm	7 mm	6 mm	5 mm	4 mm	2 mm
Max Power Frequency	80	77.5	75	86.25	102.5	77.5	80
Max Power Density	-45.6732	-43.251	-42.8908	-43.613	-43.3844	-47.3642	-54.0095

Future Work and Conclusions

- Continue work on sensor array
- Fast Switching
  - The microcontroller needs to be able to quickly switch between pairs of electrodes
- FlexTrate™ electrodes perform as well and even better than the standard Ag/AgCl surface electrode

Acknowledgements and References

[1] A. Hanna *et. al.*, "Extremely Flexible (1mm bending radius) Biocompatible Heterogeneous Fan-Out Wafer-Level Platform with the Lowest Reported Die-Shift (<6 μm) and Reliable Flexible Cu-Based Interconnects". *Proc. of Electronic Components and Technology Conference (ECTC 2018).*

LAB NAME

Laboratory for Embedded Machines and Ubiquitous Robots

FACULTY ADVISOR

Ankur Mehta

DAILY LAB SUPERVISOR

Ankur Mehta

DEPARTMENT

Electrical and Computer Engineering

Tanvi Pati

Electrical Engineering

Sophomore

STEM Education Revolutionized with Paper Robots

As the number of robots has been increasing in the world, so has their presence in our daily lives. Students are getting exposed to robotics from a younger age and some classes have even started using it as a tool for learning. However, these robots are quite expensive and challenging to make. Our lab has developed a design environment that generates a 2D pattern that an average user can print, cut, and fold to make a 3D structure for a robot. We aim to use this cheap and easy method of fabricating robots to teach middle school students a plethora of math and science topics. We have created robot designs of varying difficulty levels and built them ourselves. We have also developed lesson plans highlighting exciting activities that connect these robots to STEM concepts. We will test these lesson plans on middle school students and enhance them based on the results. This will give us a clear idea about their skill level, curiosity for learning, and what we should deliver accordingly. In using robots to teach math and science, students will be more engaged and interested in the topic as they will be learning by doing. Integrating simple and inexpensive robots into the classroom at an earlier age will give young students a fun introduction to the world of robotics.

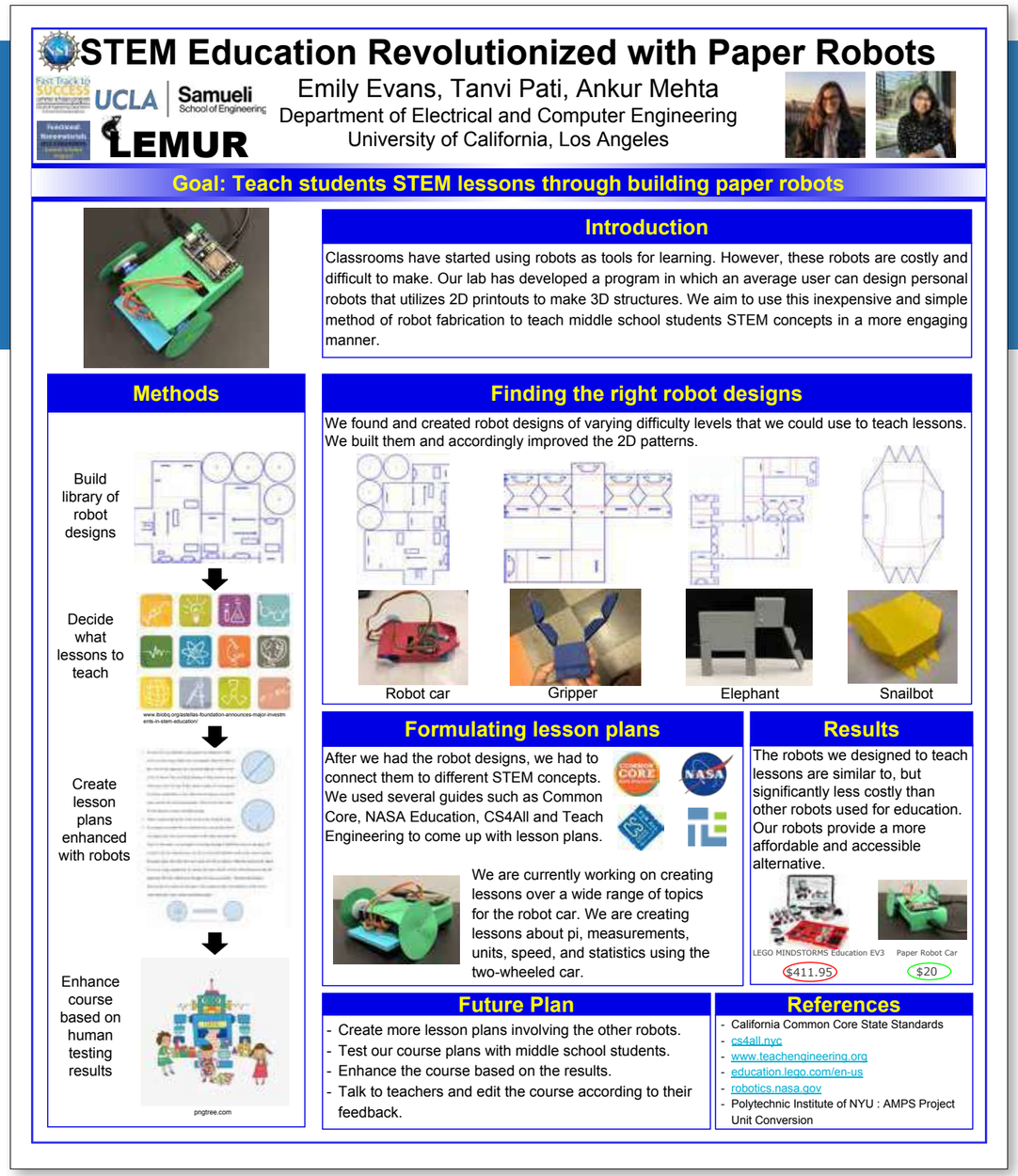

LAB NAME
CRESST

FACULTY ADVISOR
Greg Pottie

DAILY LAB SUPERVISOR
Jeffrey Jiang and Manie Tadayon

DEPARTMENT
Electrical and Computer Engineering

Logan Peters

Computer Science and Mathematics

Sophomore

Using Hidden Marker Models and Embedded Devices to Facilitate the Learning of Physicals

Many other papers have shown the efficacy of using machine learning models to provide personalized feedback and instruction for purely cognitive tasks. Our research project addresses how to teach and assess upper body skills and provide personalized feedback and instruction. We take data from cameras to establish ground truth for our experiment. Then, we use gyroscopes and accelerometers to collect data on upper limb movement such as how fast the arm is moving and in what direction. This data is subsequently used to train a Hidden Markov Model to quantitatively evaluate upper body movements. Hidden Markov Models are a simple, probabilistic models that we chose to use due to their relatively easy to interpret structure and the small amount of data required to train them. Utilizing our evaluations, we can direct the student to exercises intended to correct any deficiencies in their understanding, optimizing the student's learning of that task. Our current experimental setup involves asking the participant to memorize a pattern of LEGOs and reproduce the pattern as accurately as possible. After the participant has finished, a picture of the original setup compared to their recreation will be shown to them and this will be repeated multiple times to assess if they are getting better or worse after each trial. Our results have wide applications in teaching physical skills pertaining to vocational training or supplementing the rehab process.

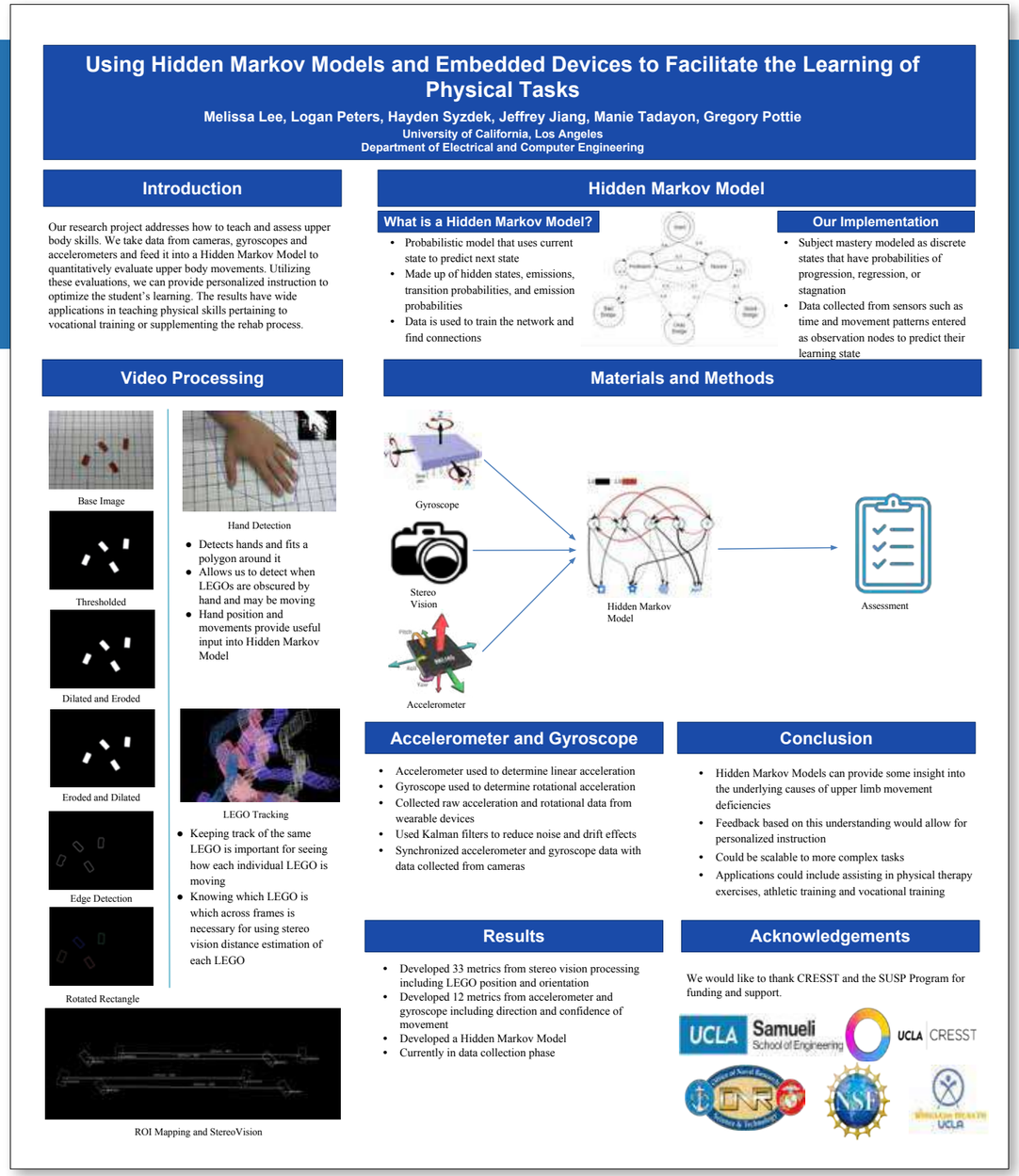

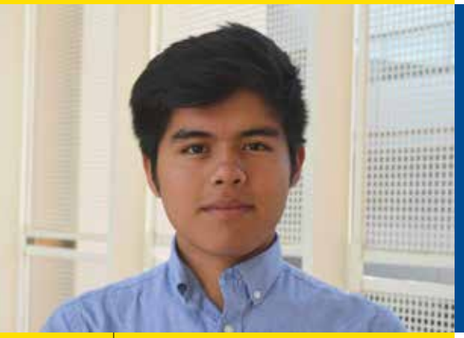

Jonathan Quintanilla

Chemical Engineering

Sophomore

LAB NAME

Simonetti Research Group

FACULTY ADVISOR

Dante Simonetti

DAILY LAB SUPERVISOR

Luke Minardi

DEPARTMENT

Chemical and Biomolecular Engineering

Effect of Aluminum Doping on Calcium Oxide Nanofiber Performance in Sorption Enhanced Steam Methane Reforming

Sorption enhanced steam methane reforming (SE-SMR) enables a cheaper and higher purity hydrogen production than traditionally used steam methane reforming (SMR). Sorbents are not often used in industry because they lack either high sorption capacity or stability over multiple carbonation-calcination cycles. Improving the stability of the carbon dioxide sorbent potentially enables reliable operation of the reformer for months at a time. In these studies, aluminum was used as a dopant in electrospun calcium oxide nanofibersto improve the stability of its sorption capacity. Calcium oxide nanofibers and calcium oxide nanofibers doped with aluminum were tested via carbon dioxide breakthroug experiments in SE-SMR at 873K, 1 atm, and a steam to carbon ratio of 3. The breakthrough time was 7473 ml g-1 and 6375 ml g-1 for calcium oxide nanofibers and calcium oxide nanofibers doped with aluminum respectively. Post breakthrough the calcium oxide was partially carbonated, and the rate of sorption fell so that CO2 was present in the products. After 10 cycles, the breakthrough time decreased 45% and 6% for calcium oxide nanofibers and calcium oxide nanofibers doped with aluminum respectively. During the pre-breakthrough time, the conversion of methane was 72% and the H2 mole fraction was 0.92, compared to 60% methane conversion and a H2 mole fraction of 0.72 for SMR. Despite the lower initial sorption capacity in doped nanofibers, they retain their initial capacity and outperform calcium oxide nanofibers after only ten cycles.

Effect of Aluminum Doping on Calcium Oxide Nanofiber Performance in Sorption Enhanced Steam Methane Reforming

Jonathan Quintanilla, Luke Minardi, Dante Simonetti

Department of Chemical and Biomolecular Engineering, University of California, Los Angeles

2018 Summer Undergraduate Scholars Program

Abstract

Sorption enhanced steam methane reforming (SE-SMR) enables a cheaper and higher purity hydrogen production than traditionally used steam methane reforming (SMR). Sorbents are not often used in industry because they lack either high sorption capacity or stability over multiple carbonation-calcination cycles. Improving the stability, the carbon dioxide sorbent potentially enables reliable operation of the reformer for months at a time. In these studies, aluminum was used as a dopant in electrospun calcium oxide nanofibers to improve the stability of its sorption capacity. Calcium oxide nanofibers and calcium oxide nanofibers doped with aluminum were tested via carbon dioxide breakthrough experiments in SE-SMR at 873K, 1 atm, and a steam to carbon ratio of 3. The breakthrough time was 7473 ml g^{-1} and 6375 ml g^{-1} for calcium oxide nanofibers and calcium oxide nanofibers doped with aluminum respectively. Post breakthrough the calcium oxide was partially carbonated, and the rate of sorption fell so that CO_2 was present in the products. After 10 cycles, the breakthrough time decreased 45% and 6% for calcium oxide nanofibers and calcium oxide nanofibers doped with aluminum respectively. During the pre-breakthrough time, the conversion of methane was 72% and the H_2 mole fraction was 0.92, compared to 60% methane conversion and a H_2 mole fraction of 0.72 for SMR. Despite lower sorption capacity in doped nanofibers, they retain their initial capacity and outperform calcium oxide nanofibers after only ten cycles.

Motivation

Thermodynamic Equilibrium

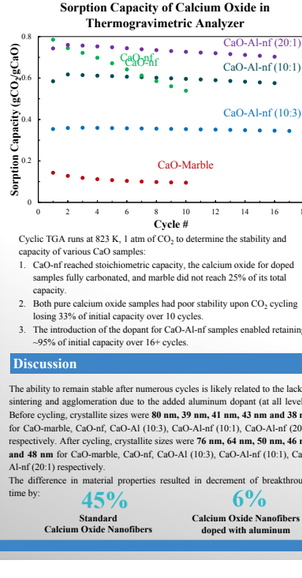

Benefits of sorbent in SMR:
- Eliminates a need for down stream processing, operating at lower temperature, higher purity product

Drawbacks of sorbent:
- Does not reach full capacity and has poor stability

Goal:
- Design a sorbent with high sorption capacity and high stability to multiple carbonation-calcination cycles using electrospinning and dopants
- Test sorbent in SE-SMR reactor to quantify improved performance

Materials Synthesis & Testing

1. Electrospinning of Calcium salt (dopant) - polymer - ethanol solution

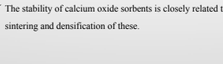

Electrospinning enables unique physiochemical properties for the development of calcium oxide sorbents. This synthesizing process enables a high porosity and a novel particulate structure.

2. Characterization of Nanofibers Properties

After synthesis, the nanofibers were characterized by Scanning Electron Microscopy (SEM) and X-Ray Diffraction (XRD). These tests help determine the physical and morphological properties of the nanofibers and how these change after testing them. Thermogravimetric analysis (TGA) is also run to determine how the sorption capacity behavior throughout each cycle.

3. Test performance CO_2 breakthrough experiment in plug flow reactor

SE-SMR breakthrough testing is done by packing the reactor with the nanofibers and nickel catalyst and operating at 823K and 1 atm for each carbonation (SE-SMR) cycle. To regenerate the calcium oxide after each cycle, the reactor was heated to 998K and held overnight while flowing hydrogen gas throughout the setup.

For each cycle, calcium oxide will react with carbon dioxide during methane reforming process. The sorbent's stability decreases due to sintering and densification after multiple cycles. By running a series of cycle, the sorbent's stability will be examined by measuring the breakthrough time carbon dioxide's concentration becomes present during the reaction.

Results

Sorption Capacity of Calcium Oxide in Thermogravimetric Analyzer

Cyclic TGA runs at 823 K, 1 atm of CO_2 to determine the stability and capacity of various CaO samples:
1. CaO-nf reached stoichiometric capacity, the calcium oxide for doped samples fully carbonated, and marble did not reach 25% of its total capacity.
2. Both pure calcium oxide samples had poor stability upon CO_2 cycling losing 33% of initial capacity over 10 cycles.
3. The introduction of the dopant for CaO-Al-nf samples enabled retaining ~95% of initial capacity over 16+ cycles.

Cyclic SE-SMR CO_2 Breakthrough using CaO-nf sorbent

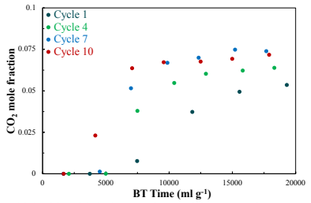

CO_2 breakthrough in SE-SMR experiments at 823 K, 1 atm, and a steam:carbon ratio of 3:
1. The initial breakthrough time was 7473 ml g^{-1}.
2. After 10 cycles, the breakthrough time decreased towards 4164 ml g^{-1}.

Breakthrough curve is sharper after just four cycles and a noticeable decrease in breakthrough time after the seventh cycle and becomes more pronounced in cycle 10.

Cyclic SE-SMR CO_2 Breakthrough using CaO-Al-nf (20:1) sorbent

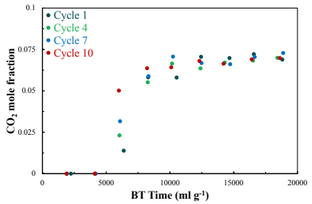

CO_2 breakthrough in SE-SMR experiments at 823 K, 1 atm, and a steam:carbon ratio of 3:
1. The initial breakthrough time was 6375 ml g^{-1}.
2. After 10 cycles, the breakthrough time decreased towards 5995 ml g^{-1}.

Breakthrough time values are retained around the initial value in each cycle, by improving its stability. Breakthrough curve is sharper after four cycles.

Discussion

The ability to remain stable after numerous cycles is likely related to the lack of sintering and agglomeration due to the added aluminum dopant (at all levels). Before cycling, crystallite sizes were **80 nm, 39 nm, 41 nm, 43 nm and 38 nm** for CaO-marble, CaO-nf, CaO-Al (10:3), CaO-Al-nf (10:1), CaO-Al-nf (20:1) respectively. After cycling, crystallite sizes were **76 nm, 64 nm, 50 nm, 46 nm and 48 nm** for CaO-marble, CaO-nf, CaO-Al (10:3), CaO-Al-nf (10:1), CaO-Al-nf (20:1) respectively.

The difference in material properties resulted in decrement of breakthrough time by:

45% — **Standard Calcium Oxide Nanofibers**

6% — **Calcium Oxide Nanofibers doped with aluminum**

Conclusions

- ✓ The inclusion of dopants for calcium oxide nanofibers retain 94% of its initial stability and 95% of its initial sorption capacity of the sorbent for 10+ cycles .
- ✓ Pure calcium oxide's stability perform poorly by losing 33% of its initial sorption capacity and 45% of its stability over 10 cycles.
- ✓ The stability of calcium oxide sorbents is closely related towards sintering and densification of these.

Acknowledgements

Acknowledgements for the Chemical and Biomolecular Engineering Department, our faculty advisor Dante Simonetti and daily lab supervisor Luke Minardi

References

Albrecht, Karl O., et al. "Application of a Combined Catalyst and Sorbent for Steam Reforming of Methane." *Industrial & Engineering Chemistry Research*, vol. 49, no. 9, May 2010, pp. 4091–4098., doi:10.1021/ie901914c.

Manuel Rivas

Computer Science

Sophomore

LAB NAME

Network and Embedded Systems Lab

FACULTY ADVISOR

Mani Srivastava

DAILY LAB SUPERVISOR

Kevin Xia and Eun Sun Lee

DEPARTMENT

Electrical and Computer Engineering

Automating Grading of Embedded Systems Assignments, Version 2.0

Grading embedded system assignments requires timeconsuming interaction between students and instructors because of the experimental setup that is only available in the laboratory. Previous work to address this problem includes EmbedInsight, a system which automates the grading cycle by allowing students to submit their codes to a server. Submissions are graded in a queue by the instructor's grading microcontroller board, which creates a long delay in feedback when many students upload code within a short period of time. We propose EmbedInsight Version 2.0, which provides distributed grading and userfriendly debugging features by giving a grading board to each student. The three components to this system are the website, a grading board, and a student board. This system establishes communication between the website and the grading board by using Google Chrome's WebUSB feature, while the grading board communicates with the student board through the use of General Purpose Input/Output pins. The grading board tests whether or not the student programmed their board to carry out specific instructions. The new website has several features such as buttons that send commands to the board and the ability to simulate an oscilloscope. The concept of this project expands the functionality of microcontrollers and could also be a very powerful tool for education. It would allow instructors to easily assign and grade embedded systems assignments at all levels of education, while also giving students a way to get more feedback to improve their learning experience.

Automated Grading of Embedded Systems Assignments, Version 2.0

Manuel Rivas, Fernando Cruz, Zhengxu Xia, Eun Sun Lee, Mani Srivastava
Department of Electrical and Computer Engineering,
University of California, Los Angeles
2018 Summer Undergraduate Scholars Program

Motivation

- Embedded systems are a combination of computer hardware and software that is designed for a specific function within a larger system
- Grading embedded system assignments requires one-to-one meeting in a designated time slot
- Extreme time investment required from instructors and students
- Debugging devices like oscilloscopes are only available in lab facilities

Oscilloscopes are used to debug and grade these assignments. We aim to provide a similar feature that is accessible from the web with our project.

Previous Work: EmbedInsight

- Automates grading cycle by allowing students to submit their codes to a server
- Grades submissions in a queue.
- Creates a long delay in feedback when many students upload code within a short period of time
- Uses only a limited number of testbeds

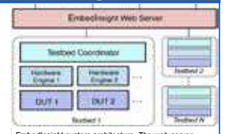

EmbedInsight system architecture. The web server communicates with multiple testbeds to grade multiple student's submissions

Introduction to EmbedInsight Version 2.0

- Provides a grading board to each student
  - Distributed grading
  - User-friendly debugging feature
- Our board communicates with the website using Google Chrome's WebUSB API
- Students' microcontroller board programmed as assigned
- Result read by the tester board through GPIO
- The tester microcontroller board facilitates communication between the browser and student board as well as the recording process

Student Board: NUCLEO-F746ZG

Tester Board: LPC1768

Example Assignment

- Example assignment: Timestamping Pulse Width Modulation (PWM) waves
- A PWM wave is an electric wave that alternates between "on" and "off"
- Dependent on two factors: period and duty cycle
- Period = time for one cycle
- Duty Cycle = (time on) / period

An example of a PWM wave that could be generated by a student's board.

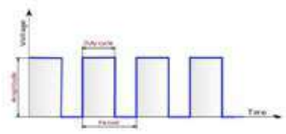

Overall Architecture

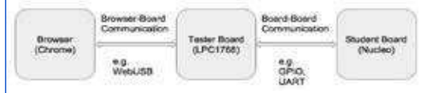

- The browser sends commands to the Tester Board, which sends signals to the Student Board
- The Student Board interprets the data as a period and duty cycle and generates a PWM wave
- The Tester Board measures the waveform coming from the Student Board and reports the data back to the browser
- The browser analyzes, grades, and then displays the data from the Tester Board

Results and Website

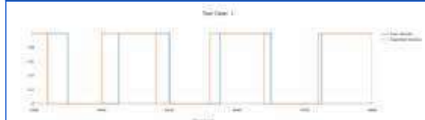

- Oscilloscope-like graphical user interface
- Graphs detected and expected waveform of the test case
- Displays grading feedback
- Other functions include turning lights on or off on the tester board
- Reliable and consistent communication between the 3 components

Conclusion and Future Work

Conclusion:

- Allow efficient distribution and grading of embedded systems assignments
- Improve students learning experience by providing user-friendly debugging features
- Give microcontrollers the capability of communicating with websites

Future Work:

- Record multiple signals simultaneously
- Flash grading algorithm directly to tester board via WebUSB
- Develop a user account system for students/instructors
- Test the current system with other types of assignments

Acknowledgements

University of California, Los Angeles (UCLA);
Networked and Embedded Systems Lab (NESL), UCLA;
Wireless Health Institute (WHI), UCLA

Tara Sadjadpour

Electrical Engineering

Sophomore

LAB NAME

Algorithmic Research in Network Information Flow

FACULTY ADVISOR

Christina Fragouli

DAILY LAB SUPERVISOR

Gaurav Agarwal

DEPARTMENT

Electrical and Computer Engineering

Security for Multiple Unicast Traffic over Combination Networks

Our research focuses on secure communication in the presence of a passive adversary wiretapping any K edges of the network. In a unicast network, which has a single source and single destination, the secure capacity is M-K, where M is the min-cut between the source and the destination. However, no such result is known for multiple unicast networks in which multiple destinations are interested in independent messages; this can be attributed to the fact that the unsecure capacity, the maximum rate at which one can communicate in the absence of an adversary, is also unknown. We focus on a class of multiple unicast networks with the combination network topology. These are 3-layer networks with a single source in the first layer, relay nodes in the second layer, and destination nodes in the third. The *m* sources are co-located at the single source node, and *m* corresponding destinations seek independent information. With the aid of numerical simulations, we compare the achievable region of a scheme with an outer bound in the secure capacity region for these networks. Using randomly generated networks, we find the outer bound's corner points and verify whether all of them are contained inside the achievable region. All of our simulations showed that the outer bound corner points are contained in the achievable region.

UCLA Samueli School of Engineering | Summer Undergraduate Scholars Program | Fast Track to SUCCESS summer scholars program | Functional Nanomaterials | Functional NanoMaterials Scholars Program REU Site funded by NSF

Security for Multiple Unicast Traffic Over Combination Networks

Tara Sadjadpour, Gaurav Agarwal, Christina Fragouli

Algorithmic Research in Network Information Flow Laboratory, Dept. of Electrical and Computer Engineering

Model

Networks represented by graphs consisting of directed edges of unit capacity

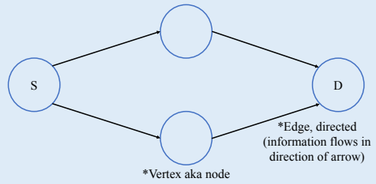

Secure Network Coding

Min-Cut Max-Flow Theorem: The minimum # of edges we can remove such that a source cannot send data to its destination equals the maximum flow of information from the source to its destination, denoted by M

Capacity: Maximum rate R at which source can communicate to destination

Unicast = single source, single destination

Mutlicast = single source, multiple destinations receiving same information

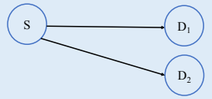

Unsecure Capacity[1]: R = M

Secure Capacity[2]: R = M–K, where K = # of edges the wiretapper has access to

Multiple Unicast Traffic

- In our scheme, all sources are co-located at a single node
- Multiple destinations associated with each of the co-located sources
- We consider the combination network topology, i.e. 3-layer multiple unicast network with single source, t relays, and m destinations (sinks)[3]
- All destinations are interested in different information

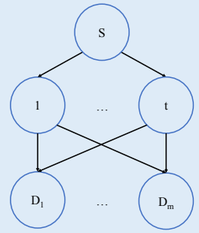

Our Work

- Goal: Numerically evaluate the performance of an achievable scheme

Outer Bound

$$\sum_{i \in I} R_i \leq \left(M_{\{I\}} - K\right)^+ \quad \forall\, I \subseteq \{1, \ldots, m\}$$

Achievable Scheme

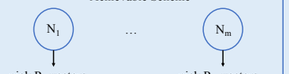

If $\sum_{i=1}^{m} R_i$ vectors are linearly independent then $(R_1, \ldots, R_m)$ is achievable

Are they the same?

- Achievable region ⊆ outer bound
- Achievable region and outer bound are convex
- Show that every corner point of outer bound is inside the achievable region

Simple Example of Our Evaluation

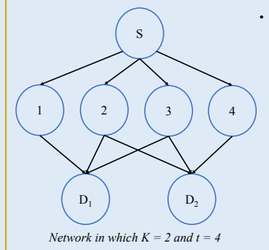

Network in which K = 2 and t = 4

- We create V_1 and V_2 for D_1 and D_2, resp., using relay–destination disconnection matrices C_1 and C_2, and an altered Vandermonde Matrix that maintains its MDS matrix characteristics over our finite field

$$V_{K\times t} = \begin{pmatrix} 1 & 1 & 1 & 1 \\ 1 & \alpha_1 & \alpha_2 & \alpha_3 \end{pmatrix}$$

$$C_1 = \begin{pmatrix} 0 & 0 & 0 & 1 \end{pmatrix} \quad C_2 = \begin{pmatrix} 1 & 0 & 0 & 0 \end{pmatrix}$$

$$V_1 = \begin{pmatrix} V \\ C_1 \end{pmatrix} = \begin{pmatrix} 1 & 1 & 1 & 1 \\ 1 & \alpha_1 & \alpha_2 & \alpha_3 \\ 0 & 0 & 0 & 1 \end{pmatrix}$$

$$V_2 = \begin{pmatrix} V \\ C_2 \end{pmatrix} = \begin{pmatrix} 1 & 1 & 1 & 1 \\ 1 & \alpha_1 & \alpha_2 & \alpha_3 \\ 1 & 0 & 0 & 0 \end{pmatrix}$$

- Using our algorithms that operate over finite fields, we find null spaces N_1 and N_2 of V_1 and V_2, resp.
- For outer bound corner point (R_1, R_2), we choose R_1 and R_2 vectors from N_1 from N_2, resp.
- Check that the vectors chosen from N_1 and N_2 are linearly independent

Results and Future Work

- Thus far, all simulation methods show that the inner and outer bounds are equal
- The outer bound has $\binom{2^m}{m}$ corner points, so we would like to find a way to conduct simulations on networks with $m > 8$ destinations. We will consider finding the following to check if their coordinates are contained in the achievable scheme
  - The maximum sum rate
  - The sum rate such that all rates are equal

References

[1] Ahlswede, Rudolf, et al. "Network information flow." *IEEE Transactions on information theory* 46.4 (2000): 1204-1216.

[2] Cai, Ning, and Raymond W. Yeung. "Secure network coding." *Information Theory, 2002. Proceedings. 2002 IEEE International Symposium on*. IEEE, 2002.

[3] Chi Kin Ngai and R. W. Yeung, "Network coding gain of combination networks," *Information Theory Workshop*, 2004, pp. 283-287.

Siddharth Somasundaram

Electrical Engineering

Sophomore

LAB NAME

Integrated Nanomaterials Core Lab

FACULTY ADVISOR

Diana Huffaker

DAILY LAB SUPERVISOR

Dingkun Ren

DEPARTMENT

Electrical and Computer Engineering

InAsSb Nanowire Multi-Spectral Photodetectors at Mid-Wavelength Infrared Using Metal Photonic Crystals

Room-temperature photodetection at mid wavelength infrared (MWIR) is extremely important for several applications, such as gas detection, heat seeking, spectroscopy, and thermal imaging. However, many state-of-the-art photodetectors at MWIR require bulky cooling accessories to minimize dark current caused by thermal generation. Nanowires, however, have unique properties, specifically small volume and capability for lattice mismatched heteroepitaxial growth, that allow for significant suppression of dark current. As a result, the nanowire-based detector platform is a promising frontier for ultra-compact, small-footprint, and efficient photodetection. Our study focuses on developing a novel nanowire photodetector structure for MWIR, composed of InAsSb nanowires with a planar gold plasmonic grating. We first perform optical simulations to optimize the plasmonic resonances at MWIR to achieve high light absorption. Then, with this optimized plasmonic structure, we integrate the outputted optical generation profile from the optical simulation into a 3-D electrical model to determine the photoresponse of the structure. While the simulations demonstrate high room-temperature detectivity at MWIR, the robust design of the gratings also promises the realization of a multi-spectral photodetector built on a focal plane array.

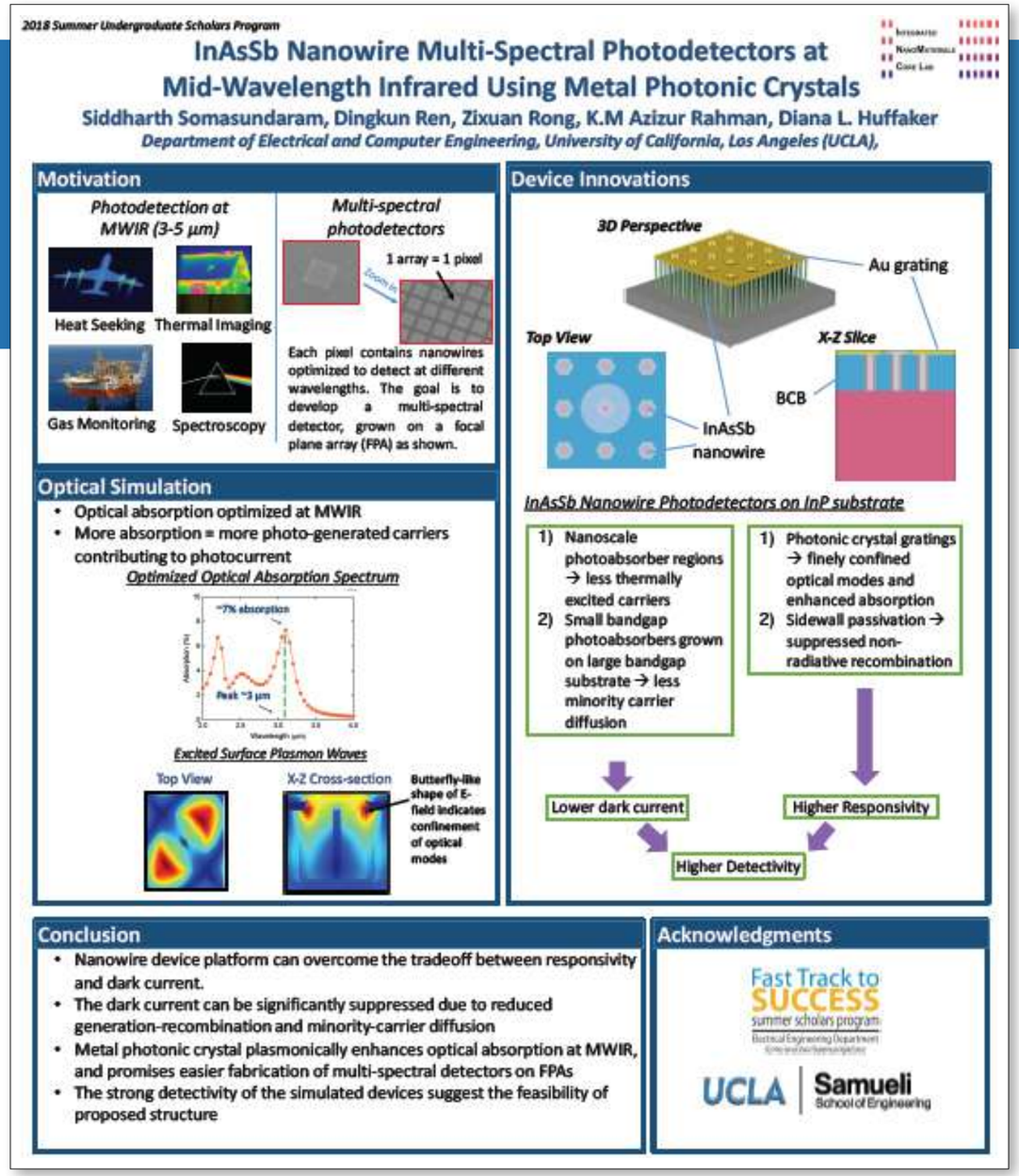

Hayden Syzdek

Computer Science

Junior

LAB NAME

CRESST

FACULTY ADVISOR

Greg Pottie

DAILY LAB SUPERVISOR

Jeffrey Jiang and Manie Tadayon

DEPARTMENT

Electrical and Computer Engineering

Using Hidden Marker Models and Embedded Devices to Facilitate the Learning of Physicals

Many other papers have shown the efficacy of using machine learning models to provide personalized feedback and instruction for purely cognitive tasks. Our research project addresses how to teach and assess upper body skills and provide personalized feedback and instruction. We take data from cameras to establish ground truth for our experiment. Then, we use gyroscopes and accelerometers to collect data on upper limb movement such as how fast the arm is moving and in what direction. This data is subsequently used to train a Hidden Markov Model to quantitatively evaluate upper body movements. Hidden Markov Models are a simple, probabilistic models that we chose to use due to their relatively easy to interpret structure and the small amount of data required to train them. Utilizing our evaluations, we can direct the student to exercises intended to correct any deficiencies in their understanding, optimizing the student's learning of that task. Our current experimental setup involves asking the participant to memorize a pattern of LEGOs and reproduce the pattern as accurately as possible. After the participant has finished, a picture of the original setup compared to their recreation will be shown to them and this will be repeated multiple times to assess if they are getting better or worse after each trial. Our results have wide applications in teaching physical skills pertaining to vocational training or supplementing the rehab process.

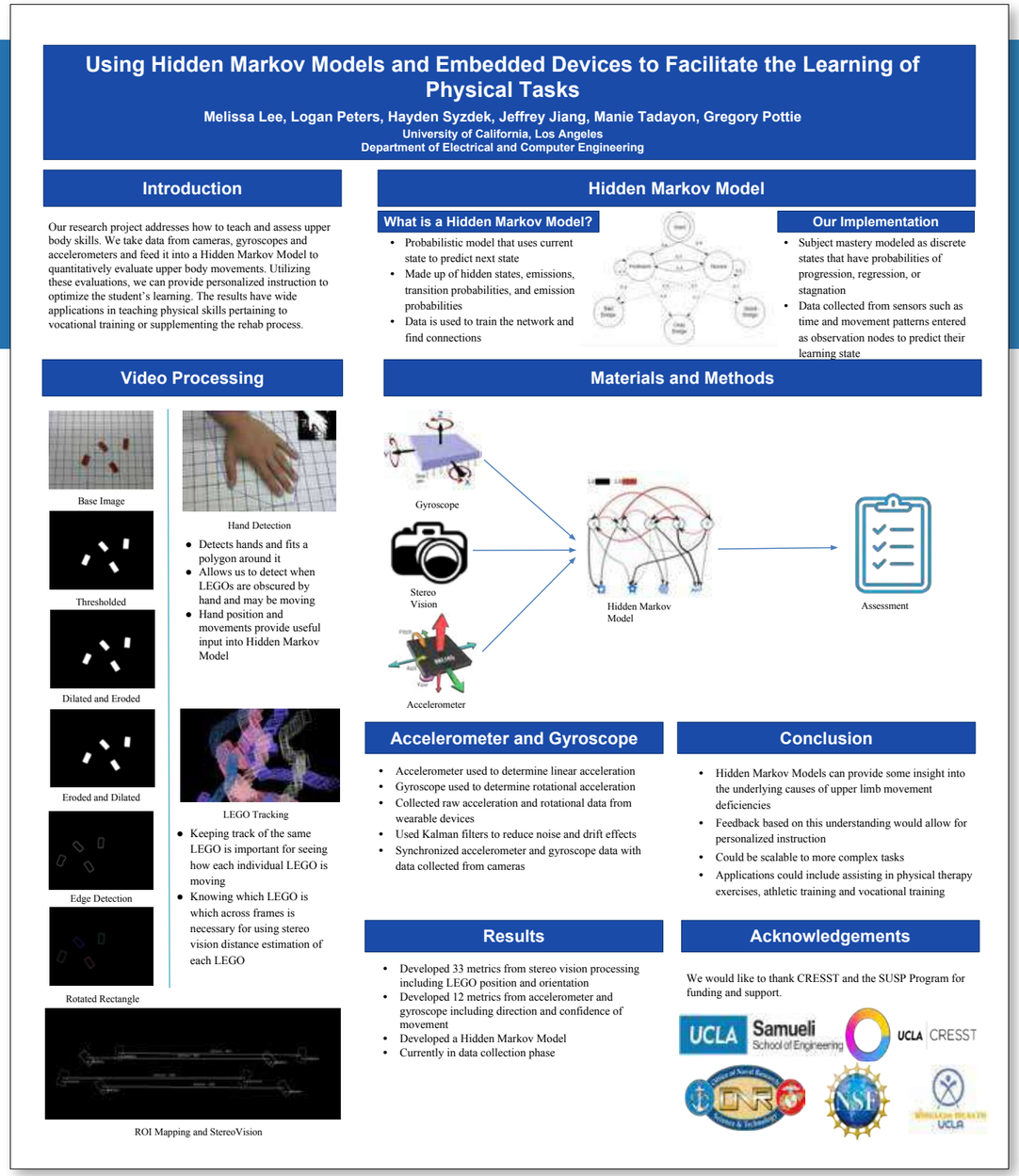

Celeste Tobar

Chemistry and Mathematics

Senior

LAB NAME

I²BL

FACULTY ADVISOR

Sam Emaminejad

DAILY LAB SUPERVISOR

Haisong Lin

DEPARTMENT

Electrical and Computer Engineering

Optimization of NIPAAm based hydrogel for wearable biofluid processing

Stimulus-responsive polymers present unprecedented opportunities to enable a wide array of sensing and actuation operations for diverse applications ranging from biomedical devices to soft robotics. Hydrogels base on N-Isopropylacrylamide (NIPAAm), a thermo-responsive polymer, have reversible volume-phase transitions and fast response to temperature, rendering them as excellent material candidates to construct biofluid actuation systems. In the course of this research, the physico-thermal characteristics of the NIPAAm based hydrogel were studied, and a process was developed for large-scale fabrication of hydrogel-based actuation interfaces with optimal thermal response. Specifically, incorporating different molar percentages of ionizable monomer and crosslinker with respect to the thermo-responsive polymer into the hydrogel's network allowed us to adjust the low critical solution temperature (LCST) and shrinkage percentage of the hydrogel. Three main hydrogels were developed with LCST's of 29, 32, and 34°C and a shrinkage percentage of 23, 17, and 34% respectively. Considering human body temperature (32°C), the gel with an LCST of 34°C was preferred. The gel with a shrinkage percentage of 34% was selected over the other gels because it allows for a wider pressure range. The pressure withstanding range was measured for the hydrogel with the best characteristics, and it was calculated to be 28-35 Pa. Moving forward the optimized hydrogel thermal response will be leveraged to realize a variety of micro-actuation interfaces for a broad range of wearable biofluid processing and biomarker sensing.

OPTIMIZATION OF NIPAAM BASED HYDROGEL FOR WEARABLE BIOFLUID PROCESSING

Celeste Tobar[1,2], Haisong Lin[1], Dr. Sam Emaminejad[1]

[1]Interconnected & Integrated Bioelectronics Lab (I²BL), University of California, Los Angeles

[2]Mount Saint Mary's University, Los Angeles

2018 Summer Undergraduate Scholars Program

Introduction

Stimulus-responsive polymers present unprecedented opportunities to enable a wide array of sensing and actuation operations for diverse applications ranging from biomedical devices to soft robotics. Hydrogels base on N-Isopropylacrylamide (NIPAAm), a thermo-responsive polymer, have reversible volume-phase transitions and fast response to temperature, rendering them as excellent material candidates to construct biofluid actuation systems. In the course of this research, the physico-thermal characteristics of the NIPAAm based hydrogel were studied, and a process was developed for large-scale fabrication of hydrogel-based actuation interfaces with optimal thermal response. Specifically, incorporating different molar percentages of ionizable monomer and crosslinker with respect to the thermo-responsive polymer into the hydrogel's network allowed us to adjust the low critical solution temperature (LCST) and shrinkage percentage of the hydrogel.

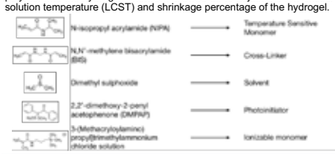

Background

Stimuli-responsive hydrogels are exceptional actuators in that they do not require an external power source to undergo volume-phase transitions. Distinct hydrogels respond to either

- Physical stimuli: temperature, electric or magnetic field, light, pressure, *etc.*
- Chemical stimuli: pH, solvent composition, ionic strength, *etc.*

A distinctive kind of hydrogel is a thermo-responsive hydrogel. Thermo-responsive hydrogels require its gel network to undergo a low critical solution temperature transition (LCST) to diffuse water out of its network. By altering the chemical composition of the hydrogel, the response can be altered. One could increase the concentration of ionizable monomer in the gels network to raise the LCST or lower the concentration of cross-linker to increase the swelling ratio. A group at the University of Wisconsin-Madison took advantage of these properties to create a Variable-Focus Liquid Microlense.

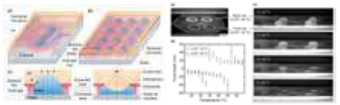

Dong, L.; Agarwal, A.; Beebe, D.; Jiang, H. Adv. Mater. 2007, 19, 401-405.

Methods

The figure below demonstrates the experimental process of creating the hydrogel to the method of testing. Every step in the experimental process affects one another. One has to take into consideration all aspects of the hydrogel when building the molds and testing.

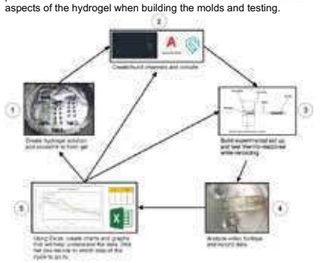

The figure below illustrates the experimental set up for testing the pressure the hydrogel can withstand. Pmax is the pressure at which the hydrogel breaks and allows for water to pass through the channel. Pmin is the pressure at which water could flow through the system after the hydrogel has shrunk. The value for Pmin and Pmax was calculated using the mathematical formulas for the volume of a cylinder and pressure.

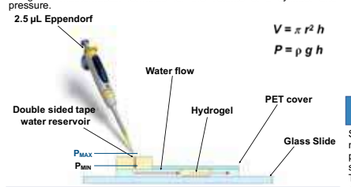

Results

For the application of the hydrogel, it was important to test them on a heat source other than a hot plate; thus micro-heaters were used. By testing multiple micro-heaters, we found that the temperature applied by the micro-heater correlates to the voltage and current being applied to the heater fairly linearly.

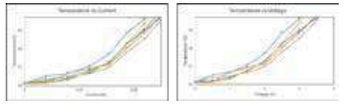

In the figure below, we see the visual effects of adding different molar percentages of ionizable monomer and crosslinker in the hydrogel's network. Vial #3, visually has a better shrinkage percentage than Vial #1 and 6.

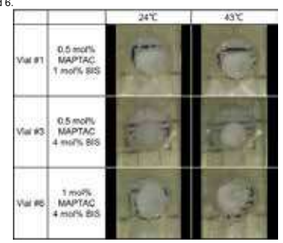

By analyzing the video footage of the hydrogel shrinkage over a period of time constantly raising the temperature, we can see that Vial #3 has a better LCST and shrinkage % than the other two vials.

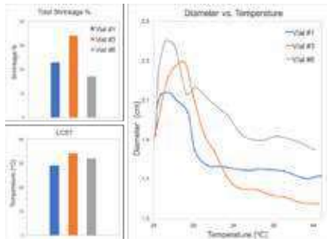

The figures below demonstrate the characteristics of the optimized hydrogel.

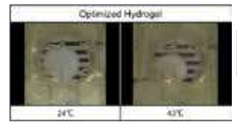

LCST	34
Shrinkage %	34
Pmin	27
Pmax	35

Conclusion

Specifically, incorporating different molar percentages of ionizable monomer and crosslinker with respect to the thermo-responsive polymer into the hydrogel's network allowed us to adjust the low critical solution temperature (LCST) and shrinkage percentage of the hydrogel. Three main hydrogels were developed with LCST's of 29, 32, and 34℃ and a shrinkage percentage of 23, 17, and 34% respectively. Considering human body temperature (32℃), the gel with an LCST of 34℃ was preferred. The gel with a shrinkage percentage of 34% was selected over the other gels because it allows for a wider pressure range. The pressure withstanding range was measured for the hydrogel with the best characteristics, and it was calculated to be 28-35 Pa. Moving forward the optimized hydrogel thermal response will be leveraged to realize a variety of micro-actuation interfaces for a broad range of wearable biofluid processing and biomarker sensing.

Future Direction

- Investigating structural effects
- Studying different chemical composition
- SEM imaging of hydrogel
- Embed optimized hydrogel into a variety of micro-actuation interfaces

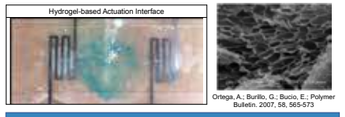

Ortega, A.; Burillo, G.; Bucio, E.; Polymer Bulletin. 2007, 58, 565-573

Acknowledgments

- National Science Foundation (NSF)
- Functional Nanomaterials UCLA Engineering Summer Undergraduate Scholars
- Fast Track to Success Summer Scholars Program, Electrical Engineering Department, UCLA Henry Samueli School of Engineering and Applied Science
- Dr. Chee Wei Wong
- Dr. Robert Candeler
- Dr. Chandrashekhar Joshi
- Willian Herrera
- Wes Uehara

LAB NAME
Neptune Lab

FACULTY ADVISOR
Chandrashekhar Joshi

DAILY LAB SUPERVISOR
Eric Welch

DEPARTMENT
Electrical and Computer Engineering

Dana Tovey

Electrical Engineering

Senior

Amplication of Picosecond Long-Wave Infrared Pulses in an Optically-Pumped High Pressure CO_2 Laser

The long-wavelength infrared range of 8-14 μm is of great interest for numerous strong-field physics research applications. For wavelengths in this range, achieving efficient amplification of pulses to gigawatt and higher peak powers using optical parametric amplification in nonlinear crystals or molecular lasers pumped via electric discharge has proven very challenging. Optically-pumped CO_2 lasers offer a promising alternative solution for amplification of 10 μm picosecond pulses. Numerical calculations are performed to model the amplification of such pulses using a 20 atmosphere CO_2 laser optically-pumped via a tunable 4 μm Fe:ZnSe laser. The optimal pump wavelength for an amplifier of length 5 cm, chosen to maximize absorbed pump energy and minimize non-uniformity of gain distribution, is found to be 4.19 μm. Simulations demonstrate that at high pressure, there is negligible difference in gain when describing the CO_2 asymmetric stretching mode as a harmonic oscillator (with a Boltzmann distribution) versus as an anharmonic oscillator (with a Treanor distribution). The difference between the cases of optical pumping and electric discharge pumping, however, is significant. It is shown that with optical pumping, using realistic conditions, gain coefficients as high as 5.6%/cm can be achieved. This system has the potential to be used for the amplification of 10 μm pulses from μJ to mJ energies as one compact stage of a scheme designed to generate multi-terawatt picosecond laser pulses. In addition to theoretical results, experimental characteristics of the Fe:ZnSe pump laser are presented.

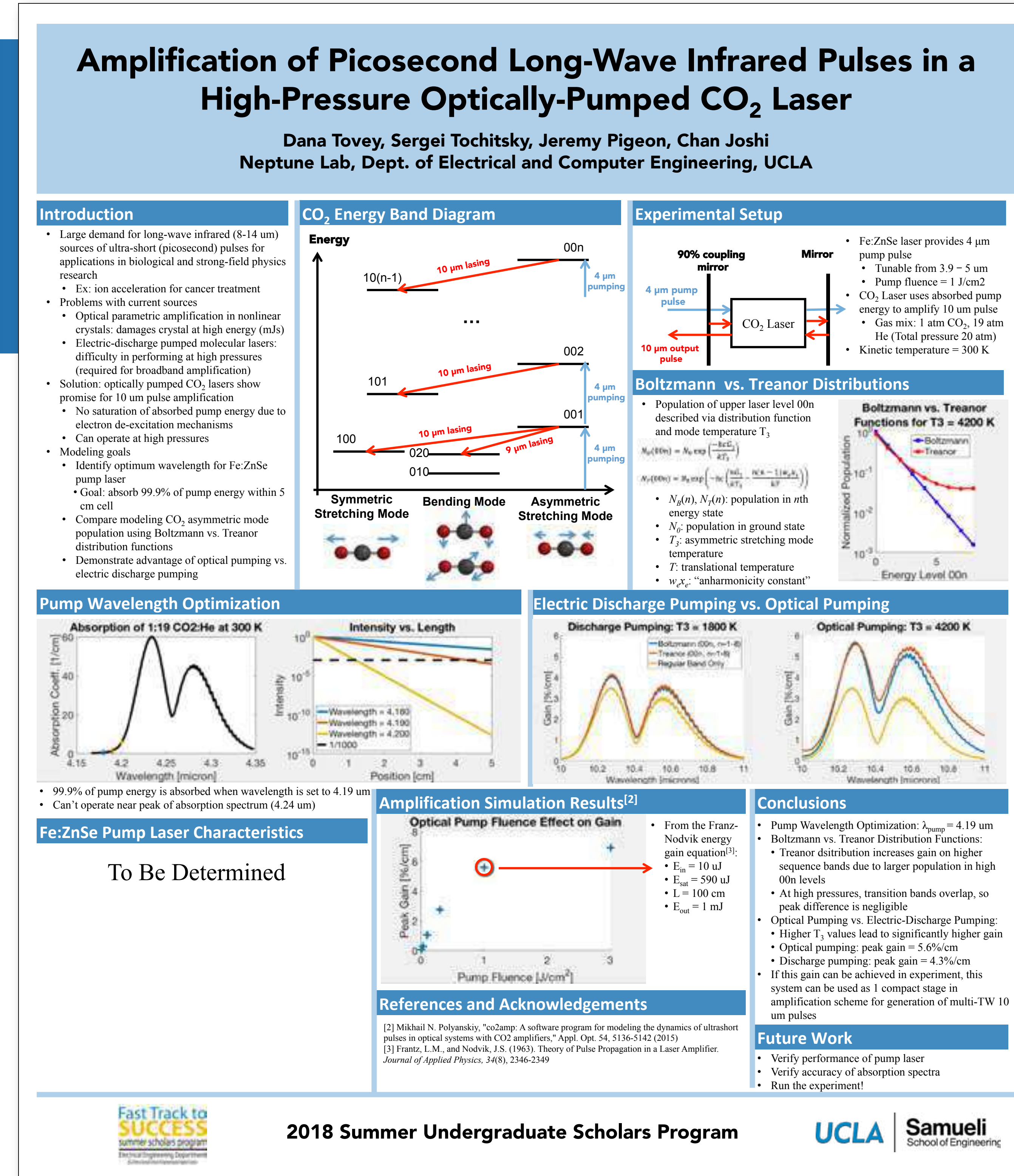

LAB NAME
Kao Lab

FACULTY ADVISOR
Jonathan Kao

DAILY LAB SUPERVISOR
NA

DEPARTMENT
Electrical and Computer Engineering

Mahak Virlley

Biology and Mathematics

Senior

Noninvasive Brain-Machine Interface Utilizing Electroencephalography

Brain-machine interfaces (BMIs) enable a nontraditional method of communication to individuals suffering from paralysis by decoding neural activity into control signals for a keyboard. This communication is dependent on an interface with the user via a continuously moving cursor. The overall goal of this research is to create a noninvasive BMI utilizing electroencephalography (EEG). In comparison to invasive BMIs, noninvasive BMIs are more affordable and involve less risk. In this study, we aim to conduct a proof of concept experiment to ensure that the external device communicates effectively and efficiently with trained deep learning models. In order to accomplish this, we aim to create a task implemented in MATLAB Simulink that consists of a series of random dots that appear on the screen, and disappear once the cursor lands on the dot. This real-time application will have computational purposes from event to response. Testing this program, by having the cursor be driven with simulated neural activity from deep learning models, will enable us to prove our concept so that we may extend the work and eventually, combine the efforts of the BMI with the noninvasive EEG imaging technique. I would like to sincerely thank the UCLA Samueli Engineering Summer Undergraduate Scholars Program, Department of Electrical and Computer Engineering and Jonathan Kao for accepting me to do research at UCLA this summer.

Noninvasive Brain-Machine Interface Utilizing Electroencephalography

Mahak Virlley, Ken-Fu Liang, and Jonathan Kao

Department of Electrical and Computer Engineering, University of California, Los Angeles

Abstract

Brain-machine interfaces (BMIs) enable a nontraditional method of communication to individuals suffering from paralysis by decoding neural activity into control signals for a keyboard. This communication is dependent on an interface with the user via a continuously moving cursor. The overall goal of this research is to create a noninvasive BMI utilizing electroencephalography (EEG). In comparison to invasive BMIs, noninvasive BMIs are more affordable and involve less risk. In this study, we aim to conduct a proof of concept experiment to ensure that the external device communicates effectively and efficiently with trained deep learning models. In order to accomplish this, we aim to create a task implemented in MATLAB Simulink that consists of a series of random dots that appear on the screen, and disappear once the cursor lands on the dot. This real-time application will have computational purposes from event to response. Testing this program, by having the cursor be driven with simulated neural activity from deep learning models, will enable us to prove our concept so that we may extend the work and eventually, combine the efforts of the BMI with the noninvasive EEG imaging technique. I would like to sincerely thank the UCLA Samueli Engineering Summer Undergraduate Scholars Program, Department of Electrical and Computer Engineering and Jonathan Kao for accepting me to do research at UCLA this summer.

Background & Rationale

- Noninvasive brain-machine interfaces are devices that offer a direct communication pathway between an individual's brain and an external device.
- For individuals with loss of motor function, BMIs offer an opportunity to once again move and communicate with the world.
- Over the last 17 years, advances in BMIs demonstrate its potential for clinical use.
- However, there are still many challenges before this can be implemented, i.e. low spatial and temporal resolution of the imaging technique.

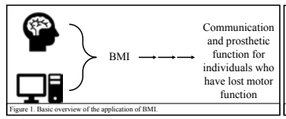

Figure 1. Basic overview of the application of BMI.

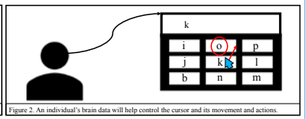

Figure 2. An individual's brain data will help control the cursor and its movement and actions.

Proof-of-Concept Experiment

It is important to first conduct a proof-of-concept experiment in which trained deep learning models and a keyboard are utilized to test communication accuracy with respect to the intended sensorimotor behavior.

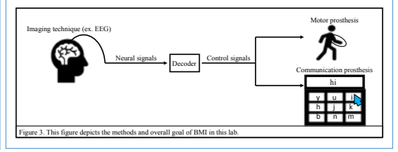

Figure 3. This figure depicts the methods and overall goal of BMI in this lab.

Methods

Translating kinematics into trajectories

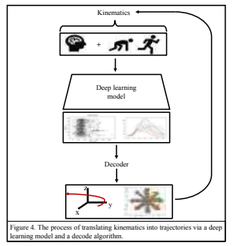

Figure 4. The process of translating kinematics into trajectories via a deep learning model and a decode algorithm.

Optimizing the deep learning model

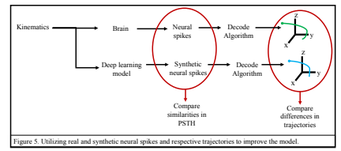

Figure 5. Utilizing real and synthetic neural spikes and respective trajectories to improve the model.

- After translating kinematics to neural spikes and their corresponding trajectories, the real and fake neural spikes are compared for similarities in the peristimulus time histogram (PSTH) which observes firing rates of neurons with respect to time.
- The trajectories will also be compared to look for differences that may assist in the improvement of the deep learning model .

Creating a task for real-time application

- A Simulink model is being created so that a real-time application of the task can be observed.
- The model specifically discusses the trial flow and trial parameters, along with other aspects of the task.

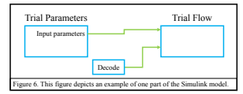

Figure 6. This figure depicts an example of one part of the Simulink model.

Conclusions & Future Studies

- Although no results have been obtained yet, the methods above consist of the current work in the lab.
- Once the task is successfully created, there will be a real-time application of the task that allows for improvement of the system.
- The brain and deep learning model will offer neural data that will be decoded by the algorithm to obtain control signals.
- The control signals will be implemented on the task via a continuously moving cursor.
- Once the cursor movement is obtained, it can be analyzed and adjustments can be made to the system according to the accuracy of the cursor movement with respect to its corresponding neural signal.

Real-time application

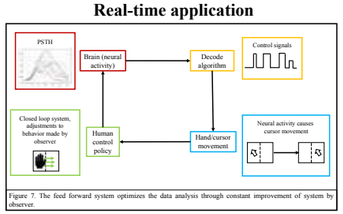

Figure 7. The feed forward system optimizes the data analysis through constant improvement of system by observer.

Acknowledgements

Functional Nanomaterials;
Summer Undergraduate Scholars Program
Department of Electrical and Computer Engineering
University of California, Los Angeles
Dr. Jonathan Kao
Neural Prosthetics Systems Laboratory of Krishna Shenoy
Jianwei Zhang
Michael Kleinman

Nikki Woo

Electrical Engineering

Sophomore

LAB NAME
ARNI

FACULTY ADVISOR
Christina Fragouli

DAILY LAB SUPERVISOR
Gaurav Agarwal

DEPARTMENT
Electrical and Computer Engineering

Exploring Secure Capacity for Communication in 1-2-1 Networks

Millimeter wave communication allows for very high data transfer rates; however, transmitting over large distances poses the issue of high information loss due to path loss. In order to minimize this path loss, we utilize beamforming, in which transmitting and receiving nodes align their antennae in order to establish a communication link. 1-2-1 networks serve as models for millimeter wave communication networks which use beamforming such that any intermediate node can only receive from and transmit to one node at a time. In our research, we analyze the secure capacity of these 1-2-1 networks in the presence of a passive adversary who has access to any K channels of her choice. Using the number of node and edge-disjoint paths of a network, we can calculate the lower and upper bounds on the secure capacity. For randomly generated graphs, we find and compare these capacity bounds with the rate achieved using a novel scheme. In our scheme, rather than starting with node-disjoint paths of a graph (which corresponds to the lower bound on capacity region), this scheme starts with edge-disjoint paths and maximizes path use while minimizing adversary access. Plotting the results of our scheme with upper and lower capacity bounds will allow us to analyze the specific network parameters that may yield a tighter lower bound.

UCLA Samueli School of Engineering | Summer Undergraduate Scholars Program

Fast Track to SUCCESS Summer Scholars Program — Electrical Engineering Department, UCLA Henry Samueli School of Engineering and Applied Science

Wireless Health UCLA

On Secure Capacity for Communication in 1-2-1 Networks

UCLA Department of Electrical and Computer Engineering

K. Daniels, N. Woo, G. Agarwal, C. Fragouli

Algorithmic Research in Network Information Flow (ARNI)

Millimeter Wave Communication

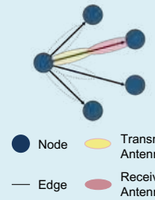

- Utilized in 5G wireless communication systems
- High frequency communication
- Large bandwidth, small components

- **Challenge**: Short range and physical barriers
- **Solution:** Utilize beamforming: two beams must align to establish a communication link

1-2-1 Network Model

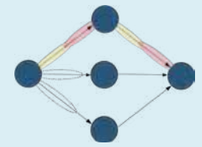

Example of a 1-2-1 Network

- Models millimeter wave communication
- Unit capacity edges
- Each node can point its transmitting/receiving beam to at most one node
- Source: can transmit to at most M nodes
- Destination: can receive from at most M nodes

Unsecure Capacity

- Unsecure capacity: Maximum flow in the absence of adversary

$$C_u = \min(M, H_e)$$

M = number of antennae on source node
H_e = # of edge disjoint paths

Scheme for Choosing Optimal Paths

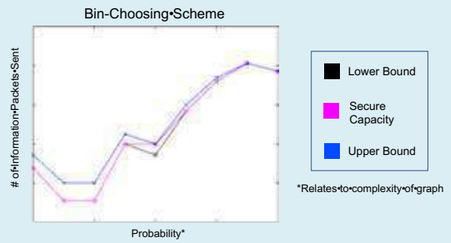

1. Group all edge disjoint paths into node disjoint bins
2. Choose paths from M different bins every iteration, always starting with the biggest bins
3. If there are any leftover paths left, use them if doing so will generate a greater overall rate

Secure Capacity Bounds

- Secure capacity = # of information packets that can be sent given adversary has access to any K edges

- Secure capacity of the network is between the following bounds:

- H_v = # of vertex disjoint paths
- M = number of antennae on source node
- H_e = # of edge disjoint paths

- Upper Bound: $H = \min(M, H_e)\left(1 - \frac{K}{H_e}\right)$
- Lower Bound: $L = \min(M, H_v)\left(1 - \frac{K}{H_v}\right)$

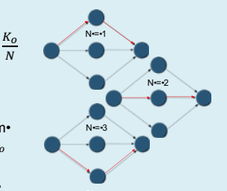

Arbitrary Network Graph

$H_e = 3 \rightarrow H = \min(1,3)\left(1 - \frac{1}{3}\right) = \frac{2}{3}$

$H_v = 2 \rightarrow L = \min(1,2)\left(1 - \frac{1}{2}\right) = \frac{1}{2}$

$$L \leq Secure\ Rate \leq H$$

Approximating Tighter Lower Bound on Secure Capacity

- The secure flow rate for any graph is given by: $R = \frac{(M*N)-K_o}{N} = M - \frac{K_o}{N}$

N = number of times network is used
K_o = number of symbols intercepted by adversary on her K channels

- We must choose paths of traversal from source to destination such that either K_o is minimized or N is maximized
- Continuously alternate paths such that adversary is severely limited

Given:
M<=1, K<=1

Secure Rate = $1 - \frac{1}{3} = \frac{2}{3}$

Conclusions and Future Work

- We observed that scheme 1 was able to yield a rate better than the lower bound in some cases
- Further generalizations can be made regarding the specific parameters needed for a network to yield a tighter lower bound
- Finding a closed mathematical expression that allows us to determine whether or not a given graph will yield a tightened lower bound
- Other sophisticated schemes may still be explored to get better rates

Acknowledgements

We would like to thank the Summer Undergraduate Scholars Program, the UCLA Electrical and Computer Engineering Department, Professor Christina Fragouli, and Gaurav Agarwal for their continuous guidance and for this opportunity to explore research in the field of network security.

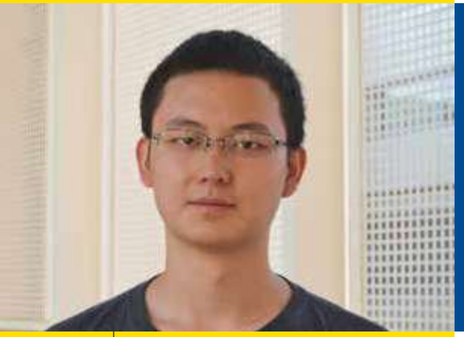

LAB NAME
LEMUR

FACULTY ADVISOR
Ankur Mehta

DAILY LAB SUPERVISOR
Ankur Mehta

DEPARTMENT
Electrical and Computer Engineering

Derek Xiao

Electrical Engineering

Sophomore

Control of a Rocket using an Off-Center Mass

As electronics get smaller and more powerful, satellites have also gotten smaller, the smallest of which are in the **1-IOg** range [1]. This makes smaller launch vehicles viable, which may make small launch operations an affordable possibility for researchers and hobbyists. We explore a controller for small rockets that uses an off center mass in order to reduce the number of actuators, potentially reducing cost and increasing flight distance. We plan to use mathematical analysis and simulations to explore the natural dynamics of the system, and later use simulation to demonstrate that the controller we come up with is able to make the rocket track arbitrary trajectories. As of this moment, I am working on extracting useful results from the mathematical analysis to compare with the simulation that I set up in the first few weeks.

[1] Z. Manchester, M. Peck, A. Filo, “KickSat: A Crowd-Funded Mission To Demonstrate The World’s Smallest Spacecraft,” 27th Annual AIAA/USU Conference on Small Satellites, SSC13-1X-5, 2013.

Attitude Control of a Rocket using an Off-Center Mass

Derek Xiao, Amir Ali Omidfar, Professor Ankur Mehta
Department of Electrical and Computer Engineering

Goal: Create control system for a rocket with only 1 DOF actuation

Background and Motivation

As electronics get smaller and more powerful, so have rocket payloads. For example, some wireless sensor networks have nodes on the order of 1-10 grams [1]. Small rockets capable of sending small payloads into space are more cost effective and accessible than big launch vehicles for hobbyists or researchers.

Active attitude control of a small model rocket was demonstrated in [2]. However it made use of 2 servo motors and a spherical bearing for the rocket engine, and 2 DC motors for flywheel roll control, which adds a lot of weight and cost to the rocket. We consider a design that uses only 1 DC motor to actuate the off-center mass.

Introduction

We propose active control of the rocket by controlling the position of an off-center mass connected to the rocket by an actuated revolute joint. This control method would reduce the amount of actuators needed for active control, and as a result potentially decrease rocket weight and increase flight distance.

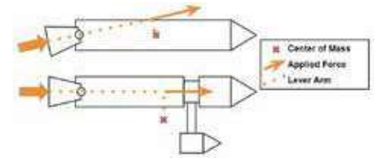

Figure 1: (Top) Rocket control using a gimbaled rocket engine (Bottom) Rocket control using an off center mass

System Model

The system is simplified as a cylinder attached to an off center mass through a revolute joint. Joint torques and external forces can be specified in simulation, and that is how I will be implementing the control system and simulating rocket thrust.

Additionally, cartesian coordinates and orientation can be exported out of the simulation, and fed into the controller, which will be implemented in simulink.

Figure 2: system model

Method

1. Simulate system with Simscape Multibody (Matlab add-on)

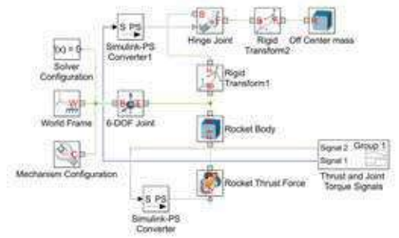

Figure 3: Simscape Multibody graphical representation of system

2. Investigate system’s natural behavior by deriving the equations of motion (current)
3. Validate the simulation software by comparing with mathematical analysis
4. Design control law
5. Demonstrate control law in simulation

Current work

I have set up a simulation environment in Matlab Simulink, using the add-on “Simscape Multibody”. However, to maintain good scientific practice, I’m currently trying to formulate predictions about the system behavior through mathematical analysis of the equations of motion.

Simultaneously, I am taking a course about underactuated robotics by Russ Tedrake to get inspiration on how to control the rocket.

Future Plan

By the end of the summer, I anticipate that I’ll have finished exploring the system’s natural behavior through mathematical analysis and compared it to observations in simulation (step 3). Hopefully, by then I can move on to designing a controller.

References

[1] Z. Manchester, M. Peck, A. Filo, “KickSat: A Crowd-Funded Mission To Demonstrate The World’s Smallest Spacecraft,” 27th Annual AIAA/USU Conference on Small Satellites, SSC13-IX-5, 2013.
[2] Kehl, Florian & M Mehta, Ankur & Pister, Kristofer. (2015). An Attitude Controller for Small Scale Rockets. Springer Tracts in Advanced Robotics. 105. 201-214. 10.1007/978-3-319-07488-7_14.

Acknowledgements

- 2018 Summer Undergraduate Scholars Program

Nicolas Zani

Electrical Engineering

Sophomore

LAB NAME

Sensors and Technology Laboratory

FACULTY ADVISOR

Rob Candler

DAILY LAB SUPERVISOR

Jimmy Wu

DEPARTMENT

Electrical and Computer Engineering

Circuit Analysis of Micromachined Electromagnet Quadruple Devices

The increasing interest in higher-energy FEL for medical and particle imaging calls for new focusing technology. The fabrication process outlined in Harrison et. al. [1] allows for the micromachining of an electromagnet, with a field parallel to the substrate plane, which makes possible the MEMS magnetic quadrupole in Harrison et. al. [2]. These quadrupoles can be utilized for FEL emission in the 100-10 nm wavelength spectrum in shorter distances than allowed by current technology. After the machining of a handful of quadrupole devices for FEL focusing on a 4mm x 4mm die, multiple technical issues surfaced surrounding the machining process, mostly shortages and other node faults, which prevent experimentation. By means of a stereoscope and probe station, identification consisted of thorough resistance mapping across individual devices, which were analysed for shorts in the electromagnet windings. This resulted in resistance fluctuation during measurement, and resistance mappings pointed to shorts located at the vias. To allow for furthering of the initial project, current was applied across shorted pads to burn the shorts; this technique working points towards “whiskers” -- small strands of metal created by the fabrication process -- being the primary cause of shortage for some devices. Some electromagnets were found to be disconnected, leading to future investigations involving FIB incision and SEM imaging.

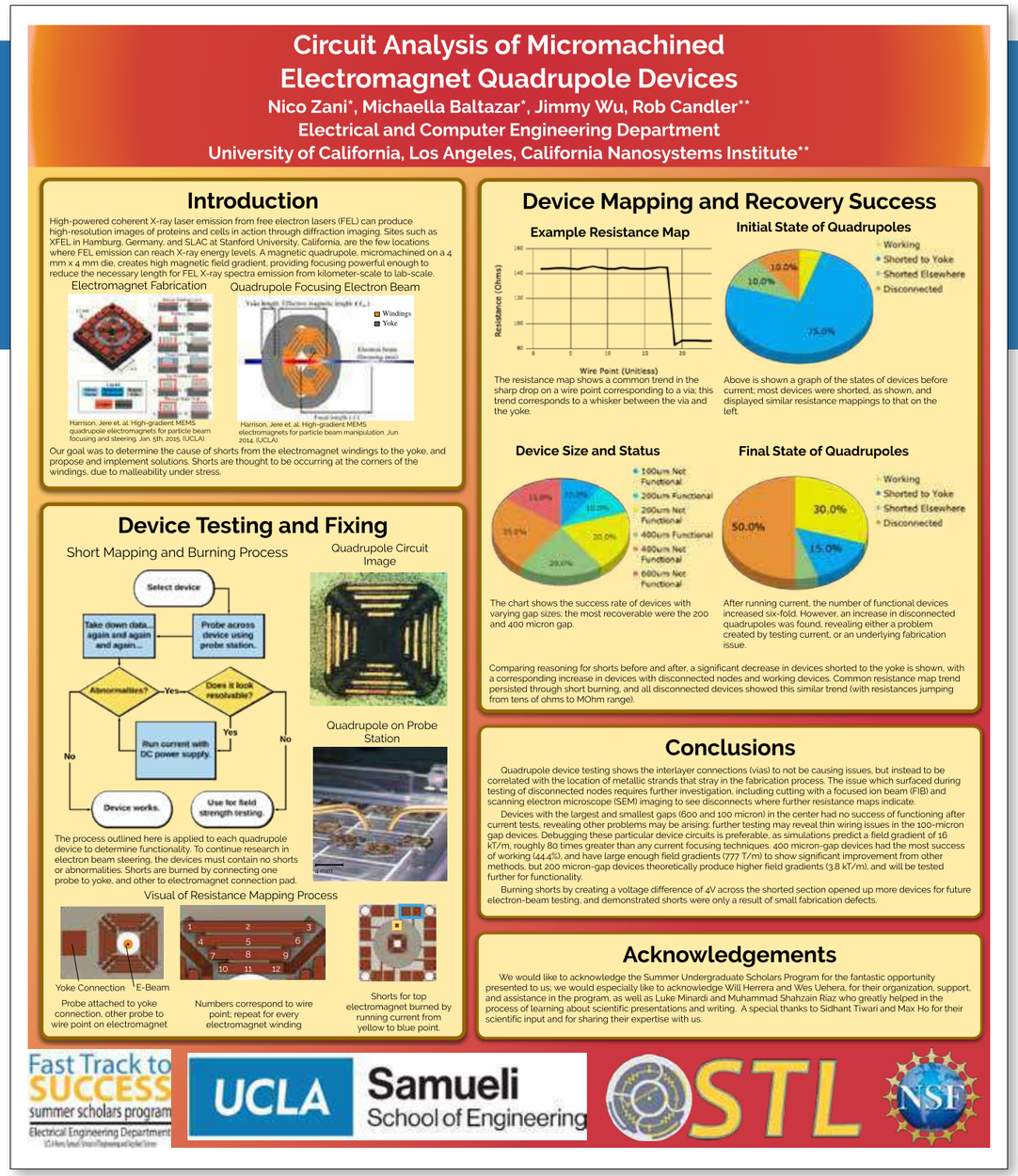

LAB NAME
Mesoscopic Optics and Quantum Electronics

FACULTY ADVISOR
Chee Wei Wong

DAILY LAB SUPERVISOR
Jaime Gonzalo Flor Flores

DEPARTMENT
Electrical and Computer Engineering

Jameson Zhang

Electrical Engineering

Sophomore

Automation of Optical Fiber Coupling Utilizing Computer Vision

Coupling optical fibers to electronic chips is an essential task for testing photonics chips. When the instruments holding the chips and the fibers lack the adequate and essential precision, a human must manually couple the optical fibers to the waveguide to prevent damaging the chip or the fiber and to ensure that the fiber is close enough to the waveguide. However, there may be hundreds of wave guides on a single chip and thousands of chips to test. Henc, it is not feasible for a human operator to couple all of them. The objective of the computer vision. To do so, we train a program to recognize key components of the chip and the fiber such as the wave guide, coupler, edge of the chip, and the head and body of the optical fibers. We train the program by feeding it many images of these components so that it can discriminate ebtween them. When the program detects these components, we align the fiber head to the wave guide. Finally, we adjust the position of the fiber automating the coupling procss through object recognition will greatly speed up coupling and the same concepts may be used to automate many other industrial task.

Automated Optical Fiber Coupling Utilizing Computer Vision

Jameson Zhang, Jaime G. F. Flores, Chee W. Wong

Department of Electrical and Computer Engineering, University of California, Los Angeles

Introduction

Photonics chips are a special type of electronic chip that take light signals from optical fibers rather than normal wires. The optical fibers must be aligned with wave guides, which are pathways for the light to travel on the chip, in order for the chip to receive the signals. This alignment process is called coupling. When people manufacture photonics chips, they must test them and to test them, they must couple fibers to waveguides first. Since optical fibers are so small, the instruments used for coupling often lack the precision to couple safely and correctly so a human must do it manually. Computer vision is a field of computer science that deals with object recognition and image analysis. We will use computer vision, specifically Haar-like features, to detect key components of the chip and optical fiber to automate the preliminary coupling of the fibers. Then, we will perform a final alignment to couple the fibers by using the maximum intensity. Maximum intensity occurs when the fibers are perfectly coupled so we place the fibers in a state where the intensity is maximized.

Background

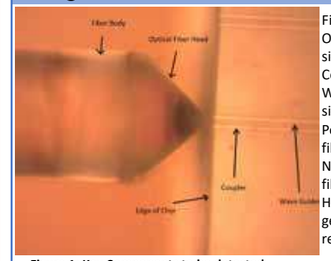

Figure 1: Key Components to be detected

Fiber Body – sends light signal
Optical Fiber head – focuses light signal
Coupler – assists in coupling
Wave Guide – pathway for light signal to enter chip
Positives – images with optical fiber present
Negatives – images without optical fiber present
Haar-like Features – Simple geometric features used for object recognition

Methods

1. Obtain positive and negatives and convert to greyscale

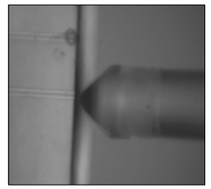

Figure 2: Greyscale positive
Hundreds of positives and negatives are used to train the program

2. Locate and crop key features (Whole fiber, fiber head and body, coupler)

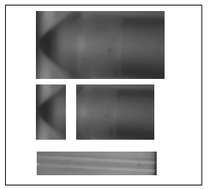

Figure 3: Key components cropped
From top to bottom: Optical Fiber, Optical Fiber head and body, Coupler

3a. Train program to detect these components
3b. Use Fourier Transform for chip edge

4a. Couple fiber by aligning components.
4b. Finish alignment by maximizing intensity detected

Haar-like Features

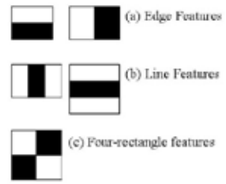

Figure 4: Rectangles for different types of features
There are different combinations of rectangles that are used to analyze different types of features

- Object detection using Haar-like features compares intensities of pixels in different features.
- Each feature becomes a value by subtracting sum of pixels in the white rectangles(s) by the sum of pixels in the black rectangle(s)
- AdaBoost is used to determine the best features to consider by finding the features that can distinguish between the most objects.
- A Haar-cascade is used instead of testing for all features at once. Features are applied to different stages (from 4 to 40 stages). If a window completes all stages, the object is detected.

Conclusion and Future Work

- A preliminary alignment of the optical fibers is made by detecting key components of the chip and fiber and aligning those.
- The position of the fiber is adjusted such that the intensity received by the chip is maximized, giving the most precise alignment.
- We will attempt to optimize and speed up object detection to achieve smoother real-time alignment

Results

Figure 4: Fiber head detected by program
Our program is able to detect key features such as the optical fiber heads

- Detecting individual key components was more consistent than detecting the fiber as a whole
- We are able to consistently detect key components with only four cascade stages
- The algorithm for final alignment is able to achieve satisfactory alignment

References

Viola, P., & Jones, M. (n.d.). Rapid object detection using a boosted cascade of simple features. *Proceedings of the 2001 IEEE Computer Society Conference on Computer Vision and Pattern Recognition. CVPR 2001*.

Acknowledgements

I would like to thank the 2018 Summer Undergraduate Scholars Program and the UCLA Electrical and Computer Engineering Fast Track to Success Summer Scholars Program and the UCLA Department of Electrical and Computer Engineering for this opportunity to conduct research. Thank you to the National Science Foundation for the funding and support

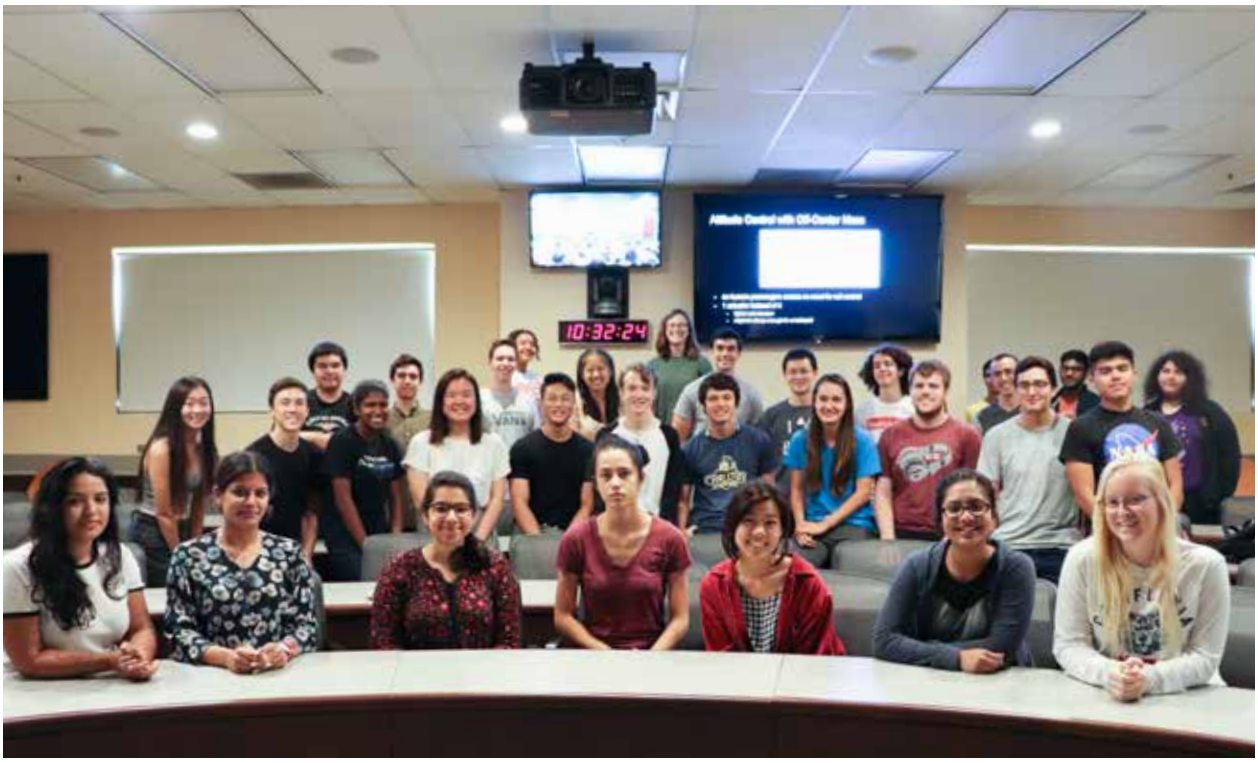

If you would like to find out more about the Summer Undergraduate Scholars Program, please contact Director William Herrera:

William Herrera
Director
Summer Undergraduate Scholars Program
310.825.9478
williamh@seas.ucla.edu
6288 Boelter Hall

Or visit our website at https://tinyurl.com/uclasusp.

UCLA Samueli School of Engineering